



Wakota Bridge Thermal Monitoring Program Part I: Analysis and Monitoring Plan

Minnesota
Department of
Transportation

**RESEARCH
SERVICES**

Office of
Policy Analysis,
Research &
Innovation

Arturo E. Schultz, Principal Investigator
Department of Civil Engineering
University of Minnesota

May 2013

Research Project
Final Report 2013-11

Your Destination... Our Priority



To request this document in an alternative format, please contact the Affirmative Action Office at 651-366-4723 or 1-800-657-3774 (Greater Minnesota); 711 or 1-800-627-3529 (Minnesota Relay). You may also send an e-mail to ADArequest.dot@state.mn.us.

(Please request at least one week in advance).

Technical Report Documentation Page

1. Report No. MN/RC 2013-11	2.	3. Recipients Accession No.	
4. Title and Subtitle Wakota Bridge Thermal Monitoring Program Part I: Analysis and Monitoring Plan		5. Report Date May 2013	
7. Author(s) Christopher J. Scheevel, Krista M. Morris, and Arturo E. Schultz		6.	
9. Performing Organization Name and Address Department of Civil Engineering University of Minnesota 500 Pillsbury Drive SE Minneapolis, MN 55455		8. Performing Organization Report No.	
12. Sponsoring Organization Name and Address Minnesota Department of Transportation Research Services 395 John Ireland Boulevard, MS 330 St. Paul, MN 55155		10. Project/Task/Work Unit No. CTS Project #2010011	
		11. Contract (C) or Grant (G) No. (C) 89261 (WO) 145	
15. Supplementary Notes http://www.lrrb.org/pdf/201311.pdf		13. Type of Report and Period Covered Final Report	
		14. Sponsoring Agency Code	
16. Abstract (Limit: 250 words) <p>In this work, a common refined design method is evaluated with respect to a recently constructed bridge. Two finite element models of the Wakota Bridge in South St. Paul, Minnesota, were produced, one using a design level program (SAP2000) and the other using a research level program (ABAQUS). These models were verified with respect to each other using linearly elastic materials and were found to behave similarly. After this verification, an arbitrary temperature load was applied to each model and the refined design method was evaluated for accuracy of reduced section properties with respect to the more descriptive progressive cracking solution simulated by ABAQUS. The refined design method was employed using two, four, and six stiffness segments at which stiffness is evaluated along the height of the pier walls. It was seen that accuracy increased as the number of stiffness segments increased and that four segments seemed to balance accuracy and time-commitment by the engineer adequately.</p> <p>A staged construction model of the Wakota Bridge was also built, using the design level program, which incorporates all time-dependent effects of the construction sequence as well as locked-in forces. A pile analysis was performed and appropriate rotational springs were found for Foundations 2 and 3. A simplified method for the determination of the rotational springs is discussed, and a range of effective lengths was found for use with this procedure. The staged construction model is used for field data correlation in Part two of this report.</p> <p>The staged construction model was also used to evaluate the different design options as described in the AASHTO LRFD. The two options given for accounting for reduced section properties were evaluated and compared. The refined analysis option and gross section option were compared for the Wakota Bridge and are shown to correlate to within about 10%. The two temperature application methods (Procedure A and B in the AASHTO LRFD) were also compared. As expected, Procedure B produced much larger design moments than that of Procedure A.</p>			
17. Document Analysis/Descriptors Temperature, Thermal stresses, Concrete, Bridge piers, Finite element method		18. Availability Statement No restrictions. Document available from: National Technical Information Services, Alexandria, Virginia 22312	
19. Security Class (this report) Unclassified	20. Security Class (this page) Unclassified	21. No. of Pages 129	22. Price

Wakota Bridge Thermal Monitoring Program Part I: Analysis and Monitoring Plan

Final Report

Prepared by:

Christopher J. Scheevel
Krista M. Morris
Arturo E. Schultz

Department of Civil Engineering
University of Minnesota

May 2013

Published by:

Minnesota Department of Transportation
Research Services
395 John Ireland Boulevard, MS 330
St. Paul, Minnesota 55155

This report documents the results of research conducted by the authors and does not necessarily represent the views or policies of the Minnesota Department of Transportation or the University of Minnesota. This report does not contain a standard or specified technique.

The authors, the Minnesota Department of Transportation, and the University of Minnesota do not endorse products or manufacturers. Trade or manufacturers' names appear herein solely because they are considered essential to this report.

Acknowledgments

The authors would like to thank the Minnesota Department of Transportation for funding this project. The authors would also like to thank the Technical Advisory Panel (TAP) members for their help and guidance during the development of this report: Dave Dahlberg, Arielle Ehrlich, Shirlee Sherkow, Keith Molnau, Paul Stenberg, Jihshya Lin and Dustin Thomas. Finally, the authors would like to thank Paul Bergson, Rachel Gaulke, Andrew Gastineau and others in the Department of Civil Engineering at the University of Minnesota for their assistance and advice.

Table of Contents

Chapter 1. Introduction.....	1
1.1 General.....	1
1.2 Wakota Background Information	1
1.3 Wakota Monitoring Project Details	4
Chapter 2. Instrumentation.....	6
2.1 Introduction.....	6
2.2 Instruments.....	6
2.3 Choosing the Instrument Locations	7
2.4 Placement of Instruments.....	9
2.5 Data Acquisition	11
2.6 Instrument Calibration and Data Storage.....	13
Chapter 3. Literature Review on Modeling and Design.....	15
3.1 Introduction.....	15
3.2 Common Refined Design Method (CRD Method).....	15
3.2.1 <i>Deflections Due to Sustained Loads</i>	15
3.2.2 <i>Application of Thermal Loads</i>	18
3.2.3 <i>General Modeling Considerations</i>	19
3.3 Finite Element Analysis Review.....	19
3.4 Thermal Loadings on Concrete Bridges	24
3.5 AASHTO LRFD and MnDOT BDM Requirements for Thermal Loadings on Bridge	26
3.5.1 <i>Uniform Temperature</i>	26
3.5.2 <i>Temperature Gradient</i>	29
Chapter 4. Research Level Modeling (ABAQUS).....	32
4.1 Introduction.....	32
4.2 Modeling Assumptions	32
4.3 Creating the Three Dimensional Model Geometry.....	33
4.4 Importing.....	34

4.5	Meshing.....	35
4.6	Verifying Convergence.....	37
4.6.1	<i>Superstructure</i>	37
4.6.2	<i>Piers</i>	40
4.7	Tie Constraints.....	41
4.8	Boundary Conditions and Loading.....	41
4.9	Cracking Behavior.....	43
4.9.1	<i>Compressive Behavior</i>	43
4.9.2	<i>Tensile Behavior</i>	44
4.10	Defining Rebar.....	46
Chapter 5.	Design Level Modeling (DLM)	48
5.1	Introduction.....	48
5.2	Development of the Model Geometry.....	48
5.2.1	<i>Superstructure</i>	48
5.2.2	<i>Pier Walls</i>	49
5.2.3	<i>Other Modeling Considerations</i>	50
5.3	Design/Calibration Model and Staged Construction Analysis (DLM3).....	50
5.4	Prestressing Strands.....	50
5.4.1	<i>Time-Dependent Effects</i>	51
5.4.2	<i>General Considerations</i>	51
5.5	Footing Restraints.....	53
5.5.1	<i>General</i>	53
5.5.2	<i>Pile Analysis</i>	54
5.6	Preliminary Correlation.....	61
Chapter 6.	Comparison of Linear Models.....	63
6.1	Introduction.....	63
6.2	Pier Lateral Movement.....	63
6.3	Pier End-Moments.....	64
6.4	Superstructure Bending.....	66
6.5	Rotational Spring Considerations.....	67

Chapter 7. Evaluation of Common Refined Design Method	69
7.1 Introduction.....	69
7.2 Pier Discretization Questions.....	69
7.3 Dependence on Loading Magnitude	73
Chapter 8. AASHTO LRFD Design Option Evaluation	77
8.1 Introduction.....	77
8.2 Loading Considerations	77
8.3 Comparison of Options	79
8.3.1 <i>Comparing Cracked Stiffness Methods</i>	79
8.3.2 <i>Comparing Temperature Application Methods</i>	81
8.4 Discussion.....	84
Chapter 9. Summary, Conclusions, and Recommendations	85
9.1 Summary	85
9.2 Conclusions.....	85
9.3 Recommendations.....	86
9.3.1 <i>For Practice</i>	86
9.3.2 <i>For Research</i>	87
References	88

Appendix A: Wakota Bridge Monitoring Program Instrumentation Plan

List of Figures

Figure 1.1: Typical cross-section close to piers [6].	2
Figure 1.2: Typical cross-section at midspan with traffic layout [6].	2
Figure 1.3: Plan view of entire structure [6].	2
Figure 1.4: Rendering of completed structure [2].	3
Figure 1.5: Elevation view of Wakota superstructure and substructure properties [3].	3
Figure 1.6: Wakota Bridge under construction.	4
Figure 1.7: Cast in place cantilever construction progress.	4
Figure 2.1: Geokon Model 4200 vibrating wire strain gauge [4].	6
Figure 2.2: HX-P420 linear string potentiometer [5].	7
Figure 2.3: Instrumented sections along length of bridge (abutments, Section 2-4U, Section 4-6D, Pier 2, Pier 4).	8
Figure 2.4: Strain gauge distribution in superstructure.	9
Figure 2.5: Pier instrumentation elevations (mm).	10
Figure 2.6: Pier 2 strain gauge locations and designations.	11
Figure 2.7: Pier 4 strain gauge locations and designations.	11
Figure 2.8: Campbell Scientific equipment connection diagram [6].	13
Figure 3.1: Effect of creep and shrinkage on fixed pier system.	16
Figure 3.2: Effect of jacking force.	16
Figure 3.3: Simplification of pier cross-section.	17
Figure 3.4: Twin-walled pier discretized for analysis.	18
Figure 3.5: Different tension stiffening models: a) Scanlon-Murray model; b) Lin and Scordelis model; c) Vebo and Ghali model; d) Gilbert and Warner model [14].	21
Figure 3.6: Tension stiffening model used in study [14].	21
Figure 3.7: Varying tension-stiffening parameters compared to test results [14].	22
Figure 3.8: Priestley's thermal design gradient [20].	25
Figure 3.9: Minimum design temperatures for concrete girder bridges with concrete decks [22].	27
Figure 3.10: Maximum design temperatures for concrete girder bridges with concrete decks [22].	27
Figure 3.11: Solar radiation zones for the U.S.A [25a].	29

Figure 3.12: Design thermal gradient [25a].	30
Figure 4.1: Superstructure cross-sections.	33
Figure 4.2: Assembled geometric 3D analysis model.	34
Figure 4.3: C3D20R element in ABAQUS [16].	36
Figure 4.4: Representative span meshing scheme.	37
Figure 4.5: Meshing refinements.	38
Figure 4.6: Stress contours of different meshing schemes.	39
Figure 4.7: Pier Table 4 used for pier wall convergence study with applied load.	40
Figure 4.8: Comparison of different pier meshing schemes.	41
Figure 4.9: Popovics/Thorenfeldt/Collins concrete material model.	44
Figure 4.10: Typical tension stiffening curve.	45
Figure 4.11: Steel reinforcing bar material model.	46
Figure 5.1: Representative cross-section from SAP2000 Model.	48
Figure 5.2: Bridge pier representation in SAP2000.	49
Figure 5.3: SAP2000 Design model for comparison of methods (no prestressing).	50
Figure 5.4: Creep coefficient (left), shrinkage strain (right).	51
Figure 5.5: General multi-linear plastic kinematic relationship.	52
Figure 5.6: Pier 2 Pile supported footing.	53
Figure 5.7: Pier 3 Pile supported footing.	54
Figure 5.8: Pier 4 spread footing.	54
Figure 5.9: Pier 2 soil profile (ϕ = angle of internal friction, γ = unit weight in lb/ft ³).	55
Figure 5.10: Pier 3 soil profile (ϕ = angle of internal friction, γ = unit weight in lb/ft ³).	56
Figure 5.11: Pier 2 pile analysis strip and applied lateral load.	56
Figure 5.12: Translational stiffness diagram.	57
Figure 5.13: Axial stiffness formula diagram.	57
Figure 5.14: Simplified rotational stiffness in pile strip.	58
Figure 5.15: Lateral deflection range for approximate ultimate loadings.	61
Figure 6.1: Estimate of appropriate moments at ends of piers.	64
Figure 6.2: Local rotation of pier base due to elastic icebreaker.	66
Figure 6.3: Qualitative vertical deflections of superstructure under self weight.	67

Figure 7.1: Pier force and moment comparison of DLM1 with CRD stiffness updating method and RLM2 with nonlinear materials.	72
Figure 7.2: Moment deviation with respect to loading magnitude using: 2 Stiffness Segments (top), 4 Stiffness Segments (bot).	74
Figure 7.3: Axial force deviation with respect to loading magnitude using: 2 Stiffness Segments (top), 4 Stiffness Segments (bot).	75
Figure 7.4: Shear force deviation with respect to loading magnitude using: 2 Stiffness Segments (top), 4 Stiffness Segments (bot).	76
Figure 8.1: Comparison of predicted pier wall end forces and moments using the refined and gross section cracked section procedure (Temperature Procedure A).....	80
Figure 8.2: Comparison of predicted pier wall end forces and moments using the refined and gross section cracked section procedure (Temperature Procedure B).	81
Figure 8.3: Percent difference in design forces when using Procedure B vs. Procedure A.....	82

List of Tables

Table 3.1: Procedure A temperature ranges [22].	26
Table 5.1 a): Foundation properties (fixed connection).	59
Table 5.2: Predicted and measured movements (mm) due to construction jack apart.	62
Table 6.1: Pier wall displacements at top under 85 °F temperature increase.	64
Table 6.2: a): Moments due to 85 °F temperature load.	65
Table 6.3: Moments with pier wall base fixed (85° F expansion load).	66
Table 6.4: a): Moments due to 85° F temperature load (with rotational springs).	68
Table 7.1: RLM2 moments and forces due to 100° F temperature load (Pier 4).	70
Table 7.2: a): DLM1 (100°F, Pier 4).	71
Table 7.3: Results from axial and lateral loading.	73
Table 8.1: AASHTO LRFD strength load cases.	77
Table 8.2: Dead weight load factors (γ_p).	78
Table 8.3: Pier wall relative stiffnesses.	83

List of Abbreviations

AASHTO	American Association of State and Highway Transportation Officials
DLM1	Design Level Model, created in SAP2000, contains no prestressing, time-dependent effects, pier wall rotational springs, or foundation rotations
DLM2	Design Level Model, created in SAP2000, no prestressing, time-dependent effects, or foundation rotations. Contains rotational springs at ends of pier walls for attempt at accounting for local rotations
DLM3	Design Level Model, created in SAP2000, incorporates staged construction, prestressing, time-dependent effects, and foundation rotation, no pier wall rotational springs
RLM1	Research Level Model, built in ABAQUS, linear material representation
RLM2	Research Level Model, built in ABAQUS, nonlinear material representation in piers
CRD	Common Refined Design
CTE	Coefficient of Thermal Expansion

Loading Notation

CR	= force effects due to creep
DD	= downdrag force
DC	= dead load of structural components and nonstructural attachments
DW	= dead load of wearing surfaces and utilities
EH	= horizontal earth pressure load
EL	= miscellaneous locked-in force effects resulting from the construction process, including jacking apart of cantilevers in segmental construction
ES	= earth surcharge load
EV	= vertical pressure from dead load of earth fill
PS	= secondary forces from post-tensioning
SH	= force effects due to shrinkage
BR	= vehicular braking force
CE	= vehicular centrifugal force
CT	= vehicular collision force
CV	= vessel collision force
EQ	= earthquake load
FR	= friction load

IC = ice load

IM = vehicular dynamic load allowance

LL = vehicular live load

LS = live load surcharge

PL = pedestrian live load

SE = force effect due to settlement

TG = force effect due to temperature gradient

TU = force effect due to uniform temperature

WA = water load and stream pressure

WL = wind on live load

WS = wind load on structure

γ_{TG} = load factor for temperature gradient

Γ_p = load factor for permanent loading

Γ_{SE} = load factor for settlement

Executive Summary

The design of reinforced concrete bridge piers for lateral loads is an ambiguous task for bridge engineers. As the piers experience lateral loads, primarily from temperature fluctuations and time-dependent effects, they undergo cracking. Because of this mechanism, bridge designers must consider cracked sections with a reduced stiffness.

The procedures required by the American Association of State and Highway Transportation Officials (AASHTO) Load and Resistance Factor Design (LRFD) Specifications and the Minnesota Department of Transportation (MnDOT) LRFD Bridge Design Manual (BDM) for determining thermal forces in bridge piers were investigated. AASHTO LRFD requires consideration of an 80 °F temperature range, corresponding to a 35 °F increase and 45 °F decrease from a MnDOT specified central temperature of 45 °F, a load factor of 0.5 for the Strength Limit State, and the use of gross section properties to model the bridge members. MnDOT requirements for typical bridges also includes a load factor of 0.5 for the Strength Limit State and the use of gross section properties for bridge members, but two different procedures are used to account for temperature effects. For the calculation of internal transverse forces, the same 35 °F increase and 45 °F decrease as specified in the AASHTO LRFD are used, but longitudinal thermal effects are calculated using a 150 °F temperature range (a 75 °F rise and 75 °F fall from a central 45 °F temperature). It is often difficult to handle the thermal loads in design, and common solutions more sophisticated analysis, such as representation of bearing and/or pile flexibility or using cracked column stiffness, or structural modifications, such as reducing the pier column size or placing a joint in the pier cap.

In this work, which is the first half of a two-part report, a common refined design method is evaluated with respect to a recently constructed major bridge with fixed twin-walled piers. Two finite element models of the Wakota Bridge in South St. Paul, Minnesota, were produced, one using a design level program (SAP2000) and the other using a research level program (ABAQUS). These models were verified with respect to each other using linearly elastic materials and were found to behave similarly. After the two models were verified with respect to each other, an arbitrary temperature load was applied to each model and the refined design method was evaluated for accuracy of reduced section properties with respect to the more descriptive progressive cracking solution produced by ABAQUS. The refined design method was employed using two, four, and six stiffness segments at which stiffness is evaluated along the height of the pier walls. It was seen that accuracy increased as the number of stiffness segments increased and that four segments seemed to balance accuracy and time-commitment by the engineer adequately.

A staged construction model of the Wakota Bridge was also built, which incorporates all time-dependent effects of the construction sequence as well as locked-in forces. A pile analysis was performed and appropriate rotational springs were found for foundations 2 and 3. A simplified method for the determination of the rotational springs is discussed, and a range of effective lengths was found for use with this procedure. The staged construction model was used for field data correlation in Part 2 of this report.

The staged construction model was also used to evaluate the different design options as described in the AASHTO LRFD and the MnDOT BDM. The two options given for accounting for reduced section properties were evaluated and compared. The refined analysis option and gross section option were compared for the Wakota Bridge and are shown to correlate to within about 10%.

The two temperature application methods (Procedure A and B in the AASHTO LRFD Articles 3.12.2.1 and 3.12.2.2) as interpreted by MnDOT BDM were also compared. As expected, Procedure B produced much larger design moments than that of Procedure A.

It was found that the CRD Method is an appropriate method for the analysis of cracked section properties in concrete piers that experience cracking, and should be used in final designs of this type of pier. The gross section method, which employs a 0.5 temperature load factor can be used for preliminary design, as it generally produces conservative results.

For conservatism, the magnitude of the uniform temperature load should be applied as per Procedure B in AASHTO LRFD when considering longitudinal effects, as this procedure produces much larger moments than Procedure A at the ends of the pier walls. Ambient air temperature at the bridge will be compared to the internal concrete temperatures in the field portion of the research, allowing for better judgments on whether the Procedure A or B temperature range is the best range to use for design in Minnesota.

Chapter 1. Introduction

1.1 General

Concrete bridge design for highway bridges is a complicated process incorporating a wide variety of design considerations and calculations. One aspect of concrete bridge design that is both ambiguous and lacking in research is the thermal analysis and design of reinforced concrete substructures that incorporate fixed connections to the superstructure. The piers must be designed to have adequate ductility to accommodate the longitudinal movement of the structure with respect to the footings. Much of the moment applied to bridge piers is due to long-term, time-dependent effects and uniform temperature changes throughout the structure. The piers are designed to crack with increasing moment, relieving much of this moment applied to them.

There are two different methods defined in the AASHTO LRFD Article 3.4.1 for the purpose of accounting for the cracked section properties in fixed pier substructures for bridges. One procedure calls for the simple application of a 0.5 load factor on the thermal loads for the analysis of the lateral loading case of the pier walls while using gross section properties. The 0.5 load factor accounts for the moment relief at the ends of the pier walls due to cracking. The second procedure requires a *refined* analysis to determine the appropriate cracked section stiffness while using a load factor of 1.0 on the thermal loads. There are also two procedures for temperature design, outlined in Articles 3.12.2.1 and 3.12.2.2: Procedure A calls for an 80 °F temperature range, while Procedure B calls for a 150 °F temperature range.

In the state of Minnesota, temperature considerations are of concern in design. It has been shown that the magnitude of thermal stresses can be comparable or even greater than dead and live loads [1]. Because of this, an accurate design method must be developed and verified for both temperature gradients and uniform expansion in bridges.

In order to investigate the effects of temperature variations on concrete bridges, the Wakota Bridge was chosen as the subject of a study to analyze and investigate thermal design methods and specifications. The construction of the Wakota Bridge spurred this study because the time of its construction allowed for convenient installation of a data collection system, and because its use of twin-bladed fixed-flexible piers allowed for an investigation both into the behavior of a pier type whose response to changing temperature was not well-researched as well as into the behavior of bridges in general in the state of Minnesota with respect to temperature.

1.2 Wakota Background Information

MnDOT Bridges 82855 and 82856, together known as the Wakota Bridge, carry the west and eastbound lanes respectively of Interstate highway 494 across the Mississippi River, as well as over the Union Pacific Railroad and Verderosa Avenue. Construction of the Wakota Bridge started in 2002 and was completed in the summer of 2010 [2]. Construction of the westbound structure, Br. 82856 was completed in 2006; Br. 82855 was completed in 2010. The bridge considered in this project was the eastbound bridge, Br. 82855.

The superstructure consists of a post-tensioned double box girder concrete section. It has a total length of 1886 ft and a total width of 85 ft at center. The longest span stretches 471 ft.

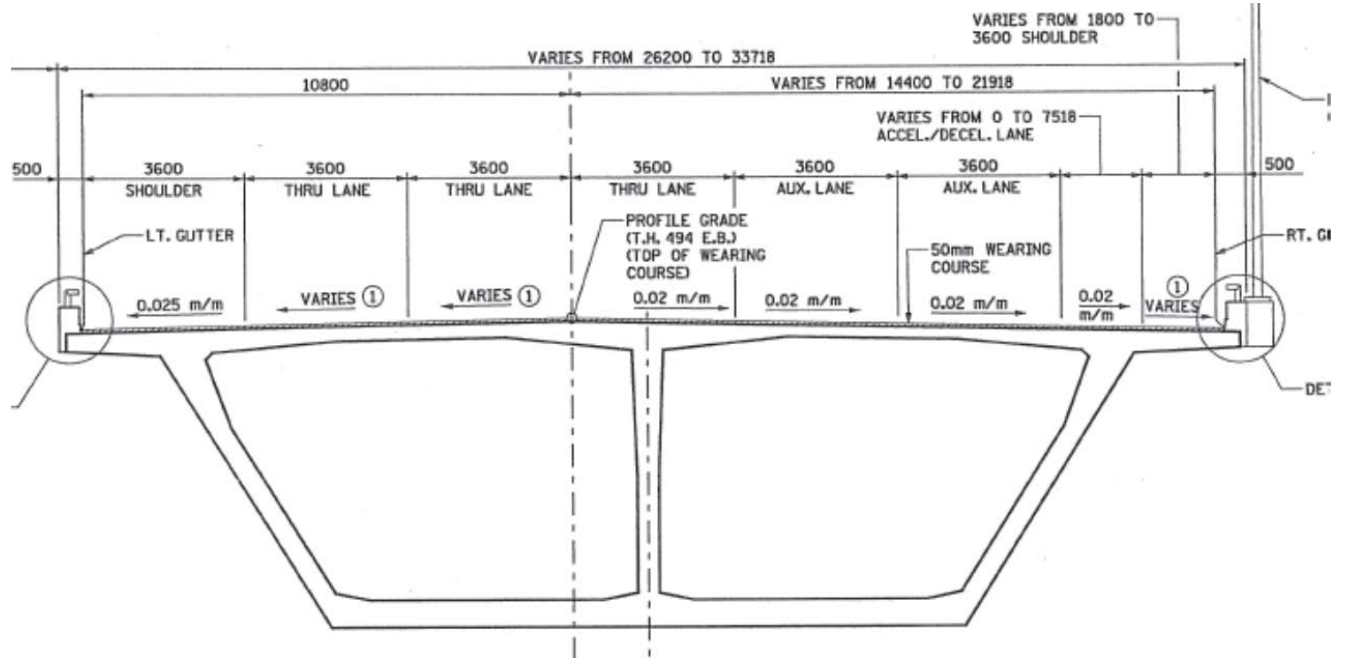


Figure 1.1: Typical cross-section close to piers [6].

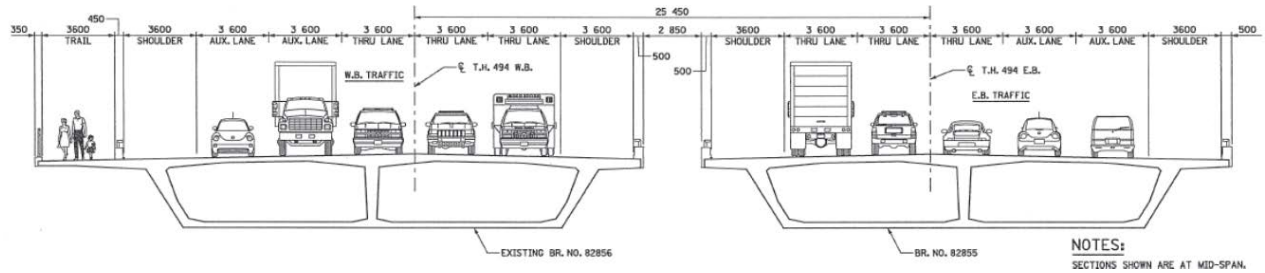


Figure 1.2: Typical cross-section at midspan with traffic layout [6].

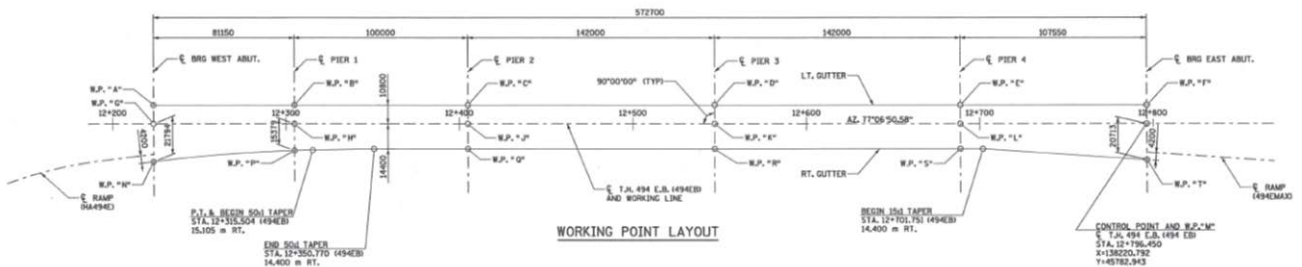


Figure 1.3: Plan view of entire structure [6].



Figure 1.4: Rendering of completed structure [2].

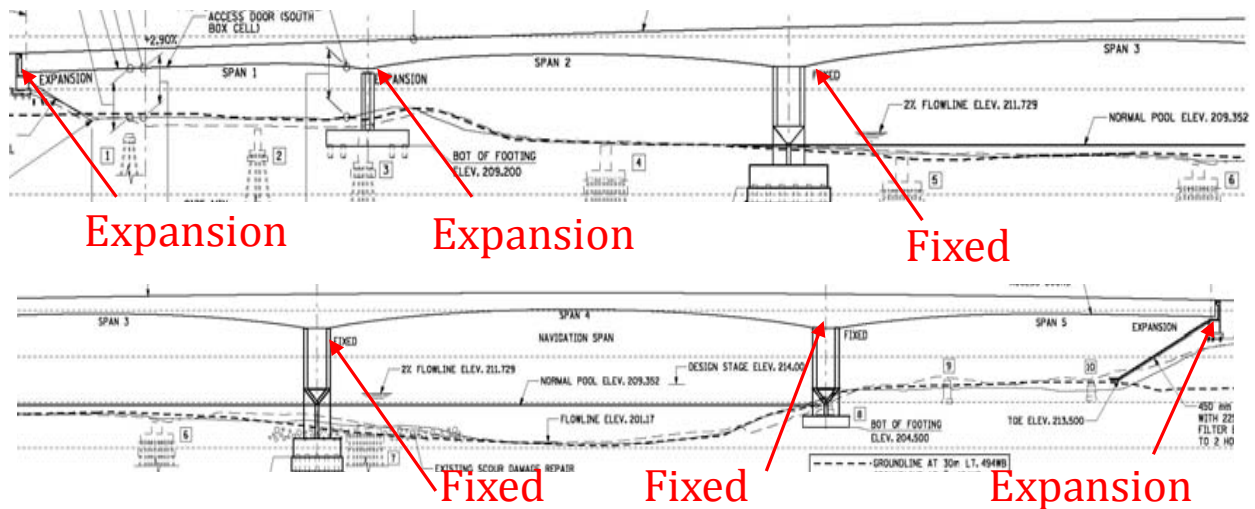


Figure 1.5: Elevation view of Wakota superstructure and substructure properties [3].

The substructure consists of three twin-walled, fixed flexible reinforced concrete piers and one single-walled pier fitted with an expansion bearing to allow translation of the superstructure over the pier. Piers 2, 3, and 4 are fixed as shown above, and Pier 1 has the expansion bearing. The abutments are also fitted with expansion bearings. There is no prestressing in the substructure and all footings except the Pier 4 footing are pile supported, with the Pier 4 footing being a spread footing on rock.



Figure 1.6: Wakota Bridge under construction.



Figure 1.7: Cast in place cantilever construction progress.

1.3 Wakota Monitoring Project Details

The Wakota monitoring project was initially designed to be a two year program funded by MnDOT, although due to construction delays with the contractor, the project had to be extended by approximately 1 year. The premise of the project is that daily and seasonal temperature changes generate fluctuations in the length of the bridge superstructure. Due to bridge support conditions, the length fluctuations generate changes in member forces. Of primary interest were the magnitudes of the changes in pier axial forces, bending moments and shear forces. The pier forces from the field measurements were used, in conjunction with analyses of the bridge, to evaluate AASHTO LRFD procedures for thermal effects.

Although the primary focus of the Wakota monitoring program was investigation of the forces in the twin-blade pier walls, it was also desired to investigate the behavior of the concrete box girder superstructure. With the incorporation of instrumentation in the superstructure as well as the substructure, valuable information was obtained on the forces present in the box-girder due to the restraint forces imposed by the fixed substructure.

The first objective that was considered, and which is the main focus of this report, was the evaluation of the commonly used refined design method to account for cracked section properties and reduction in pier end moments. In order to evaluate the method, two finite element models were developed. The first model to be developed was a research level model, which incorporated fully three-dimensional properties as well as nonlinear concrete behavior accounting for the cracking that occurs in the pier walls. This model was then compared to a design-level model using a common refined design technique for the pier walls used by many designers. It was desired to obtain a degree of confidence in the refined design method based on the nonlinearly behaving research level model. As well as affirming the accuracy of the method, it was desired to determine recommendations for its employment and to recognize convergence tendencies, if any.

As well as the evaluation of the common refined design method, a model was desired for the correlation of field data. Because the instrumentation in the structure was sparse, a model was needed to gain insight on the behavior of the structure as a whole, incorporating all loads on the structure, including time-dependent effects. Using the field data, this model was to be calibrated and used to monitor and predict bridge behavior. However, it was necessary to independently evaluate and compare the two AASHTO LRFD design methods for cracked section properties using the aforementioned model containing time-dependent effects. This model should give accurate prediction of stresses due to the different design methods.

Chapter 2. Instrumentation

2.1 Introduction

In order to investigate thermal forces, an instrumentation plan was developed. This chapter provides an overview of the instrumentation installed in the bridge. The instrumentation described here was used to monitor changing strains in the bridge superstructure as well as the changing strains in the critical elements of the bridge substructure, namely, the double pier walls as the effect of thermal loading takes place. The results obtained from these instruments were analyzed and used to calibrate the finite element model constructed in this study, and to confirm its reliability. Calibration of the finite element models with respect to collected data is reported in Phase II of this report. A complete description of the instrumentation can be found in Appendix A.

2.2 Instruments

Two different types of instruments were used in the instrumentation of the Wakota Bridge, vibrating wire strain gauges and linear string potentiometers, the most prevalent of which was the vibrating wire strain gauge. Vibrating wire strain gauges are effective and accurate when a static change of strain measurement is desired. The particular gauges used in the structure were the Model 4200 concrete embedment gauges from Geokon Inc. Because these were embedment gauges, they had to be placed in the cross-sections prior to pouring concrete during the construction process.

Vibrating wire strain gauges are constructed with a barbell configuration and work by using an excitation wire located in the gauge. The tensioned wire is excited by a controlling peripheral and the frequency is read by the peripheral. A fast Fourier transform is then performed on the frequency signal and the resonant frequency is separated from noise signals that may be polluting the reading, resulting in very low susceptibility to noise effects in the signal. Changes in strain over the gauge length translate to increases or decreases in the wire tension, and these tensile force changes produce proportional changes in the frequency of the vibrating wire. This approach allowed the use of very long lead wires from the gauges to the controlling peripheral without distorting the signal, which was an advantageous attribute because the structure is large and required long lead wires.

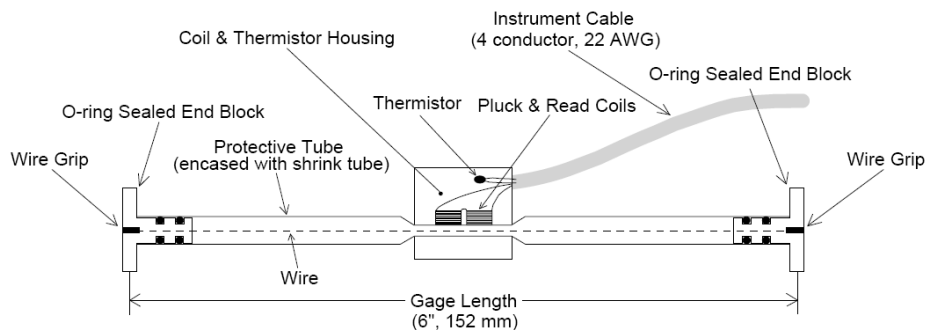


Figure 2.1: Geokon Model 4200 vibrating wire strain gauge [4].

The other type of instrument employed in the monitoring process was the linear string potentiometer. Linear string potentiometers (also called “string pots”) are simple devices that allow displacement measurements with a high degree of accuracy over a relatively long range of measurement. The specific model of string pot used in this application was the HX-P420 manufactured by Unimeasure, Inc. This string pot outputs variable current depending on the extension of the wire from the transducer located in the device core. The current output ranges from 4-20 mA and values depend on the range of the produced potentiometer. A range of 15 inches was selected due to the fact that the expansion bearings at the end abutments of the bridge were designed for a displacement of ~12 inches. The 15-inch range gave some margin for error for the neutral setting at installation. The output of the HX-P420 was correlated to the displacement as a simple ratio of the displacement of the measuring wire to the total range. For example, if the range of the string pot were 15 inches, a reading of 5 mA would have corresponded to a displacement of $\frac{5-4}{20-4} * 15\text{inches} = 0.9375$ inches.



Figure 2.2: HX-P420 linear string potentiometer [5].

2.3 Choosing the Instrument Locations

It was important to choose appropriate locations for instrumentation as limited resources were allocated to this task. A representative description of the overall bridge thermal behavior was desired with few instruments. Because this was the case, two sections in the box girder superstructure and two double-pier walls were selected for instrumentation.

The choice of superstructure sections to be instrumented was intuitive. The behavior to be studied was the stress due to thermal loadings in the superstructure, so sections were selected based on the spans that would see the largest stresses due to thermal loadings. In the case of the Wakota Bridge, it can be seen that the spans of this nature are Spans 3 and 4 (Figure 1.5). Because of the presence of expansion bearings at both the east and west abutments and in Pier 1, the thermal expansion of the superstructure in Spans 1, 2 and 5 is unrestrained and thus, stresses would be minimal when compared to the stresses seen in Spans 3 and 4, which are restrained against longitudinal expansion.

Two cross-sections in the superstructure, one each in Spans 3 and 4, were chosen for instrumentation (Figure 2.3). The superstructure cross-sections were chosen based on two criteria. The first criterion was that the instrumented cross-section needed to be close to a live load inflection point of the structure. This followed from the fact that the thermal loading effects on the structure were the only ones sought. Being close to a live load inflection point minimized the loading effects due to traffic and other variable loads that were not of interest. The live load inflection points had to be close to the piers, if not above them, so the cross-sections chosen were to be away from center-span. The second criterion for choosing the cross-sections was the construction progress. Because the instruments installed were embedment gauges, the installation needed to be correlated with construction progress. The final choices for instrumented cross-sections were Section 2-4U and Section 4-6D.

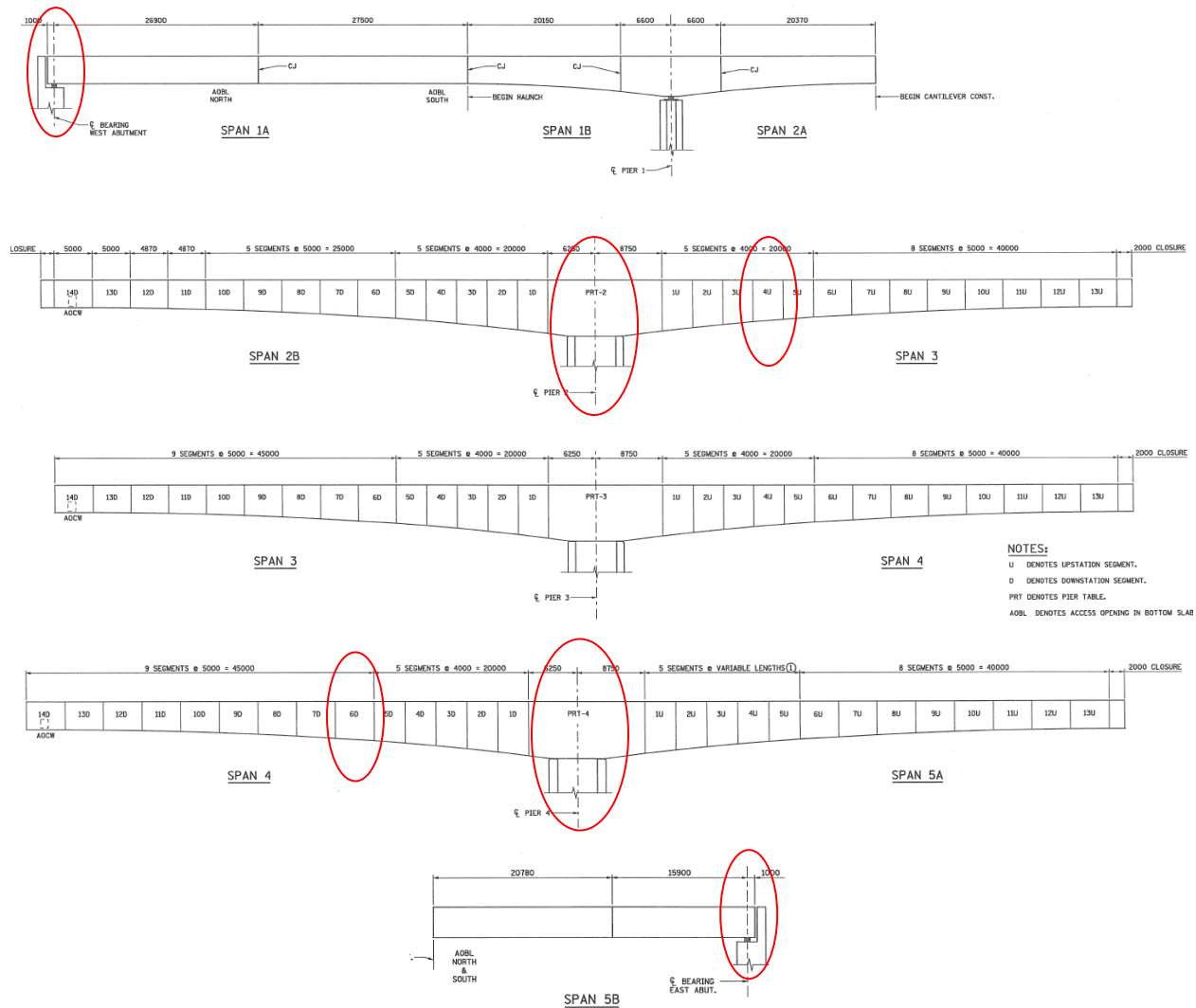


Figure 2.3: Instrumented sections along length of bridge (abutments, Section 2-4U, Section 4-6D, Pier 2, Pier 4).

Choosing the piers to be instrumented was a similar task and the same logic could be applied. Since Piers 2, 3 and 4 are fixed flexible piers, and Pier 3 is exactly equidistant from Piers 2 and 4, Piers 2 and 4 were expected to see the most stress from thermal effects due to the expansion of the superstructure about Pier 3 (Figure 2.3). Therefore, the double pier walls of Piers 2 and 4 were chosen to be instrumented and the focus of this study. Each of the abutments was instrumented with linear string pots to measure overall expansion/contraction of the bridge.

2.4 Placement of Instruments

The instruments were placed in the chosen sections in a manner that would give the most representative description of section behavior. In the span sections, 20 strain gauges were distributed evenly around the cross-sections as shown in Figure 2.4. All gauges were oriented horizontally in order to give longitudinal strain information. In the two selected piers, both pier walls were instrumented at two different elevations, one near the top of the wall and one near the base. This was chosen because the maximum stresses will occur at the ends of the walls: as the bridge expands the piers will deform in double curvature. At each elevation, the strain gauges were paired and distributed across the width of the wall as can be seen in Figure 2.5. In all, 28 vibrating wire strain gauges are installed in Pier 2, and 16 are installed in Pier 4. Pier 2 contains more gauges than were necessary for data collection; these extra gauges were installed to investigate other aspects of the pier response to give a fuller picture of the pier behavior. All gauges were oriented vertically so as to capture bending and axial strains. This configuration captured strain on both sides of the pier walls.

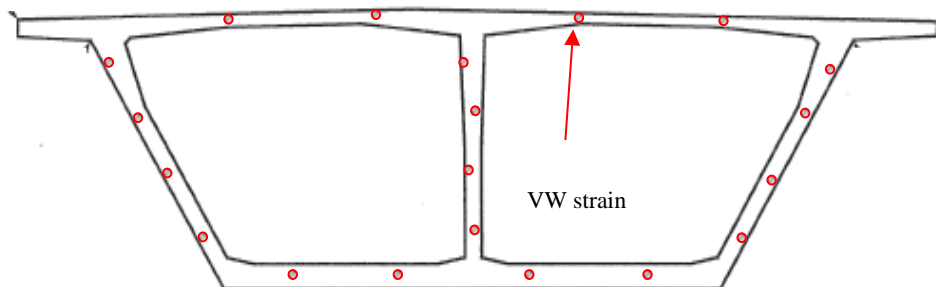
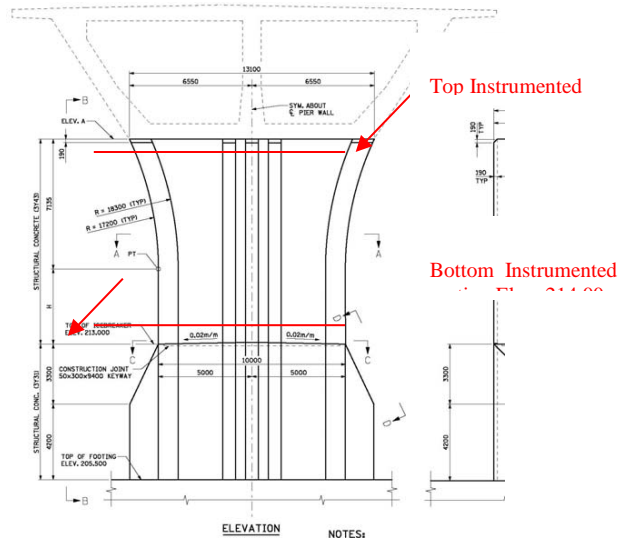


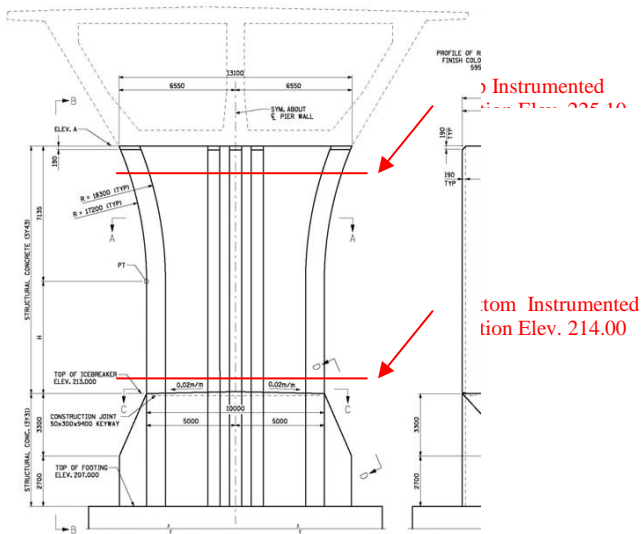
Figure 2.4: Strain gauge distribution in superstructure.

TABLE OF ELEVATIONS AND DIMENSIONS		
	ELEV. A	DIM. H
UPSTATION WALL	224.230	4095
DOWNSTATION WALL	224.100	3965



Pier 2

TABLE OF ELEVATIONS AND DIMENSIONS		
	ELEV. A	DIM. H
UPSTATION WALL	226.080	5945
DOWNSTATION WALL	226.120	5985



Pier 4

Figure 2.5: Pier instrumentation elevations (mm).

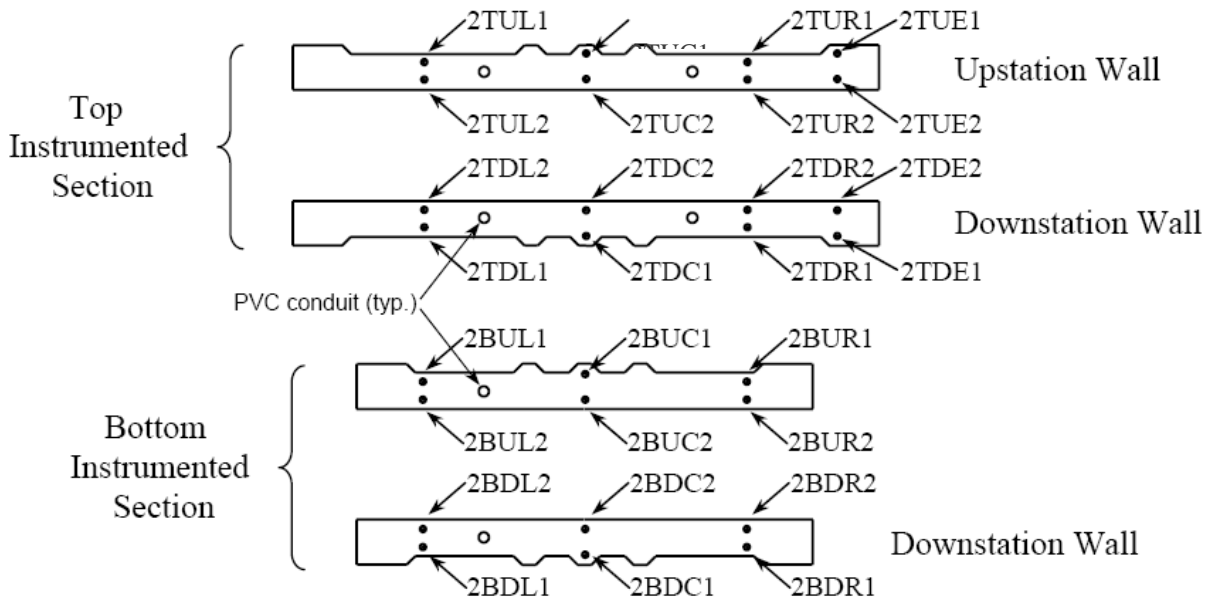


Figure 2.6: Pier 2 strain gauge locations and designations.

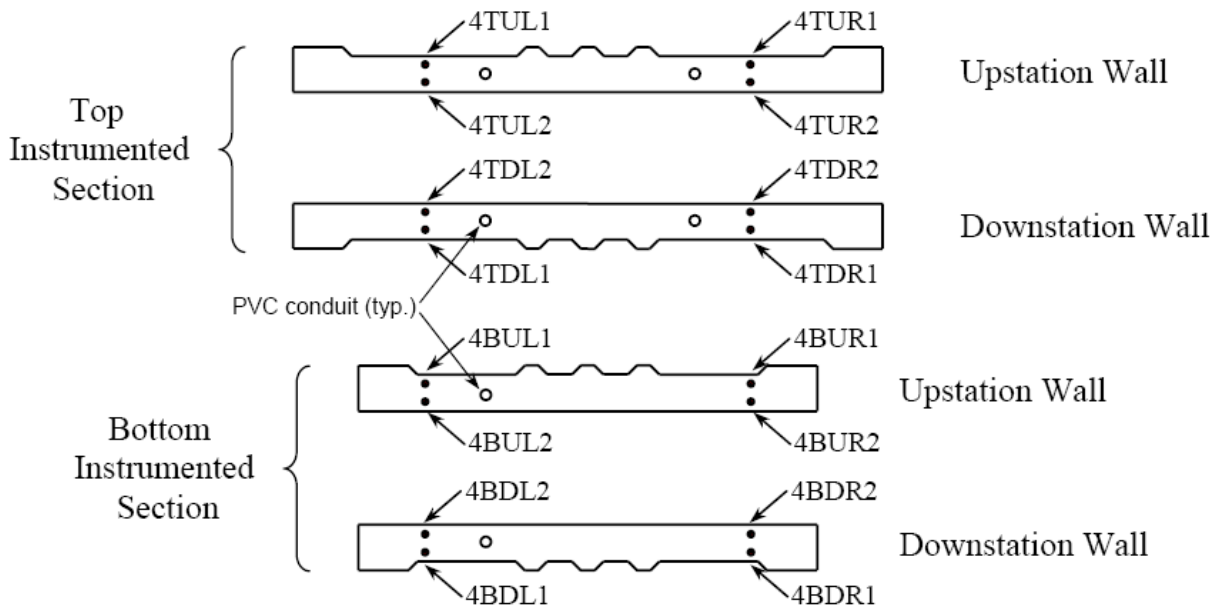


Figure 2.7: Pier 4 strain gauge locations and designations.

2.5 Data Acquisition

A data acquisition system was required to collect and organize the data transmitted by the strain gauges and the linear string potentiometers. To achieve an efficient data collection system and one in which minimal human interaction was required, equipment from Campbell Scientific was

used and a system was designed to monitor all instruments concurrently. The equipment used was as follows:

- CR1000 datalogger (two units)
- AVW200 Vibrating Wire Interface (four units)
- AM16/32B multiplexer (six units)
- Raven XTV cellular modem
- MD485 multidrop interface (three units)
- PS100 power source (two units)
- 12V 7Ahr sealed rechargeable lead-acid battery (two units)

The following are short descriptions of the functions and capabilities of each piece of equipment used.

CR1000

The CR1000 datalogger was the central component of the data acquisition system. This unit collected and stored all incoming information from the sensors distributed in the structure. It did this through the use of an onboard processor and 4 MB hard drive. Using the CR1000, the user could manipulate data on board (in real time) and do simple calculations on the stored data, such as converting frequency to strain using calibration data.

AVW200

The AVW200 vibrating wire interface acted as the controlling device for the vibrating wire strain gauges installed in the structure. It interacted with the strain gauges by exciting the wires inside the strain gauges and then reading the corresponding output frequency. A fast Fourier transform was then performed on the output frequency whereby the noise in the signal was eliminated and the resonant frequency was sent to the datalogger for collection. Up to four AVW200 modules could be connected to one CR1000.

AM16/32B

The AM16/32B multiplexer extended the number of instruments that the AVW200 could read at a time. Sixteen strain gauges could be connected to each AM16/32B. The multiplexer then stepped through each connected instrument consecutively and relayed the signals to the vibrating wire interface and the datalogger. Two AM16/32B multiplexers were connected to each AVW200, allowing up to 32 strain gauges to be read by one AVW200.

Raven XTV

The Raven XTV cellular modem allowed the data from all incoming data to be relayed over a cellular signal via Verizon Wireless' broadband service. This modem communicated over a common telemetry account in which an IP address was assigned. All data was then retrieved from a computer at the University by accessing the IP address for the instrument.

MD485 Multidrop

This device allowed the data from the two datalogger locations to be connected and transmitted to a single location near the Raven modem for cellular transmission. One MD485 was placed at each datalogger site as well as at the location of the Raven modem.

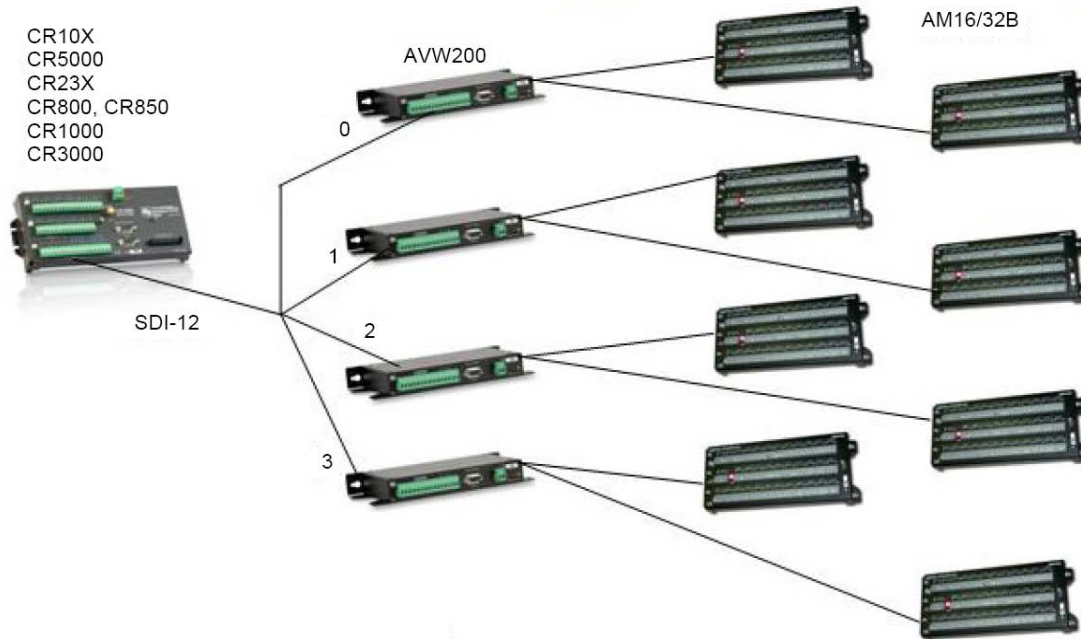


Figure 2.8: Campbell Scientific equipment connection diagram [6].

In the current study, two CR1000's were needed to collect the data from the 84 vibrating wire strain gauges due to the fact that the instrumented sections of the bridge are far apart and excessively long lead wires would be needed to connect all of the strain gauges to one datalogger in a central location. Because of this, two equipment groups were used and function independently as described in the instrumentation description in the appendix.

The expansion information collected by the linear potentiometers at the abutments was also collected by the two CR1000 dataloggers. The lead wire of each string pot was run to the closest CR1000.

2.6 Instrument Calibration and Data Storage

Because the strain gauges transmitted a frequency signal and the incorporated thermistors in each strain gauge transmit resistance, calibration factors needed to be incorporated to attain strain and temperature readings. The calibration factors can be found in the Geokon model 4200 strain gauges manual and incorporated in the Campbell Scientific equipment. Strain is related to frequency by the following relation:

$$\epsilon = G \times freq^2 \quad (1)$$

where $G = 3.304$ for the model 4200 VW strain gauge

Temperature is related to resistance by the following (Calibration constants determined experimentally for the Geokon model 4200) [4]:

$$T = \frac{1}{A+B(\ln(R))+C(\ln(R))^3} - 273.2 \quad (2)$$

where R = output resistance, T = temperature in °C, A = 1.4051 E -3, B = 2.369 E -4, and C = 1.019 E -7.

A program was written and sent to the datalogger to incorporate these calibration factors and thereby store only the desired outputs in a table for analysis. The program was also written to output an average reading for a specified time period. For example, readings could be taken every minute but the datalogger would only store one reading per hour as the average of the sixty readings during that hour.

The calibration pertaining to the linear potentiometers was simple. The output current depended on the position of the measuring cable in the transducer range. The range of the transducer could be set to the desired values within the manufacturing limiting range, which in the case of the purchased HX-P420 string pots, was 15 inches. The datalogger would then be programmed to calculate the linear correlation of current to distance as mentioned earlier and a displacement was calculated.

Chapter 3. Literature Review on Modeling and Design

3.1 Introduction

Before this study could be properly conducted, some background information was needed. A review of current literature was conducted as well as a review of the current procedures used in practice. Among the topics to be reviewed were:

- 1) Common refined design method for bridge piers
- 2) Finite element modeling of reinforced concrete
- 3) Thermal loadings on concrete bridges
- 4) AASHTO LRFD and MnDOT BDM requirements for thermal loadings on bridges

3.2 Common Refined Design Method (CRD Method)

In Section 3.11.1 of the MnDOT BDM, it is stated that the designer of a non-typical bridge with fixed piers must consider the reduced pier stiffness along the height of the pier using a *refined* method. It states,

A 3-D model of the bridge with appropriate elastic restraints at supports may be required (especially for curved bridges) to determine the direction of movement, magnitude of thermal forces, and interaction between piers for determination of the appropriate cracked section reduction in stiffness. The final solution may require several iterations and may be bracketed using an upper-bound and lower-bound stiffness matrix (i.e., - gross sections, partially cracked sections, etc.) so that the final solution falls within an acceptable range for the particular structure. In cases where several piers are fixed to the superstructure, consideration of ambient temperature at anticipated time of construction (including adjustments for closure pours as necessary) should be considered.

The suggested method for doing this task is not specified and it can be a complex task to carry out. The following is a summary of a typical refined method used to determine the percentage of gross stiffness along the height of the piers for use when considering pier design for temperature and lateral deformations.

3.2.1 Deflections Due to Sustained Loads

Although temperature is the most obvious factor contributing to the lateral forces and moments on the pier walls, creep and shrinkage are also important factors when analyzing prestressed concrete bridges and must be taken into account when considering the appropriate reduced stiffness along the height of the pier. Consider a post-tensioned reinforced concrete bridge with two sets of twin wall fixed piers. As the tendons apply a constant force on the bridge superstructure, the concrete will creep and shrink corresponding to that force, causing the piers to bend inward toward the center of the bridge span and therefore lead to cracked section properties even before a temperature loading is applied. Note also that the piers themselves will undergo creep and shrinkage due to the applied dead load of the superstructure and any moments that are

induced due to the construction process and prestressing. This may occur before the temperature loading is applied.

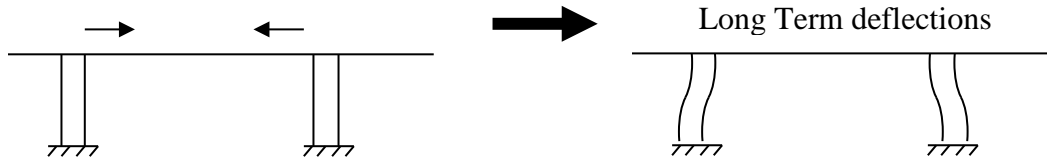


Figure 3.1: Effect of creep and shrinkage on fixed pier system.

This complicates the procedure because the cracked section properties must be analyzed at each moment in time during the staged construction of the piers and superstructure before temperature loadings are applied.

Also to be considered in the cracked section properties of the piers is the initial jacking force applied before the closure pours in each span in a segmentally constructed bridge. This will initially lead to an outward bow of the pier walls and to a curvature reversal when the creep and shrinkage deformations develop. The jacking force to be applied is calculated so as to lead to the maximum reduction in pier moments at the end of service life when all creep and shrinkage has occurred while staying within the required stress limits during service life. Often, the amount of physically applicable force is the limiting factor on the amount of jacking. The jacking force will lead to an outward bow in the piers (Figure 3.2) as mentioned earlier and will thus lead to cracking considerations which will complicate the analysis once again. Because of this, it is recommended that the jacking force not be applied in a fashion that leads to cracking of the piers [7]. This recommendation will simplify the procedure because gross section properties can then be used for the piers when bowed outward at the beginning of service life. Temperature considerations should be assessed at this point in the construction because a positive temperature change will lead to an increased outward bow of the piers and thus may lead to cracked sections unless properly accounted for, although this will rarely be the controlling load case.

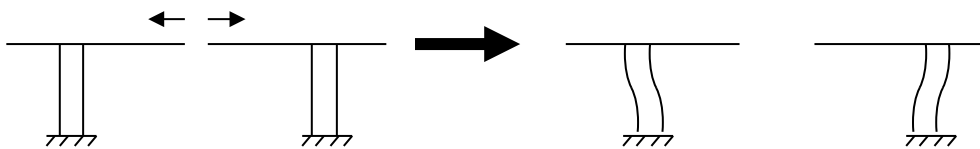


Figure 3.2: Effect of jacking force.

A bridge analysis model must be constructed to utilize the following common refined design (CRD) method. (The model could take the form of a two-dimensional or three-dimensional model. For curved bridges, as stated above, a three-dimensional model is required although a 2D model could be sufficient for straight bridges (3 dimensions must still be considered in the sectional analysis program). The analysis software to be used needs the ability to incorporate staged construction with prestressing and time-dependent analyses (if bridge construction is segmental as was the case for the Wakota Bridge). One such program is SAP2000 [10]. The

model should incorporate all prestressing components present in the bridge design. Many bridges with fixed piers are built using segmental construction, this should also be taken into account, as the age of each segment will play a role in the magnitude of creep and shrinkage inherent in the system. SAP2000 has the ability to account for this parameter using a construction scheduler and incrementing time between each task and loading condition for the calculation of loss parameters in each stage of construction. For example, a segmental balanced cantilever post tensioned bridge is analyzed by adding one segment, applying the post-tensioning and dead loads, calculating the losses and deflections occurring from time of addition to the time of the erection of the next segment, and using the found stress state and deflections as initial conditions for the next segment. This process is iterated until all segments are erected and stressed. All long term deflections occurring after the completion of construction can then be calculated based on the conditions directly after completion of the construction process. The lateral deflections of the piers based on sustained loads can then be used as the basis for additional lateral loads to be applied.

Piers in these types of bridges often have complex geometric characteristics, such as V-shaped piers or piers that change in dimensions along the height. To account for this, an approximate shape with similar sectional properties is often assumed and used for the analysis [8].



Possible assumed analysis cross Section

Figure 3.3: Simplification of pier cross-section.

This analysis is further complicated if the piers are found to be cracked, as they surely will be under even small lateral deflections. To account for the cracked behavior of the piers, there are two options for analysis. The first option is nonlinear analysis with a concrete material model representative of the behavior of concrete. The second option is the CRD method, which is an iterative approach for percentage of gross stiffness used to converge to the correct cracked section stiffness along the height of the pier. This is the most commonly used approach because although the first approach can be the more accurate if done right, it is more difficult to employ nonlinear analysis techniques than linear analysis.

In the CRD method, pier stiffness is estimated using an iterative approach. One procedure is to first discretize each pier into a number of segments at which stiffness is to be updated (each segment could consist of multiple elements in the finite element (FE) model, the number depends on the desired accuracy, but approximately five or more elements has been suggested by a bridge design professional [8]). Each stiffness updating segment in the pier should then be assigned an assumed percentage of gross stiffness. A good starting point for a pier in double curvature is to assume a stiffness of $EI_{Gross}/2.5$ for the elements with maximum moment, those being the ones connected to the superstructure and the footing [8]. This starting point comes from ACI 318-08 section 10.10.6.1 concerning members in compression [9]. The element(s) at mid-height can be assumed to have a stiffness of EI_{Gross} . Once the stiffnesses are assumed for each segment along the height of the piers, a linear analysis is executed for deflection of the structure at a moment in

time. A sectional analysis program such as Response-2000 is then used to compare the sectional response and cracked section to the one assumed in the bridge model. Based on this comparison, the stiffness of the piers in the model can then be refined to match the results of the Response-2000 output and the analysis run again. This process is repeated until the modeled pier stiffness and deflection agree with the stiffness and deflection computed by the sectional analysis program within a reasonable tolerance.

Because of the nonlinear behavior of concrete, a linear analysis cannot be run for the duration of the life of the structure. At each point in time the piers will have a unique percentage of gross stiffness along the height of the pier and therefore a unique analysis needs to be run for the deflections at the instant in question. This is not usually a significant inconvenience because the worst case scenario is usually desired, the worst case will occur after all creep and shrinkage losses have occurred towards the end of the life of the structure and the maximum negative temperature load is applied.

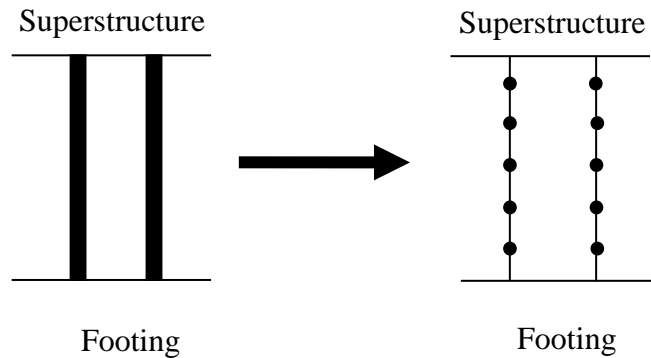


Figure 3.4: Twin-walled pier discretized for analysis.

3.2.2 Application of Thermal Loads

As can be seen in Figure 3.2, the controlling case for lateral loads will occur when the temperature drops and therefore contributes to the shortening of the span between the fixed piers and consequently, the curvature of the piers. An increase in temperature will reduce the stresses on the piers because it acts to counteract the creep and shrinkage deflections.

After the deflections due to sustained loads are calculated, the temperature changes are applied. The applied temperature changes will, like the sustained loads, change the piers' relative stiffness. This can be accounted for in the same manner described above, or some conservative assumptions can be made. When a designer is considering the application of thermal loads, there are two situations to be considered: strength and serviceability. If strength is the consideration, it is seen that the stiffer the piers are, the larger the moments will be at the ends of the piers. Because of this, it is conservative to leave the stiffness of the piers unchanged from the sustained load lateral deflection procedure. This will result in a pier that has a larger stiffness than is realistic and will result in a conservative design. If serviceability is being considered, an excessively large stiffness will lead to underestimated deflections and steel strain values. If conservative deflections are sought, the pier walls can be assumed not to restrain the superstructure movement and simply move with it. This assumption will lead to larger than

actual displacements and steel strains. Although these procedures will produce adequate designs, it may be preferable to use the previously described iterative approach for application of thermal loads as well as sustained loads to reach the most economical and realistic design.

Some modeling programs cannot apply a temperature change as specified in the AASHTO LRFD directly. In order to achieve this effect, the restraint stresses can be computed separately and superimposed on the stress state of the superstructure and piers at the point of interest.

3.2.3 General Modeling Considerations

The finite element model used in the above analysis must take into account all properties of the bridge and encompass all of the following:

- Correct cross-sectional geometry
- Foundation springs – both rotational and translational springs based on realistic footing analysis. Foundations in soil will rotate and translate to provide stress relief in the piers. Appropriate foundation springs can be found by executing a foundation analysis. Reasonable assumptions should be used when dealing with uncertainty in foundation movements.
- Points of connection of piers to superstructure modeled at correct positions
- Superstructure frame elements modeled to provide force output at the section's center of gravity to provide accurate pier moment computations
- Footings can be modeled with rigid link elements because they are excessively stiff compared to the pier walls.

3.3 Finite Element Analysis Review

The design of reinforced concrete bridges is a complex task that readily lends itself to the creation of computer models in order to predict behavior based on design loads and predicted structure-environment interaction. Computer models allow for refinement in design that could not be performed by hand and therefore are invaluable tools that must be used in contemporary engineering practice. Complex mathematical codes have been developed and combined with convenient graphical user interfaces for pre- and post-processing and provide a simple modeling environment for an experienced user. These programs are powerful analysis and design tools *if used correctly*, and if the user is aware of all limitations of the software. If they are not used correctly, or if the user does not fully understand the input necessary or the output results, incorrect analyses will result. To avoid this problem in the current study, a literature review was conducted to ensure proper analysis.

Concrete is a difficult material to model due to its nonlinear response. This problem has been a central focus of research for many years and information regarding advancements and strategies in concrete modeling are readily available [11]. Information is available in the technical literature on improvements of RC modeling to produce accurate models [11].

From the first application of finite element analysis to reinforced concrete by Ngo and Scordelis in 1967 [12], finite element modeling has evolved dramatically. The manner in which cracking of concrete is modeled, the interaction of steel and concrete, and steel yielding considerations

have all become increasingly accurate and complex. The first report on the finite element analysis of concrete submitted to the American Society of Civil Engineers (ASCE) occurred in 1982. At this time it was agreed that finite element analysis of concrete had progressed much faster than the actual understanding of reinforced concrete itself. In order to bridge the gap of understanding, Vecchio and Collins (1982) performed tests on RC members. This allowed finite element models to be correlated to specific experimental data with complex loading histories [11].

The method of concrete modeling must be an iterative process because of the nonlinear behavior and cracking. The most important aspect of modeling concrete structure behavior is the manner in which cracking is taken into account. Many different approaches have been taken in attempt to capture cracking behavior. Early researchers used “smeared” cracking models that reduced the stress across regions that would crack to zero immediately after a predefined limiting tensile stress was reached. This led to numerical instability and was not representative of the actual behavior of concrete. Although the steel in reinforced concrete carries the total tensile load across the cracks, intact concrete still has the ability to carry a small amount of tensile stress and the loss of tensile strength occurs over a narrow range of tensile strain. Many different methods were tried by researchers to capture this concrete cracking behavior. Bashur and Darwin (1978) tried to represent cracking as a continuous process by integrating through the depth of the slab, Hand, Pecknold, and Schnobrich (1973) tried representing it by using layered finite elements and evaluating cracking as a step by step process, Jiang and Mirza (1993) used a layered element and fracture energy principles [13], and many researchers tried representing it using a descending stress branch after cracking. The idea of a descending stress branch eventually dominated the modeling of cracking in concrete [11].

First introduced by Scanlon and Murray (1974), ‘tension stiffening’ as it is referred to, is a descending stress-strain curve that ranges from the cracking stress of the concrete at cracking strain to zero stress at a specified strain after cracking. It refers to the transfer of tensile stress from the concrete near the vicinity of a crack to the steel. This treatment has been widely investigated and has been shown to produce accurate results when compared to experimental test data. It is also beneficial in that it aids in the numerical stability of the solution. It is now the predominantly used cracking model in finite element modeling. Although this method can be reliable, the necessary parameters should be calibrated to the application. The shape of the tension-stiffening curve can change based on material properties and amount of reinforcing steel present in the section. Because of this variability, much research has been performed to determine appropriate values for the tension-stiffening curve for common applications such as steel reinforced concrete beams and columns.

Nayal and Rasheed (2006) report on the different models proposed and attempt to determine an appropriate generalized curve for tension stiffening behavior for common steel reinforced concrete sections [14]. Four models are reviewed: Scanlon-Murray, Lin and Scordelis, Vebo and Ghali, and Gilbert and Warner.

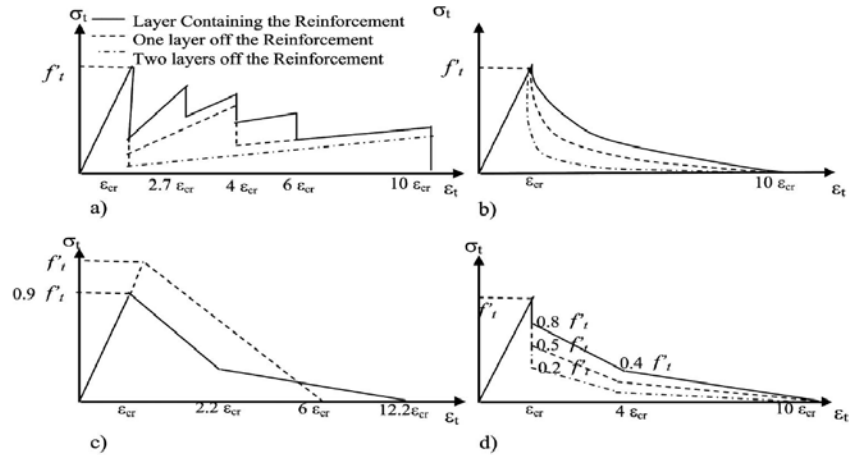


Figure 3.5: Different tension stiffening models: a) Scanlon-Murray model; b) Lin and Scordelis model; c) Vebo and Ghali model; d) Gilbert and Warner model [14].

After these models are summarized, experimental tests performed by previous researchers were compiled and tested against finite element models with varying tension-stiffening curves as a parameter study. A generalized curve was chosen similar to the Gilbert and Warner model and the four variable values on the curve were manipulated.

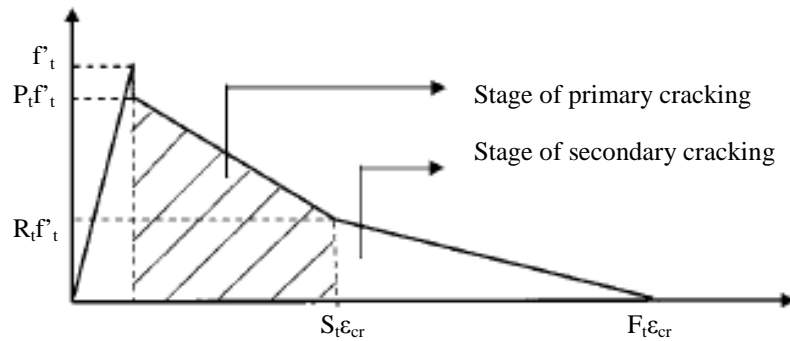


Figure 3.6: Tension stiffening model used in study [14].

A representative set of results on one member is shown below.

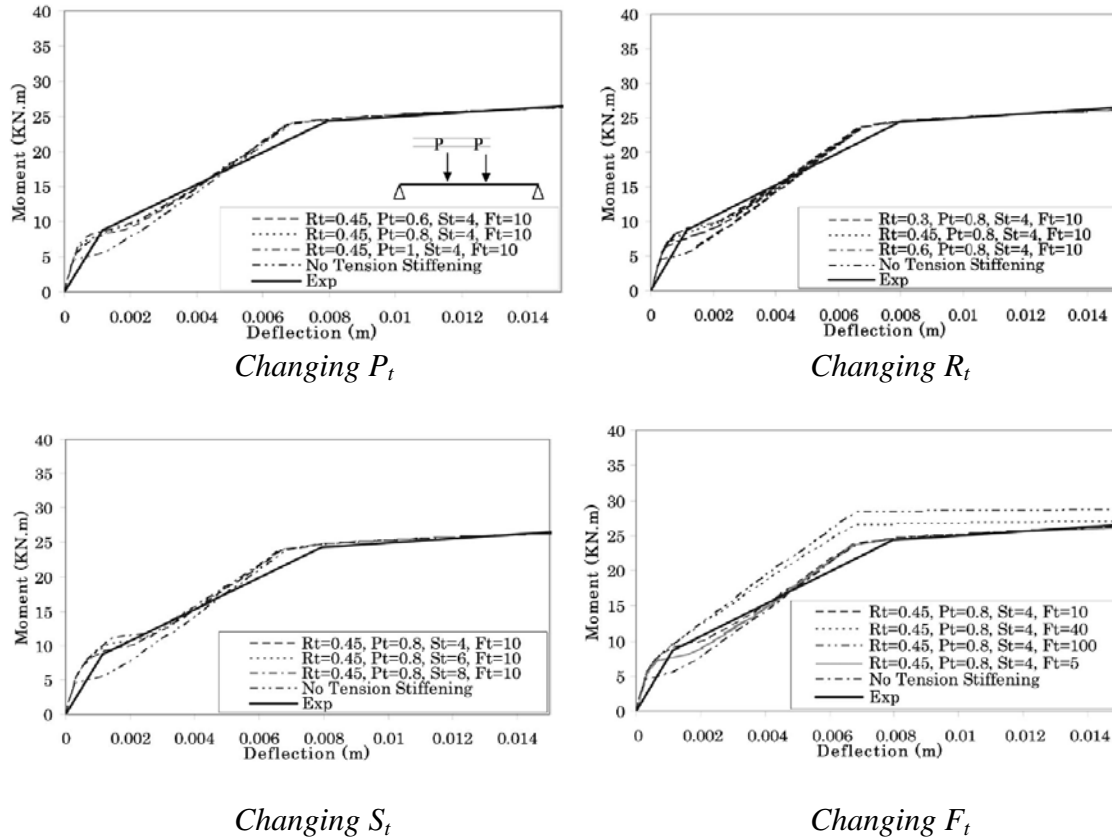


Figure 3.7: Varying tension-stiffening parameters compared to test results [14].

The best set of parameters found to match the experimental data was $S_t=4$, $R_t=0.45$, $P_t=0.8$ and $F_t=10$, where, as can be seen by Figure 3.7:

- S_t is a dimensionless number that, when multiplied by the cracking strain, ϵ_{cr} , produces the strain at the onset of secondary cracking occurs.
- R_t is a dimensionless number that, when multiplied by the tensile strength of concrete, f'_t , produces the stress at the onset of secondary cracking.
- P_t is a dimensionless number that, when multiplied by the tensile strength of concrete, f'_t , produces the stress just after the first crack occurs.
- F_t is a dimensionless number that, when multiplied by the cracking strain, ϵ_{cr} , produces the strain when stress reduces to zero.

This data was shown to be accurate for test data ranging from many different researchers with varying beam sizes. Among the parameters, F_t can be seen to be the most important in the response of the RC members. Stramandinoli and Rovere (2007) employ a similar value of strain at zero stress (F_t) in their tension-stiffening model and likewise get good experimental agreement [15]. ABAQUS, a commercial finite element code, also recommends this value in its user analysis manual [16].

Tension stiffening inherently incorporates some bond characteristics in its cracking representation because of the empirical derivation of the curve. Although this is the case, the question of bonding should be considered. Most finite element models assume a perfect bond between steel and concrete although it is well known that some bar slip does occur in experiments. A perfect bond relationship is often considered adequate, however, because test results show that the load-deflection response of reinforced concrete members is often insensitive to bond-slip [11]. Isenburg [11] states, “The small amount of slip occurring in most reinforced concrete members has little effect on the load-deflection behavior, and a model which disregards that local slip will not cause in a significant error in the predicted load-deflection, unless the failure mode is a bond failure”.

Reinforcement properties must be considered next. The constitutive model of reinforcing material has been paid little attention to compared to that of the concrete, possibly because steel has a very simple behavior and can be generalized as elastically-perfectly plastic or elastic with strain hardening. In a survey of papers performed by the ASCE [11] most researchers specified reinforcing steel as elastically perfectly plastic and as a uniaxial material, therefore ignoring dowel action of the rebar. This has led to models of acceptable accuracy and is therefore recommended. There are three techniques that can be used to represent the reinforcement in the concrete.

- 1) The steel is represented as ‘smeared’ steel in which the constitutive matrix is simply added to the constitutive matrix of the concrete.
- 2) The steel is represented as a discrete element. This leads to a restriction on the mesh because the concrete mesh is forced to have nodes at reinforcement locations.
- 3) The steel is represented as an embedded element in which reinforcing node displacements are forced to coincide with concrete element node displacements. The difficulty with this method is that a special finite element formulation is needed that some codes do not possess.

The shear modulus of elasticity of concrete is another consideration in RC modeling. Introduction of the shear modulus increases numerical stability and realism of cracking behavior. In order to introduce this factor into cracking behavior, researchers have suggested a shear reduction factor after cracking representing aggregate interlock. Although this parameter is important, researchers report little sensitivity with values of the reduction factor between 0.1 and 0.5 [11].

Although tension and cracking dominate structural behavior of RC structures, compression should still be considered. The compressive behavior of concrete in analysis is almost always modeled non-linearly and this has been shown to produce accurate results.

Other considerations must be taken into account in modeling including, but not limited to, mesh shape and size, load step, and higher order elements. Mesh shape is recommended to be based on brick elements if building a solid model as these converge quickly compared to other elements. Higher order brick elements can also be useful in achieving convergence with a small number of elements although they may lead to numerical instabilities. Mesh sensitivity studies are usually needed to determine the appropriate mesh size. Also to be considered is the load

step size. A load step that is too large can produce inaccurate results. And most importantly, good judgment must be used when building a finite element model.

3.4 Thermal Loadings on Concrete Bridges

Much research has been conducted to determine the effect of temperature on the response of bridges. This focus on temperature loadings on bridges is well justified, as the stresses produced by temperature changes has been shown to be comparable or larger than that of live loads [1]. Of primary interest in much of the obtained research is the amplitude of the thermal gradient caused mainly by solar radiation on the top of the bridge deck. This gradient produces a stress state in the bridge superstructure, which is also felt by the piers if they are integral with the superstructure, as is the case with the twin-wall piers in the Wakota Bridge. Also investigated is the magnitude of uniform temperature change throughout concrete bridges corresponding to the climate in which the bridge is immersed.

Many researchers have investigated the values and shape of the gradient curve and the stresses they produce in the structure. These attempts include thermal analysis attempts and field observations. Saetta et al. (1995) proposed a numerical finite element analysis to determine values of thermal loading at different points in a box girder [17]. Branco and Mendes (1993) used a numerical method employing the Fourier heat transform equation to solve for the temperature gradient in a cross-section [18]. Researchers using field observations for temperature gradients include Shushkewich (1998) who used a large number of thermocouples to obtain temperature data throughout the cross-section of a typical precast prestressed concrete box girder, and which agree favorably with AASHTO LRFD recommendations for critical temperature gradient [19]. Possibly the most cited and proven research concerning temperature gradient though, is by Priestley [20]. The following is a short summary of Priestley [20], which was used in the current study.

Predicting temperature distribution throughout a typical concrete box section was the first objective of Priestley's study. First, heat conduction equations were considered through the depth of the cross-section and solved using one dimensional finite difference methods and compared with two and three dimensional finite element solutions.

Stresses were then found from the temperature distribution using simple statics methods. Expressions for the restraint stress, axial force, and internal moment were derived for simple and continuous spans. Experimental and theoretical solutions were compared and shown to be in close alignment for both deflection and stress.

A design thermal gradient was then established for concrete bridges. The critical design gradient is defined as the thermal gradient likely to occur in the lifespan of the bridge. This definition was used in a parameter study of the various influences on temperature gradient in the structure: wind, ambient temperature variation, blacktop thickness, and surface solar absorptivity. The parameter study was conducted on seven typical prestressed concrete bridge sections including slabs, box girders, and beam and slab sections. An analysis of the bridge sections led to a universal design temperature gradient. The design temperature gradient consists of two parts. The first is a fifth order curve ranging from 0 °F at a depth of 47.2 inches below the deck of the bridge to a maximum temperature value T at the deck, which depends on the blacktop thickness.

The second part is a linear increase in temperature over the bottom 7.9 inches of the section. This design gradient is currently in use for concrete bridges in New Zealand and has proven very accurate based on numerous in-field tests to determine temperature gradient.

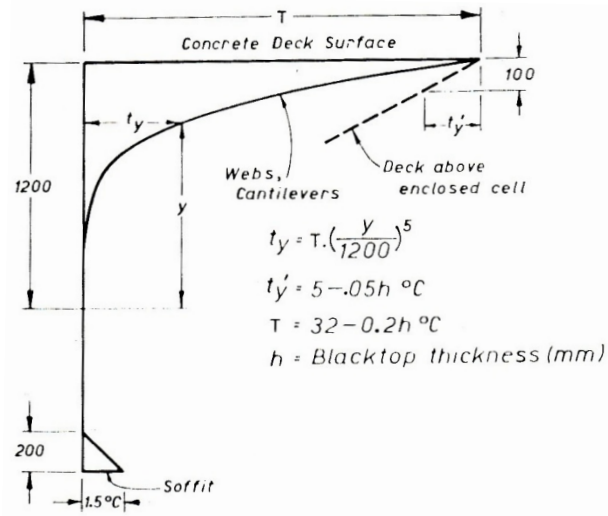


Figure 3.8: Priestley’s thermal design gradient [20].

The significance of the thermal response is then discussed; both at serviceability and at ultimate. It is mentioned that for normal reinforced concrete bridges, cracking will have occurred with the applied dead and live loads, therefore greatly reducing the continuity moments and the chance that thermal loadings will cause fatigue problems. This argument is also applied to certain cases of prestressed concrete bridges. The response for ultimate loadings is discussed next and it is contended that thermal loadings have a small effect on ultimate behavior and are therefore mostly a serviceability concern when designing bridges. Priestley states, “A further consequence of the loading is that thermal effects are generally insignificant when assessing the ultimate load characteristics of a concrete bridge, and need only be considered during serviceability checks.”

It is proposed in the conclusions that partial prestressing to reduce thermal stresses and control cracking seems attractive but more research needs to be conducted to establish reasonable design specifications for this method.

This study provides valuable temperature distribution information. Other papers cite and accept this temperature gradient to be reliable and accurate for application on different types of concrete bridges.

Although temperature gradients are important to take into account in the design of bridges, uniform temperature changes are more important in the design of the pier structure. The most powerful research conducted as to the change in concrete bridge ambient temperature was conducted by Roeder in 2002 [21]. In his study, Roeder created contour maps of the United States based on the extreme temperature data of 1273 different locations in the United States with a minimum history of 60 years of continuous temperature data. His temperature maps are now adopted as an optional procedure in the AASHTO LRFD and are used to determine design

temperatures based on location, which leads to the next topic of discussion; current design specifications for thermal loadings as prescribed by AASHTO LRFD and the MnDOT BDM.

3.5 AASHTO LRFD and MnDOT BDM Requirements for Thermal Loadings on Bridges

The design of bridges for thermal forces and moments is an important aspect of bridge design. Described below is a quick overview of the design requirements that were generated as a product of the research that has been conducted on reinforced concrete box girder bridges such as the Wakota Bridge as well as general design requirements that are applicable to all types of bridges. Both AASHTO LRFD requirements [22] and Minnesota state requirements [23] are considered here.

The design of concrete bridge superstructures for thermal loadings is fairly well researched and documented. While the superstructure forces are not the main concern in this study, they need to be reviewed because the forces produced by superstructure movements are the main contributor to the forces in the twin-wall flexible bridge piers. AASHTO LRFD outlines their design guidelines in “Thermal Effects in Concrete Bridge Superstructures [24]” as well as in the more current “AASHTO LRFD Bridge Design Specifications [22]”, whereas the MnDOT BDM has its own set of guidelines.

All bridges must be designed to accommodate the stresses and movements resulting from both the design uniform temperature change and the design temperature gradient that is produced largely from solar radiation on the deck of the bridge.

3.5.1 Uniform Temperature

There are two different procedures specified in the AASHTO LRFD [22]: Procedure A is outlined in Article 3.12.2.1 and Procedure B is outlined in 3.12.2.2.

Procedure A: Article 3.12.2.1

This is the classically used procedure and is also the less conservative of the two in the state of Minnesota. Procedure A uses the temperature range shown in Table 3.5.1.1 below, where a moderate climate is defined as a climate where the number of days with an average temperature below 32 °F is less than 14 [22].

Table 3.1: Procedure A temperature ranges [22].

Climate	Steel or Aluminum	Concrete	Wood
Moderate	0-120°F	10-80°F	10-75°F
Cold	-30-120°F	0-80°F	0-75°F

Procedure B: Article 3.12.2.2

This is a relatively new procedure that is a result of research done in 2002 by Roeder [21]. The temperature range in this procedure is determined by contour temperature maps of the United

States. One map shows the maximum design temperature and another shows the minimum design temperature. The designer obtains the design temperature range as the difference of the maximum and minimum temperatures at the desired location in the United States. There are two sets of maps: one for concrete bridges and one for steel bridges.

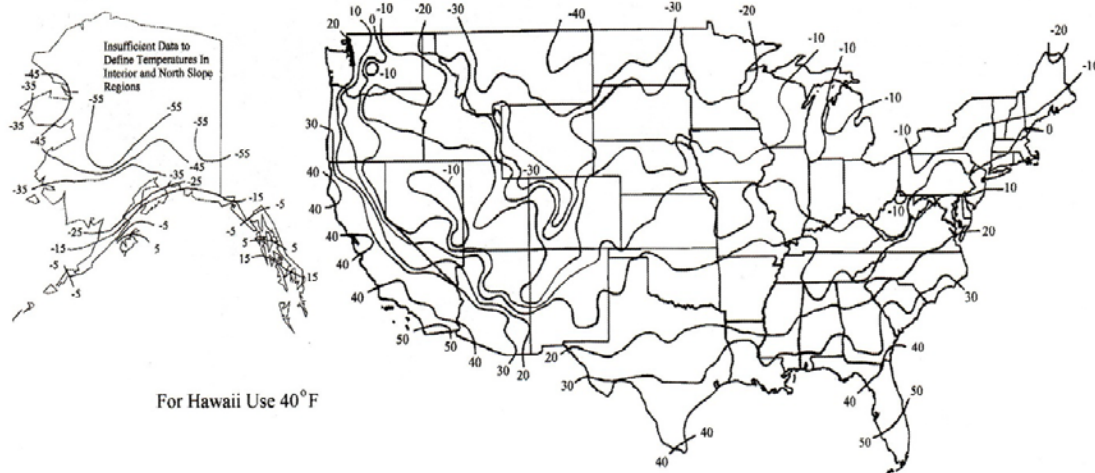


Figure 3.9: Minimum design temperatures for concrete girder bridges with concrete decks [22].

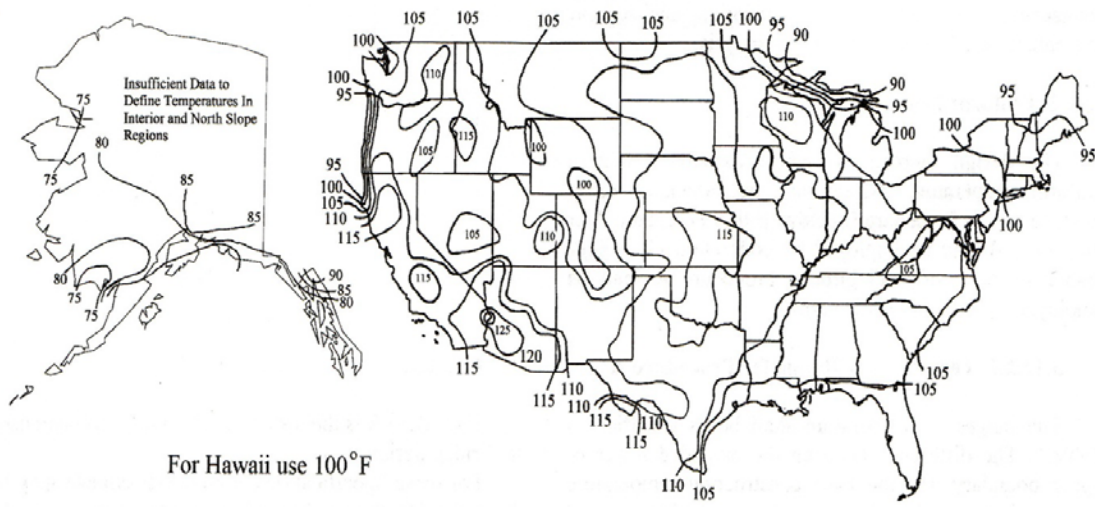


Figure 3.10: Maximum design temperatures for concrete girder bridges with concrete decks [22].

Thermal Movements

The thermal movements to be designed for are based on the temperature range and the coefficient of thermal expansion.

$$\Delta_T = \alpha L(\Delta T),$$

where Δ_T is the thermal design movement, α is the CTE (coefficient of thermal expansion), and ΔT is the temperature range.

MnDOT BDM Requirements: Article 3.11.1

Although either method is acceptable according to AASHTO LRFD, the MnDOT BDM requires that Procedure B be used for non-typical bridges, whereas Procedure A can be used for the internal pier frame forces in typical bridges [23]. A typical bridge is defined as one that generally includes:

- Routine multiple span prestressed beam, steel beam, and slab bridges
- Bridges with two or less fixed piers
- Bridges with piers less than 20 ft tall

Procedure A allows for a temperature range of 80 °F in Minnesota according to AASHTO LRFD Article 3.12.2. Designers are recommended to use a base temperature of 45 °F and apply a 45 °F temperature fall and a 35 °F temperature rise. Also, for flexible pier considerations, a strength limit state load factor of 0.5 can be applied to the thermal loads to account for the reduction of stiffness in the piers due to cracking in the concrete while using gross section properties. For longitudinal effects, MnDOT BDM requires Procedure B to be used [23]. The MnDOT BDM interprets the maps in Procedure B to display a temperature range of 150 °F; designers are recommended to use a base temperature of 45 °F and apply a 75 °F temperature fall and a 75 °F temperature rise. A strength limit state load factor of 0.5 can still be used with gross section properties in lieu of a refined method for typical bridges [23].

For non-typical bridges, designers are required by MnDOT BDM to use Procedure B for Minnesota. When analyzing non-typical bridges, the following factors must be considered [23]:

- Pier Stiffness – Use refined method to determine the appropriate percentage of gross stiffness along the height of the pier
- Bearing fixity and flexibility – Account for the stiffness of expansion bearings in determination of the overall bridge movements.
- Construction method, staging, temperature range at erection, and its effect on the connectivity of the structural system.
- Foundation stiffness – Elastic shortening of the piles provides a significant relaxation to forces applied to the pier. Also, horizontal displacements of piling will provide moment reduction.
- For joint and bearing sizing, use a 150 °F range at Service Limit State conditions. Use a thermal movement load factor of 1.2. Also use this movement to determine horizontal force requirements for guided bearings.
- For Strength Limit State, use a thermal load factor of 1.0 with the 150 °F range for longitudinal force effects. For transverse effects within individual pier frames, an 80 °F range with a 45 °F base construction temperature may be used. A 3-D model of the bridge with appropriate elastic restraints at supports may be required (especially for curved bridges) to determine the direction of movement, magnitude of thermal forces,

and interaction between piers for determination of the appropriate cracked section reduction in stiffness. The final solution may require several iterations and may be bracketed using an upper-bound and lower-bound stiffness matrix (i.e. gross sections, partially cracked sections, etc.) so that the final solution falls within an acceptable range for the particular structure. In cases where several piers are fixed to the superstructure, consideration of ambient temperature at anticipated time of construction (including adjustments for closure pours as necessary) should be considered. Setting of bearings and joints within the structure may require special provisions that call for contractor submittals which state the intended method of bearing and joint installation to obtain a neutral position at the mean temperature.

3.5.2 Temperature Gradient

All bridges must be designed to withstand the design temperature gradient caused mainly by solar radiation [22]. AASHTO LRFD Article 3.12.3 outlines the requirements for design for thermal gradient. The design temperature gradient is based on a topographical map in which the United States is divided into 4 solar radiation zones. A temperature distribution is specified for each radiation zone based on a simplified piecewise linear distribution. A negative temperature gradient due to rapid cooling of the structure is also to be accounted for. The values for the negative gradient are the positive gradient values multiplied by a factor of -0.3 for plain concrete decks and -0.2 for concrete decks with an asphalt overlay [22].

Zone	T_1 (°F)	T_2 (°F)
1	54	14
2	46	12
3	41	11
4	38	9

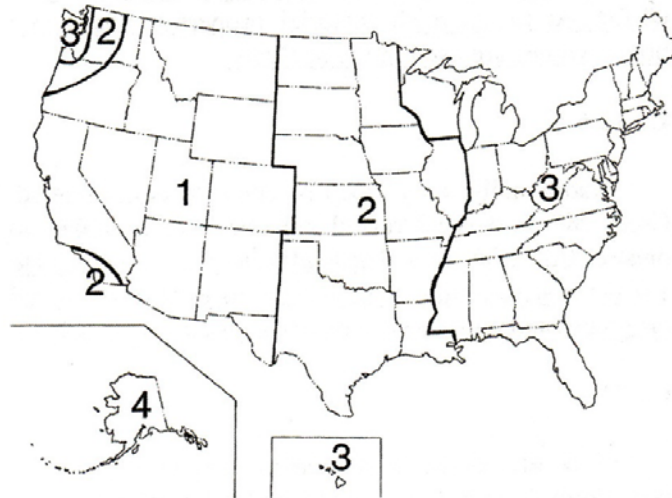


Figure 3.11: Solar radiation zones for the U.S.A [25a].

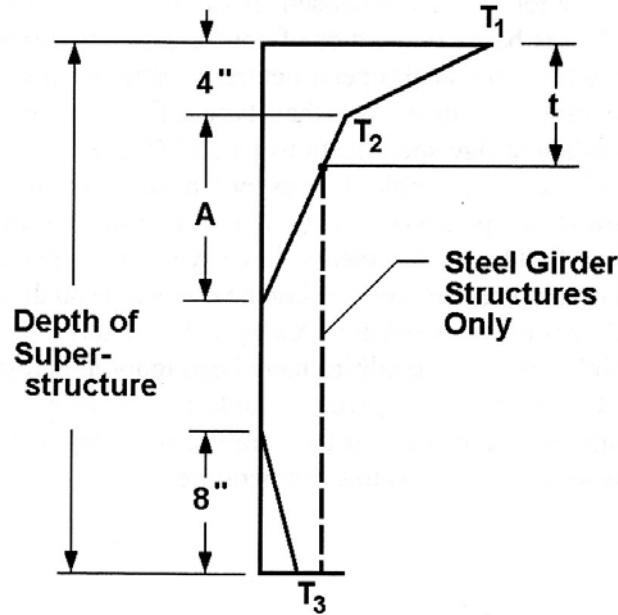


Figure 3.12: Design thermal gradient [25a].

Dimension A in Figure 3.12 is taken as 12 inches for concrete superstructures that are 16 inches or more in depth, 4 inches less than the actual depth of the section for concrete sections shallower than 16 inches, and 12 inches for steel superstructures. Temperature T_3 is taken as 0 °F unless data from the site shows otherwise, but it shall not exceed 5 °F.

AASHTO LRFD specifies “Where determination of force effects due to vertical temperature gradient is required, the analysis should consider axial extension, flexural deformation, and internal stresses” [22]. AASHTO LRFD provides guidelines in Article 3.12.3 in order to analyze all of these effects.

- Axial Expansion due to uniform component of gradient and axial end force

$$T_{ug} = \frac{1}{A_c} \int \int T_G dw dz \quad (3)$$

$$\epsilon_u = \alpha(T_{ug} + T_u) \quad (4)$$

$$N = EA_c \epsilon_u \quad (5)$$

- Flexural Deformation and fixed end moment effects

$$\phi = \frac{\alpha}{I_c} \int \int T_G z dw dz = \frac{1}{R} \quad (6)$$

$$M = EI_c \phi \quad (7)$$

- Internal Stress

$$\sigma_E = E[\alpha T_G - \alpha T_{ug} - \phi z] \quad (8)$$

where:

ϵ_u = strain due to uniform temperature

ϕ = curvature

N = Axial Force
 T_G = temperature gradient (Δ °F)
 T_{ug} = temperature averaged across the cross-section (°F)
 T_u = uniform specified temperature (°F)
 A_c = cross-section area – transformed for steel beams (in.²)
 I_c = inertia of cross-section – transformed for steel beams (in.⁴)
 α = coefficient of thermal expansion (in./in./ °F)
 E = modulus of elasticity (ksi)
 R = radius of curvature (ft.)
 w = width of element in cross-section (in.)
 z = vertical distance from center of gravity of cross-section (in.)

Design examples are provided in “AASHTO Guide Specifications: Thermal Effects in Concrete Bridge Superstructures” [24].

Now that a sufficient background has been presented on the relevant topics, the study at hand can be detailed and explained.

Chapter 4. Research Level Modeling (ABAQUS)

4.1 Introduction

In order to be able to analyze and evaluate the CRD method as it pertains to the Wakota Bridge structure, a research-level analysis model is needed. This model will be used to compare to a common design-level model utilizing the previously reviewed CRD. In order to compare the two types of models, a well-planned research level model was needed. The modeling considerations are discussed in the following sections.

4.2 Modeling Assumptions

The structure of the Wakota Bridge is quite complex. It has many members with variable dimensions including the overall width, depth, web, and slab thicknesses of the superstructure. Along with the variable geometric parameters, the structure of the Wakota Bridge employs pile-driven footings, fixed flexible piers, post-tensioning, and 5 superstructure spans. All of these complexities provide for a challenging modeling process that requires significant consideration and some simplification. It is desirable to eliminate features of the structure that will play little or no role in the behavior of the structure. Using a degree of judgment, many aspects of the Wakota Bridge were eliminated from the modeling process. A brief description and reasoning for the eliminated aspects follows.

I. *Profile Elevation*

It was chosen to exclude the incorporation of the profile elevation in the three dimensional model. The reasoning behind this is that the bridge has a relatively small slope along the length of the structure and this slope will have minimal effects on stresses due to thermal effects in the structure because thermal loadings will act mainly in the longitudinal direction of the superstructure. This longitudinal expansion/contraction will be affected very little by a small slope in the structure. This simplification allows for a much easier application of thermal gradient loadings because the gradient is dependent on deck elevation.

II. *Pier Flanges*

The architectural flanges on the pier walls perpendicular to the longitudinal direction of the bridge (as can be seen in Figure 2.6 and 2.7) were left out of the analysis model because they complicate the nonlinear analysis due to odd shaped elements and based on the assumption that they will play a negligible role in overall pier behavior.

III. *Traffic Railing*

While the concrete base is included in the analysis model, the attached steel railing is ignored because it is assumed to provide essentially no stiffness contribution to the structure when compared with the stiffness of the concrete superstructure.

IV. *Abutments*

Abutments are not modeled because they are attached to the superstructure via expansion bearings (Figure 1.5) and will therefore not affect the behavior of the main

bridge structure. The abutments are replaced with idealized support conditions at the end of the superstructure.

V. *Diaphragm Openings*

The openings in the diaphragms on the interior of the superstructure were ignored. These elements are assumed to have no impact on the behavior of the structure because of their small dimension relative to superstructure dimensions. They are used only for accessibility to the interior of the bridge.

4.3 Creating the Three Dimensional Model Geometry

The geometry of the double box girder cross-sections was also simplified. Small fillets were removed from the geometry of the interior of the box girder. These fillets were small with respect to the rest of the cross-section. In order to compensate for the small area change in the cross-section due to this simplification, connecting lines were extended over the fillet area in a way that would produce a similar cross-sectional area and still simplify the geometry. This simplification is necessary because the ability to produce a quality mesh without extreme computational cost is undermined by the existence of small edges. Also, the concrete railing base located on the flanges of the superstructure was idealized as a rectangle and the overhanging portion was modeled as being level with the bottom of the box girder flange (see Figure 4.1).

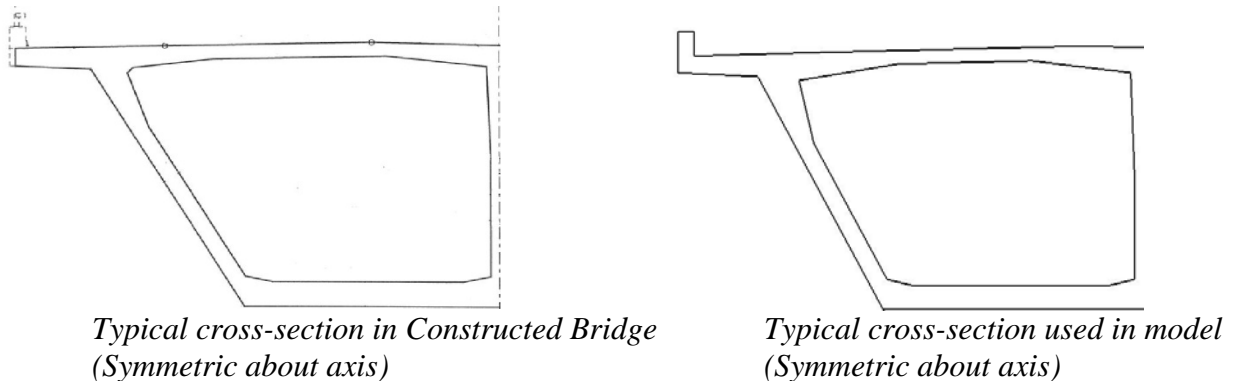


Figure 4.1: Superstructure cross-sections.

The geometry was defined using a common CAD program [25]. This was done by creating cross-sections as shown in the bridge plans at various locations (along bridge length). A total of 136 separate planar sketches were created, one of which is represented in Figure 4.1, to construct the superstructure with dimensions as specified by the bridge plans [3]. Volumes were then created to connect the separate sketches to create the superstructure. Each pier was created as a separate part in the program to be combined in the finite element program of choice. Piers 2, 3, and 4 were created as shown in the bridge plans without the architectural flanges. Pier 1 was simplified by replacing the specified pedestal and expansion mechanism combination with a single block element that was assigned connection properties in the finite element program. This will not affect the study because pier 1 is not of concern in this study. The pier could be modeled simply with boundary conditions, but for completeness it is included. The complete, assembled geometric model is shown below (Figure 4.2).

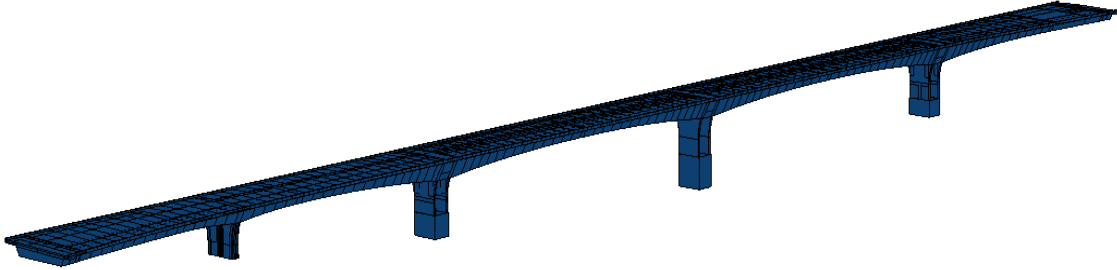


Figure 4.2: Assembled geometric 3D analysis model.

4.4 Importing

In order to be useful, this model must be imported into an advanced finite element program for analysis. Although importing a model seems as though it would be a trivial task, it proved to be labor intensive. The F.E. program chosen to carry out the analysis for the model was ABAQUS. ABAQUS has many desirable qualities that prompted its choice, including a very user friendly user interface, a large variety of meshing capabilities, and perhaps most importantly, the ability to model concrete cracking through either the concrete smeared cracking material model or the damage-plasticity model.

The geometric model was first exported from the CAD program as a STEP file (a common file format), as this is the only mutually compatible format for both ABAQUS and the CAD program in use. One convenient function inherent in the CAD program is the ability to export only the visible portion of the model. This allowed small portions of the model to be exported and imported into ABAQUS at a time. This was desirable because every portion of the model that was imported needed to be verified and possibly corrected. Upon import, ABAQUS often altered the geometry and these alterations needed fixing. This quality is well noted by the developers of ABAQUS and many features are available to troubleshoot imported parts that have problems associated with them. Perhaps the most useful of these features is the “combine edges” tool. Upon import, ABAQUS, in many cases, divided single line segments and edges into multiple line segments and edges. While this was not apparent immediately when looking at the imported part, it complicated further processes in the program and thus all divided lines needed to be replaced by the original line segment. The “combine edges” tool, in most cases, accomplished this task very easily. In the event that this ABAQUS tool did not solve the problem, it was a more difficult process to fix. In order to fix this problem, a small dimension change to the corresponding line was needed in the CAD program from which the STEP file was exported. The change in all cases was small (< 1 mm). This import error most likely occurred because of numerical rounding after being converted from metric to English units.

The general nature of ABAQUS is to separate the imported geometry into many separate ‘parts’ corresponding to the volume objects created in the CAD program. Because of this, the superstructure initially contained 131 separate ‘parts’. This was not desirable because each part needed to be meshed separately. Having 131 ‘parts’ to be meshed would create more labor than was necessary and would require constraints to tie each ‘part’ together, which would require excess computing cost. To reduce this problem, all parts with continuous geometry were merged into one larger model ‘part’, where “continuous” in this case means that there were no drastic

cross-section changes such as a span connected to a solid diaphragm. The merged parts must be continuous in order to facilitate the desired meshing technique, which will be discussed in entirety shortly. After continuous parts were merged, the superstructure consisted of 23 'parts'. The merging process did not create any geometric inconsistencies, but allowed for the simplification of the meshing process.

4.5 Meshing

After the geometry was completely imported and all import irregularities removed, a mesh was assigned for analysis. Many aspects needed to be considered before assigning a meshing technique to a geometric model. Some of these aspects include: element type, integration process, cracking, and partitioning for loading application, among others.

The first aspect of the mesh that was considered was the element type and integration process. The element chosen was the C3D20R 20-node hexahedral element with reduced integration. There are advantages involved with the use of the hexahedral element that make it desirable. These advantages include:

- *Quick convergence compared to tetrahedral elements*
- *A more uniform mesh than tetrahedral elements*
- *Provide solution at less computational cost*

Along with the choice of the hexahedral element, the 20-node quadratic formulation was chosen over the 8-node linear formulation. Reasons for this choice include:

- *Faster convergence*
Fast convergence is imperative when considering computational cost. Because the smallest dimension in the Wakota model is much smaller than the largest dimension, slow convergence leads to a large increase in the number of elements needed.
- *Can model curved surfaces with fewer elements*
This is important when used with virtual topology as discussed shortly.
- *Very effective in bending problems*

Reduced integration is also a very desirable in the element choice. Advantages of using reduced integration include:

- *Reduced computational cost*
Integration uses only 8 integration points instead of 27, reducing computing time by a factor of about 3.5.
- *Generally yield more accurate results than fully integrated counterpart*
- *Eliminates shear and volumetric locking*

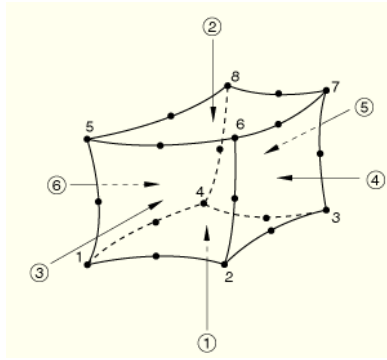


Figure 4.3: C3D20R element in ABAQUS [16].

Before the geometry was meshed with the chosen element, two aspects of the model needed to be considered: loading conditions and the presence of cracking behavior. Loading conditions may affect the mesh scheme if they need to be applied to only certain regions of a section of the model. In this case, each section needed to be partitioned in ABAQUS prior to meshing in order to apply loads to the specific regions in the model. This is imperative if a temperature gradient is to be applied to only the top of the cross-section along the span of the bridge. In order to facilitate this loading, a partition was created at the appropriate elevation below the deck of the bridge for the applied loading. Secondly, the presence of cracking needed to be considered because if cracking occurs, rebar will be needed to be included in the geometry to run a stable nonlinear analysis. Luckily, ABAQUS contains an embedment constraint that simulates the interaction of the embedded rebar in the concrete cross-section. Therefore, the geometry can simply be meshed as solid concrete and rebar can be embedded into the mesh at a later time if needed.

Much trial and error was needed to achieve a desirable mesh on all 23 superstructure ‘parts’, as described previously, and 7 substructure ‘parts’. While every element was desired to have an aspect ratio of 1 and all angles to be 90 degrees, this was not possible on a complex geometry as is used here. Because of this, a practical decision was made on the limits of the angle and aspect ratio of the elements involved in the structure. The limits for the Wakota model were limited to a smallest angle of greater than 30 degrees, a largest angle of less than 150 degrees, and an aspect ratio of less than 4. In order to achieve these limits, some simplification of the model geometry was needed. The simplification took the form of the “virtual topology” toolset in ABAQUS. This toolset allows for the combination of faces and edges on the model geometry. By combining faces in the geometry, nodes are not forced at the intersection of the two faces and therefore much more flexibility is achieved when the mesh is generated. Because a node is not forced at the face intersection when this function is used, the elements create an interpolation over the intersection if a node is not located there. This interpolation causes small geometry changes in the model but it is trivial for faces that intersect at close to 180-degree angles. The only faces combined were ones of this type, therefore the meshing was simplified at little or no accuracy cost.

Using the “virtual topology” toolset, the desired element limits were met and additionally, less than 1% of all elements in the model have angles smaller than 45 degrees or greater than 135 degrees. This was determined to be a mesh of sufficient quality. A mesh that is representative of the model is shown in Figure 4.4.

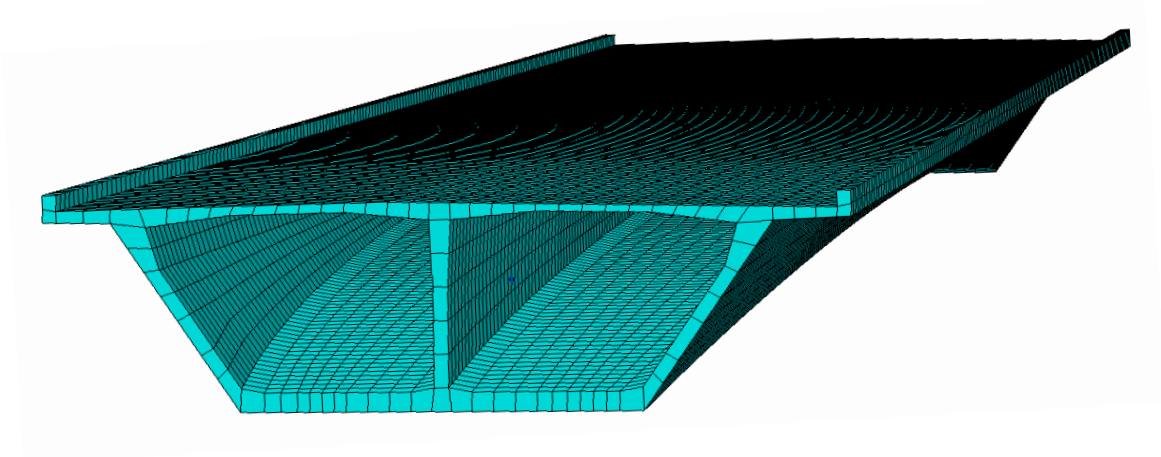


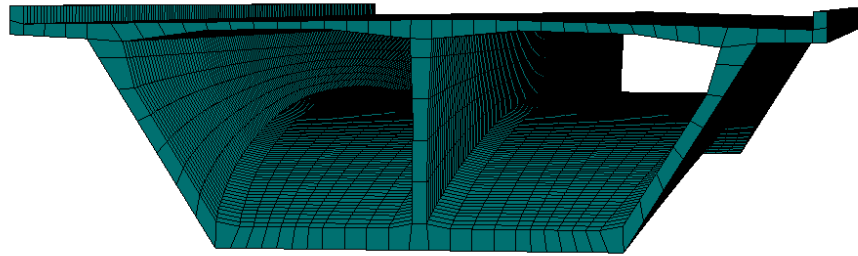
Figure 4.4: Representative span meshing scheme.

4.6 Verifying Convergence

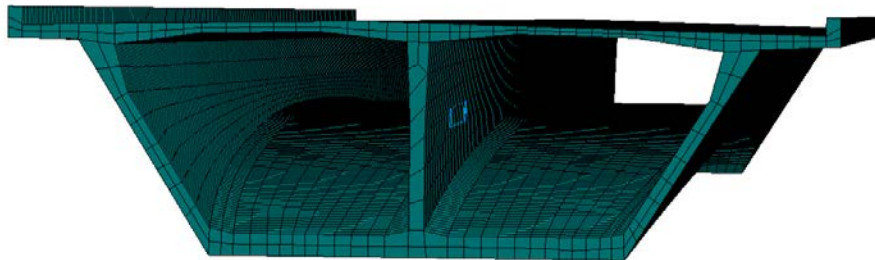
4.6.1 Superstructure

A convergence study was needed to verify that the bridge response values being obtained are of satisfactory quality. Because finite element models tend to converge to the exact solution as the number of elements is increased, a common strategy to verify convergence is to double the number of elements contained in the tested region and compare stress gradients. In the case of this model, it was considered adequate to test only one of the five spans for convergence. If the mesh for the tested span was sufficiently refined, it would be assumed that the mesh quality was adequate throughout the entire structure.

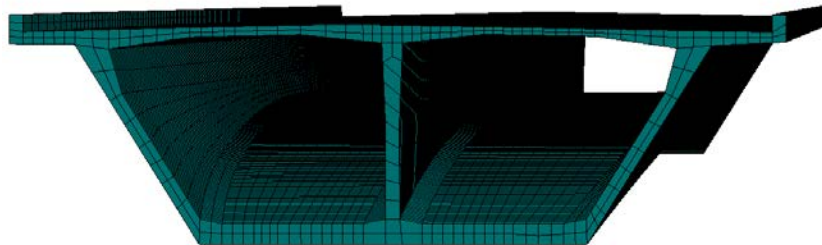
Span 3 was used to conduct the convergence study because it is one of the spans that will experience the most stress from temperature changes. Three separate meshing schemes were produced for Span 3 as shown below in Figure 4.5 (a-c). Mesh 1, 2, and 3 contained: 14,560, 45,600, and 81,656 elements respectively. All meshes used the C3D20R 20 node hexahedral reduced integration element as described previously.



a) Coarse mesh: 14560 elements



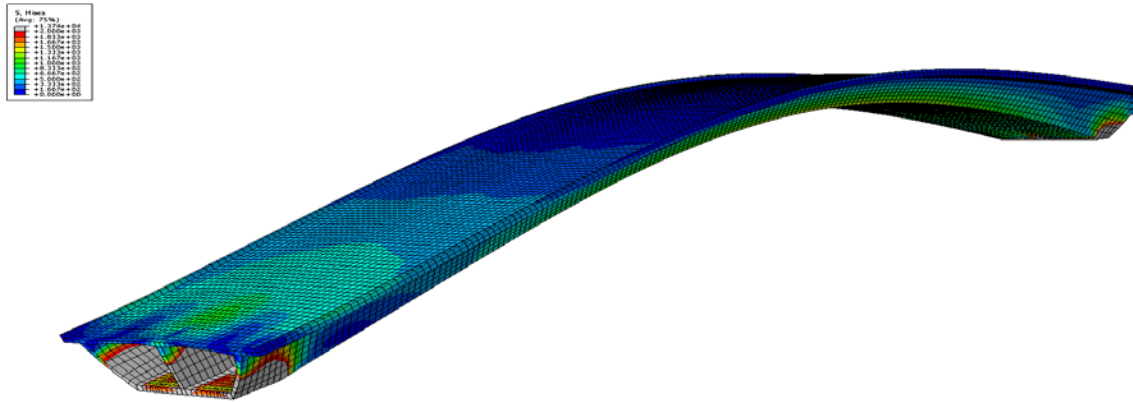
b) Refined mesh: 45600 elements



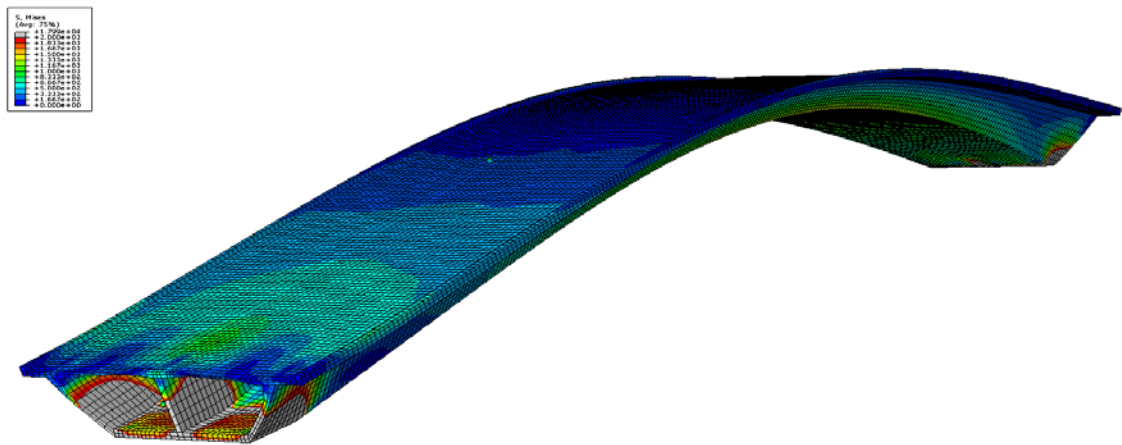
c) Most refined mesh: 81656 elements

Figure 4.5: Meshing refinements.

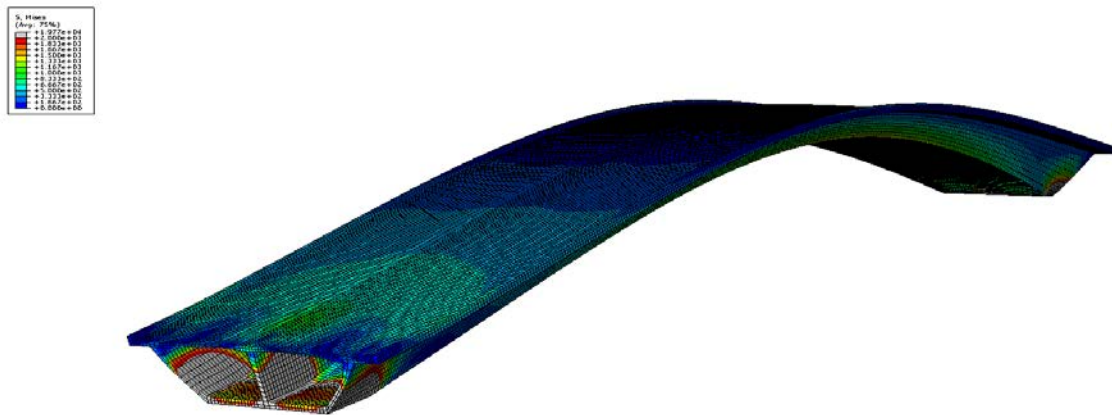
The three meshes were then subjected to a 50° F uniform temperature loading with fixed boundary conditions on the faces located closest to the piers on the underside of the box girder. The three cases were then analyzed and the stresses were observed. As can be seen in Figure 4.6, the stresses are virtually identical in all three cases. The only differences in the three stress plots are stresses at a few points located near the fixed boundary conditions. These points are not of concern because the behavior of the structure as a whole was the desired outcome and these stress concentrations were simply the result of imposed boundary conditions. If exact stresses at points like these were desired, this would be of more concern, but since that was not the objective of this study, the course mesh shown in Figure 4.6 (a) was determined to be of sufficient accuracy. In each of Figure 4.6 (a-c) the contour values are set to capture the most important aspects of the behavior, therefore the stresses at the corners (grey in the plots) are not captured.



a) Coarse mesh: 14560 elements



b) Refined mesh: 45600 elements



c) Most refined mesh: 81656 elements

Figure 4.6: Stress contours of different meshing schemes.

4.6.2 Piers

Equally as important as the convergence of the superstructure model in the case of this study was the accuracy of the stress levels in the pier wall structures. Changes in temperature affect both superstructure and substructure, and proper modeling of both was necessary to achieve an understanding of the global behavior of the bridge structure. In order to verify the convergence of the pier structures, a separate convergence study was conducted on the pier wall/pier table assembly. Although quadratic elements were used in the superstructure, linear elements were used in the case of the pier walls. The reason for this element choice is that cracking behavior in a solid element model is more stable when a linear element is used as opposed to a higher order element. When a higher order element is used in a cracking formulation, convergence is hard to achieve and tension stiffening parameters may need to be set at high levels to represent the influence of steel reinforcement. However, the influence of steel reinforcement on the fracture properties of reinforced concrete is not well understood.

Pier table 4 was isolated for the observation of pier wall stresses. A uniform pressure was applied to the diaphragm on one side of the pier table as shown in Figure 4.7 as four different meshing schemes were observed in a loading test of pier table 4 in the convergence study. The four meshing schemes were as follows:

- 2 elements along the thickness of the pier – reduced integration.
- 2 elements along the thickness of the pier – full integration.
- 4 elements along the thickness of the pier – full integration.
- 5 elements along the thickness of the pier – full integration.

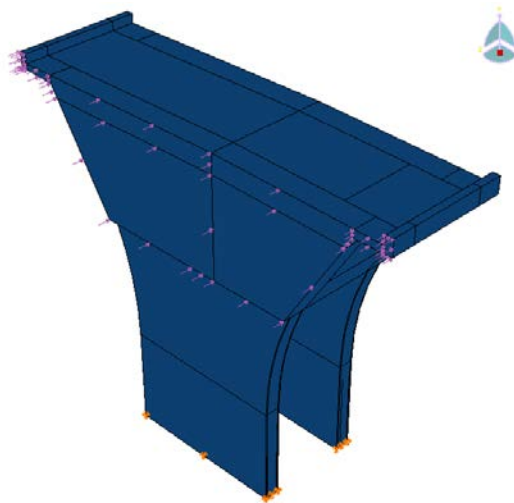


Figure 4.7: Pier Table 4 used for pier wall convergence study with applied load.

All analyses were carried out with linear material properties although nonlinear analyses were used when the global model was analyzed. It was observed that the reduced integration mesh produced imprecise results compared to the other three; therefore a fully integrated element was selected. The other three meshes can be seen to converge to common values. The two element and four element fully integrated meshes were compared to the values of the five-element mesh

in Figure 4.8. As can be seen, the results appear to have converged, and a mesh with four elements along the thickness of the pier looks to be a sufficiently converged mesh and the three-element mesh looks adequate as well, while preserving the efficiency of the model. The four-element mesh was chosen for analysis.

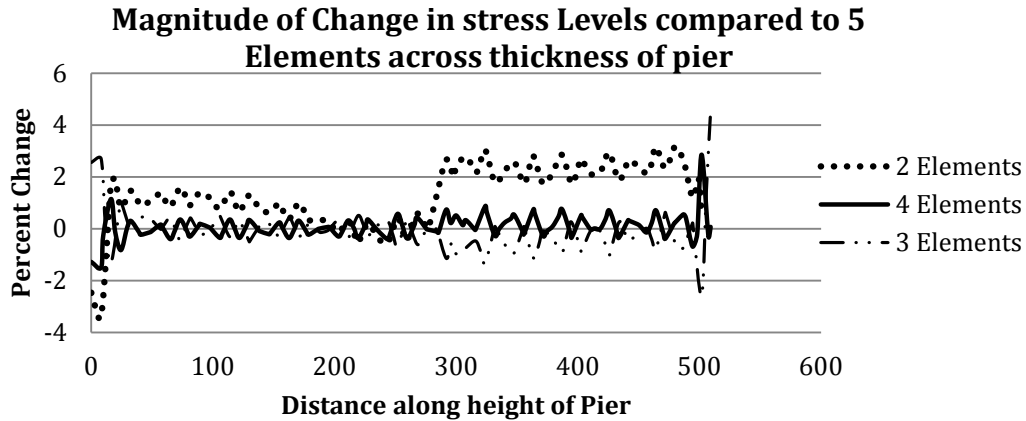


Figure 4.8: Comparison of different pier meshing schemes.

4.7 Tie Constraints

After a satisfactory mesh had been developed for each of the 23 geometric ‘parts’ of the superstructure and the 7 ‘parts’ of the substructure, they needed to be tied together. There are two options for achieving this task in ABAQUS, one being interaction properties, and the other being constraints. The latter tends to produce fewer complications with the analysis so it was consequently chosen. All surfaces were tied together using a simple surface to surface tie constraint except the interaction between Pier 1 and the superstructure because Pier 1 contains an expansion bearing. Tie constraints in ABAQUS cause the nodes of one of the contacting surfaces to conform to the deformation of the other contacting surface at the corresponding node. In order to do this, a ‘slave’ and ‘master’ surface assignment is required, of which the slave nodes conform to the master surface. The ABAQUS manual recommends using the surface with the larger cross-sectional area to be used as the master surface. Therefore, the tie constraints containing a diaphragm always have the diaphragm defined as the master surface.

Pier 1 did not employ a tie constraint as the other piers did. Pier 1 contains an expansion bearing and therefore cannot be tied to the superstructure. Instead, an interaction property was used in which the vertical displacement component of the superstructure was restrained to zero relative vertical displacement with respect to Pier 1. Displacements in the longitudinal and transverse directions of the bridge were left unrestrained.

4.8 Boundary Conditions and Loading

For initial observations, the boundary conditions of the Wakota Bridge model were kept simple. The surfaces at each end of the superstructure where the abutments would connect if they were to be modeled were constrained to zero translation in the vertical direction. Also, each pier base was fixed in all directions.

Loading conditions were similarly kept simple for initial observation. A few different loading conditions were applied separately and an analysis carried out to determine if the model was performing reasonably. The question of how realistic loading conditions could be applied was of importance. A uniform temperature loading was first considered. This loading condition would likely have the largest effect on the pier walls in the substructure of the bridge. A uniform temperature increase of 50° F was chosen for initial observation. Using this loading condition only, it was determined that the piers in the substructure will indeed crack under extreme temperature loadings, as expected.

Another loading condition of interest was a temperature gradient loading on the superstructure deck. Temperature gradient analysis was conducted for completeness, though it was not a part of the comparison between temperature design Procedures A and B. This gradient would impose bending moments at the piers and affect both the piers and the superstructure. This loading condition was more difficult to apply to the model than the uniform temperature loading because the gradient must be applied as a continuous function over the depth of the model. This was made more difficult by the fact that AASHTO LRFD design gradient is a piecewise linear function varying with the width of the deck, as discussed in Chapter 3. Because of the difficulty in applying this loading condition, and the fact that this as a simplification of the actual temperature distribution in the deck, a less approximate and simply applicable distribution was sought. The distribution found to achieve these conditions was the temperature distribution presented by Priestley (Figure 3.8) and discussed in Chapter 3. Priestley's distribution has been found to compare favorably with experimental results of an experimental segmental bridge in Pennsylvania [19] and consists of one continuous function; therefore this was a desirable distribution to be applied to the bridge model because ABAQUS more easily facilitates the application of a continuous function than a piecewise function as defined in the AASHTO LRFD [22] and discussed in Chapter 3.

Knowing the gradient function to be applied to the analysis before the mesh was created was important for the application of this loading condition in ABAQUS because the geometry in ABAQUS needed to be partitioned at the point that the gradient temperature reaches 0° F before the mesh was created. The geometry of the model was partitioned 47.2 inches (1200 mm) below the deck surface of the superstructure for this gradient to be applied because the dimension 'y' in the gradient starts at a location 47.2 inches below the deck (Figure 4.8). An arbitrary loading case was executed with this loading and results were visually inspected to confirm that they exhibited the expected behavior, which involved a bowing up of the superstructure deck in between piers.

The dead load of the bridge also had to be accounted for, as this will undoubtedly be the main component of the compressive force on the piers. The dead load will essentially be the weight of the reinforced concrete structure as other loads, such as traffic, will likely be small. The self-weight of the model can be represented using the gravity loading function in ABAQUS. The gravitational acceleration constant is defined in the loading step. Using this constant and the mass density of each element and the gravitational acceleration, ABAQUS calculates the self-weight as a body force. The weight used for the calculation of the mass density of the concrete was 152 lbs/ft³. This value combines the weight of normal weight concrete (145 lbs/ft²) and a weight contribution from the reinforcing bar assuming an average reinforcement ratio of 0.02. The concrete wearing course was not included in the self-weight loading. The wearing course

can be accounted for by the use of a distributed load on the deck if needed. It was assumed that other dead loads such as utilities were negligible compared to the weight of the concrete structure. This assumption was consistent with the bridge design assumptions. The model behaved as expected with the incorporated self-weight load.

4.9 Cracking Behavior

Because tensile stresses exceeding the cracking strength in the concrete were observed in the analyses, a nonlinear solution algorithm was needed to capture the cracking behavior of the piers. In order to accomplish this task, one of the nonlinear solution methods offered in ABAQUS was used. Two choices are offered for the modeling of concrete cracking in ABAQUS: concrete smeared cracking and concrete damage-plasticity. The former method was selected for analysis of the Wakota Bridge piers due to ease of use and the fact that damage was not a concern in this analysis; therefore a damage model was not considered.

The concrete smeared cracking method does not propagate cracks through the material when it reaches its tensile capacity. It works by reducing the effective stiffness based on the concrete material model and the stresses in the model as the load is incrementally ramped up from zero. To employ this method, a nonlinear material model for the concrete was defined.

4.9.1 Compressive Behavior

The compressive material model chosen for the analysis was the Popovics/Thorenfeldt/Collins concrete model found in Response-2000 [26], a common sectional analysis program. This concrete model is widely used and it captures the nonlinear behavior of the concrete in compression. This model was then combined with a tension behavior model that incorporates tension stiffening in order to let the solution achieve an equilibrium state. Although this model gives stress in terms of strain directly, ABAQUS calls for stress as a function of plastic strain. The plastic strain can be found by subtracting the elastic strain from the total strain. Because of this definition, an elastic modulus was assumed. In the case of the adopted model, the elastic modulus was taken as $E = 57000\sqrt{f'_c}$ (psi), as defined by ACI 318, and the concrete was assumed to be linear up to a stress at which the Popovics/Thorenfeldt/Collins curve is no longer approximately linear. The stress after this point was determined by the model given in Response-2000.

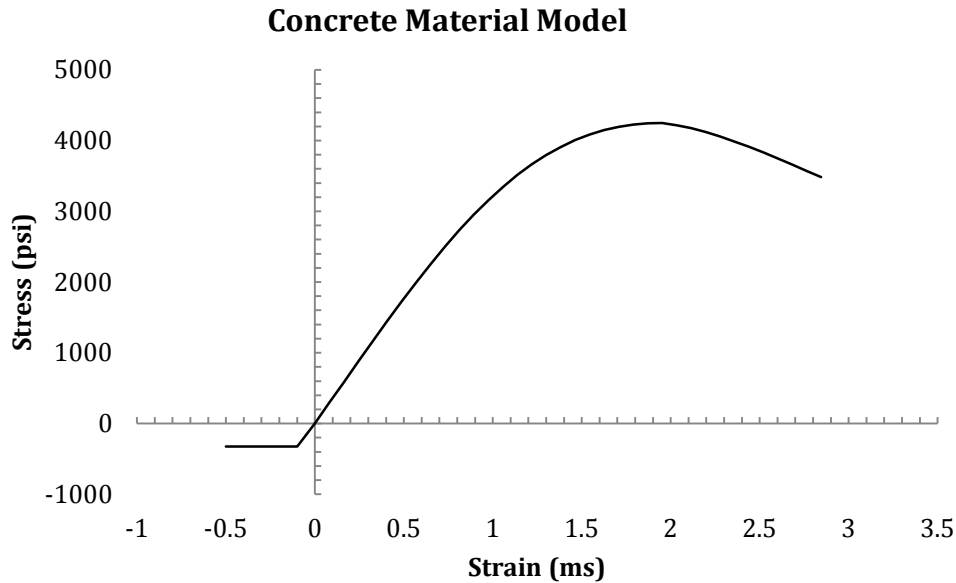


Figure 4.9: Popovics/Thorenfeldt/Collins concrete material model.

4.9.2 Tensile Behavior

The tensile behavior of concrete in a nonlinear finite element analysis is possibly the most important as well as the most challenging for defining a nonlinear material. Although the tensile ultimate strength is fairly easy to measure, the strength with increasing strain after cracking is hard to define. This strength after cracking is known as either tension softening or tension stiffening. Without tension stiffening, the finite element model will most likely not converge to a solution and the equilibrium equations will not be satisfied.

Tension stiffening is the process whereby the energy stored in the material is converted into fracture energy as cracks develop, and as the cracks advance the concrete ‘softens’. Reinforcement provided in the concrete stiffens the response by providing resistance against this softening behavior and engaging the concrete in the presence of cracks. The stiffening effect allows the average concrete stress to decrease to zero as cracking increases. Tension stiffening must be estimated; it depends on many different parameters including the reinforcement ratio, the mesh, and the bond between the rebar and concrete [16]. Local bond-slip and tension stiffening are two different but interrelated phenomena that cannot easily be separated from each other; therefore tension stiffening models take into account both of these effects [14]. Although tension-stiffening parameters should be calibrated to every case in which an analysis is desired, there are recommendations as to the stiffening curve that may be used as a starting point for analyses because it is difficult to determine by experimental testing.

The ABAQUS User’s Manual [16] suggests using a tension stiffening parameter that reduces the stress to zero at about ten times the strain at initial cracking. The strain at which most standard concretes fail in tension is approximately 10^{-4} , so a tension stiffening curve that reduces the stress to zero at 10^{-3} is reasonable [16]. Nayal and Rasheed confirm this range [14]. Although this is a good starting point for the tension stiffening parameter, the ABAQUS User’s Manual

states that “Too little tension stiffening will cause the local cracking failure in the concrete to introduce temporarily unstable behavior in the overall response of the model. Few practical designs exhibit such behavior, so that the presence of this type of response in the analysis model usually indicates that the tension stiffening is unreasonably low” [16]. Also, it was found that the tension-stiffening curve does not affect the results of the analyses reported here as is the case in many analyses. This fact was determined by running a number of analyses with the only changing parameter being the tension stiffening parameter. The analyses showed essentially no change in results and therefore it was decided that this parameter is not of significance in the present study and an arbitrary curve with increased tension stiffening was picked to enhance solution convergence.

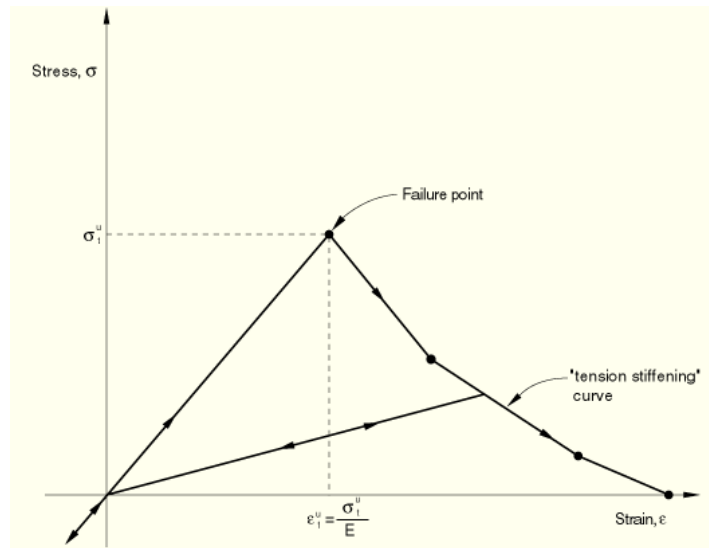


Figure 4.10: Typical tension stiffening curve.

Another factor that was found to be very important in the convergence of a nonlinear material model with smeared cracking is the choice of elements. It was difficult to achieve a converging solution in the nonlinear model while using higher order elements such as the 20 node brick elements used in the superstructure concrete or even with fully integrated linear elements. Because of this fact, the best meshing scheme that could be achieved while generating a solution at sufficiently large temperature loadings was a mesh containing linear 8-node reduced integration elements. A large number of meshing schemes and material properties and variations in the model were investigated and none could produce results with more accurate elements. Because of the need for reduced integration elements, the previously chosen fully integrated element meshing scheme was discarded for the piers that incorporated cracking, and a reduced integration pier mesh needed to be verified. For this purpose, the full bridge model was run with two different meshes on Pier 4 with a uniform 100 deg. F. temperature loading and the resulting end moments were compared with each other to determine if the mesh produced a converged solution. The first mesh consisted of 8904 elements in one stem wall of Pier 4, the second consisted of approximately twice the number of elements in the first mesh, 16,900. The analysis was run with both meshing schemes and the resulting difference in end moments was less than 0.5%. Because of this small change, the first meshing scheme consisting of 8904 elements in each stem wall of Pier 4 was determined to be adequate.

4.10 Defining Rebar

Rebar must be defined if a nonlinear analysis is to be used, as was discussed in the previous section. The assumption that only the piers will crack requires implementation of rebar in the pier walls only. The superstructure was assumed to be uncracked due to the post-tensioning, which suppressed cracking, and because the superstructure was not the main concern in this study. Therefore, the superstructure was assumed to behave linearly, which simplified the analysis and reduced the computing costs. Although rebar is not accounted for in the superstructure, it was desirable to include the contribution to stiffness of the rebar. In order to accomplish this, the modulus of elasticity of the superstructure was increased. Assuming a reinforcement ratio of 0.02, the increased modulus of the concrete is taken as $0.02 * E_{steel} + 0.98 * E_{concrete}$. For $f'_c = 6$ ksi and $E_{steel} = 29000$ ksi, the increased modulus of elasticity is about 4900ksi.

Although the pier walls are heavily reinforced with a large number of rebar, the rebar in the pier walls was defined quite simply using distributed reinforcement. Because the reinforcement in the pier wall sections is placed in planar arrangements, a distributed reinforcement option was possible. ABAQUS allows rebar to be defined at a set spacing with an individual rebar area in a fixed orientation over a shell element of small thickness. Because this was an option, a shell object was defined for each layer of rebar in each pier wall section and the appropriate amount of rebar was distributed throughout each shell object. The object could then be assigned material properties with almost zero stiffness while the rebar layers could be assigned steel properties. In this way, each shell object acts similar to individually assigned bars throughout the pier with much less input.

These shell objects were then embedded in the concrete pier wall section using constraints available in ABAQUS known as embedment constraints. The additional mass and stiffness due to the embedded elements were added to the model automatically. Bond for the rebar that is embedded is taken into account by the tension stiffening defined in the material properties of the concrete model. The simplified steel model shown below was used to capture the steel behavior and a dummy material of modulus of elasticity of 10^{-14} ksi was used for the plate as a whole. The dummy material of almost no stiffness ensures that the only contributor to the model stiffness was the rebar in the shell part. A modulus of 0 was not used for the dummy material because ABAQUS does not allow it; a finite value must be defined.

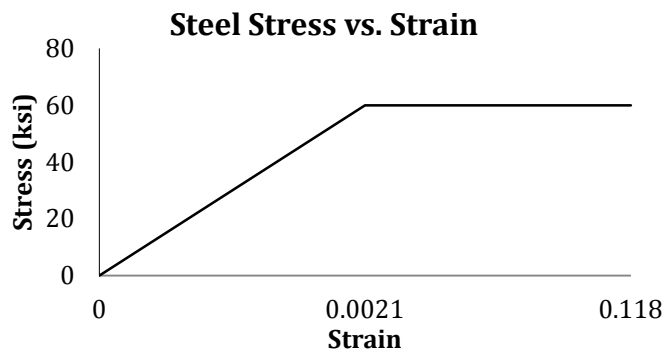


Figure 4.11: Steel reinforcing bar material model.

The model produced in ABAQUS will be referred to as the RLM (Research-Level Model) from this point on. Two versions of this model are referred to in the contents of this report: RLM1, which uses a linear material representation in the entire structure, and RLM2, which incorporates nonlinear materials in the pier walls using the smeared cracking representation in ABAQUS for concrete in tension and the Popovics/Thorenfeldt/Collins model for concrete in compression.

Chapter 5. Design Level Modeling (DLM)

5.1 Introduction

One of the main objectives of this study was to evaluate the current design practices for fixed, flexible bridge piers and make suggestions for more accurate analysis. In order to do this, a model consistent with the current design methodology was developed. A commonly available commercial design software package for this type of analysis is SAP2000. SAP2000 provides a user-friendly environment that lends itself to quick modeling with many convenient features for quick data entry and pre-processing provided to make the modeling process quick and efficient. It deals primarily with beam, frame, and truss elements, the preference of structural designers. Additionally, SAP2000 cannot evaluate the nonlinear cracking behavior of a reinforced concrete member. However, the nonlinear analysis to simulate cracking behavior is too tedious for practical design. Three different versions of the DLM were used in this report: The first one (DLM1) contains neither prestressing, time-dependent effects, nor rotational springs (at the base of the piers), DLM2 is similar to DLM1 except for the addition of rotational springs at the base of the piers, and DLM3 incorporates all loadings including prestressing and time-dependent effects as well as foundation rotations.

5.2 Development of the Model Geometry

5.2.1 Superstructure

The superstructure of the Wakota Bridge involves variable geometry, and this feature can make the model building process tedious and time consuming. To aid in this process, SAP2000 has a “bridge designer” option in which concrete box girder superstructure development is greatly simplified, although some geometric approximations needed to be made in order to use it. Dimensions of the concrete box structure can be defined at a starting point and each dimension assigned a variation along the length of the bridge. The program then automatically computes the cross-sectional properties at each varying section along the length of the bridge. The superstructure dimensions were input as accurately as possible within the capabilities of SAP2000. The most significant simplification that was made concerned the idealization of the top of the girder cross-section being flat instead of having a slight curve (i.e., crown) as in the field. Other dimensions were slightly modified to account for the change in area due to this simplification. A representative section used in the SAP2000 design model is shown in Figure 5.1.

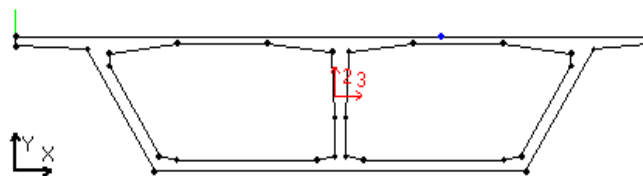


Figure 5.1: Representative cross-section from SAP2000 Model.

After the geometry of the superstructure was defined, SAP2000 automatically generates a superstructure frame model incorporating all of the cross-sectional properties from the defined sections. The superstructure was discretized at each construction segment as shown in the bridge plans with sectional properties averaged throughout each section. This choice allowed for “staged construction” analysis to simulate the effects of creep and shrinkage deformations, which greatly affects the stresses in the pier walls.

5.2.2 Pier Walls

The piers will undergo much more cracking than the superstructure, causing them to be of greater concern in the modeling process. Because of this, a few considerations must be noted. The pier walls had to be connected to the superstructure frame elements at the correct vertical location. To do this, rigid link elements were used to position the pier wall elements the correct distance below the centerline of the deck elements. This is a common practice and assumes the pier table deck section is very stiff compared to the pier wall sections. This assumption was considered appropriate because of the difference in relative stiffnesses of the two connected elements.

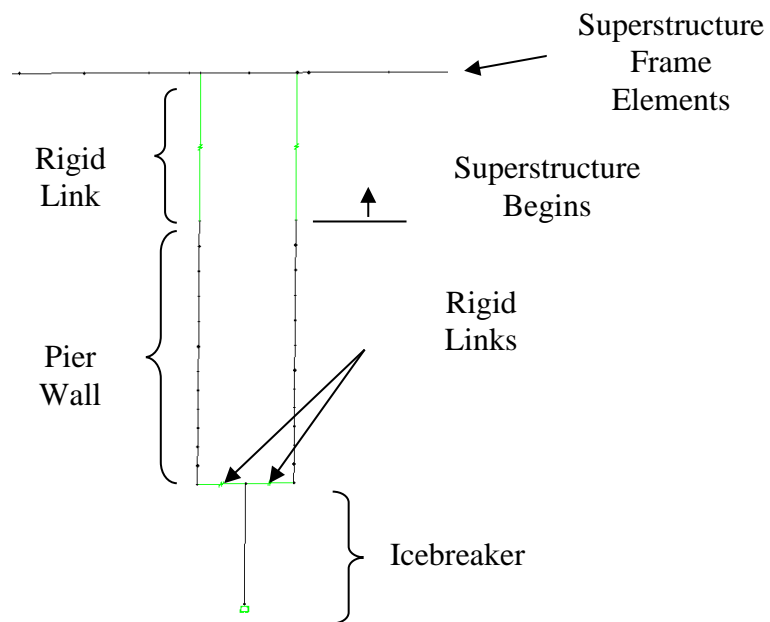


Figure 5.2: Bridge pier representation in SAP2000.

The icebreaker was also modeled as a frame element rigidly connected to the twin pier walls. The links used to connect the pier walls and the icebreaker allowed no rotation or translation relative to the attached element.

The gross section stiffness of the pier walls had to be correctly modeled with the contribution of the rebar included in the section properties. In order to do this, the transformed moment of inertia for each pier wall segment was calculated using Response-2000 to account for rebar and pier wall dimensions.

5.2.3 Other Modeling Considerations

The following assumptions were also made in developing the SAP2000 models.

- All materials in the design model behave linearly and thus do not exhibit cracking behavior discussed earlier.
- The ends of the superstructure are restrained against translation in all directions except along the skew direction.
- Footings were fixed in all DOF's for comparison to the RLM models.
- Footing springs were applied for design evaluations.
- All diaphragms modeled with appropriate thicknesses
- Bridge elevation modeled as horizontal as was done for the RLM models.

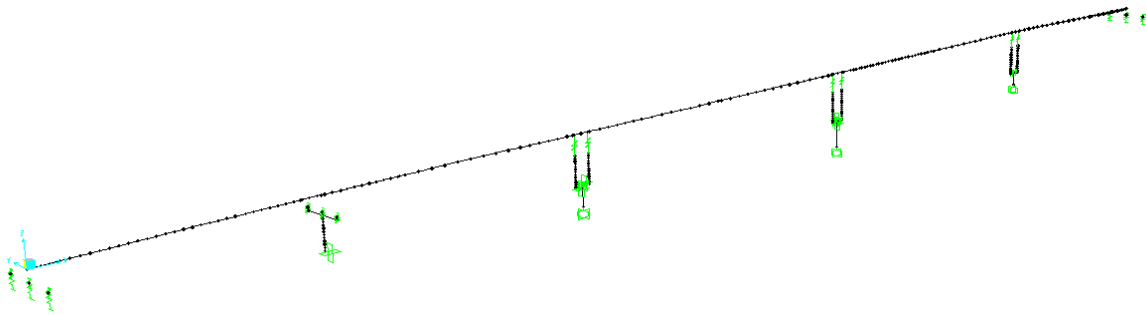


Figure 5.3: SAP2000 Design model for comparison of methods (no prestressing).

The model created in SAP2000 at this point will be referred to as the DLM1 (Design Level Model) in future sections of this report. This model was used for evaluation of the reviewed CRD method in Phase II of this project.

5.3 Design/Calibration Model and Staged Construction Analysis (DLM3)

In order to develop a model that represents the actual behavior of the structure as a whole, time-dependent effects and prestressing forces were incorporated in the analysis. These effects were not previously accounted for in the RLM models or in the DLM1 model that were used for evaluation of the CRD method. Because of the fact that the Wakota Bridge was built using cast-in-place cantilever construction, a staged construction model was required to capture these effects. This task was accomplished by first placing the longitudinal prestressing tendons in the model and then using the staged construction add-on package in SAP2000 to facilitate the time-dependent analysis. The model incorporating these effects, the DLM3 (Design Level Model 3), was used for the evaluation of design method and loading choices in the AASHTO LRFD.

5.4 Prestressing Strands

All forces due to post-tensioning tendons were considered in the staged construction model, although some simplifications were made.

- 1) Only longitudinal strands were considered.
- 2) All tendon paths were idealized as a straight path through the superstructure.
- 3) Tendons were simplified to one path through the center of the girder although the actual layout consists of tendon paths at the top of each girder web (3).

All tendons were modeled as individual elements at the appropriate vertical position in the depth of the superstructure. The loads applied consisted of the forces from the as-built stressing tables and were stressed from the specified end using specified frictional loss properties. All prestressing strands were stressed the day after the concrete section was constructed in the model as was done in the field.

5.4.1 Time-Dependent Effects

Time-dependent effects of the construction and loading were modeled using the CEB-FIP model code. This model was chosen both because it was supported by the SAP2000 program as well as because it was allowed by MnDOT. The creep and shrinkage curves for the concrete is generated internally in SAP2000 after four parameters are input as defined in the CEB-FIP model code. These parameters include the notional size of the section considered, the shrinkage coefficient, B_{sc} , which identifies the type of concrete used, the relative humidity, and the shrinkage start age. One value for the notional size was used for the superstructure in this case although it is a continually varying parameter that depends on the ratio of the concrete area to the perimeter of the section. The value used was taken as the average of the two extreme values computed at midspan and at the piers, which is a common design assumption. The curves for creep coefficient and shrinkage strain as computed by SAP2000 for the superstructure are shown in Figure 5.4 below. Separate values were obtained for each pier in the system.

The shrinkage, creep, and relaxation of the prestressing strands are also computed internally based on the CEB-FIP model code for grade 270 prestressing strand.

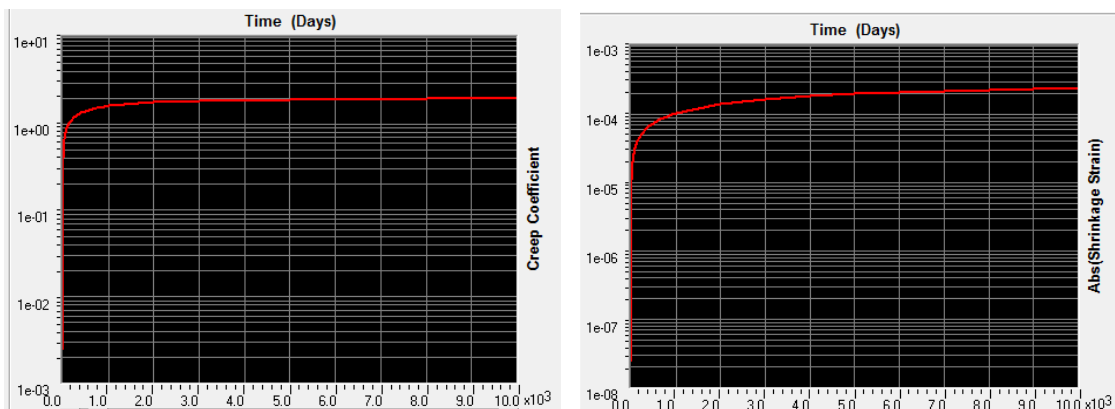


Figure 5.4: Creep coefficient (left), shrinkage strain (right).

5.4.2 General Considerations

In order to get the most accurate results, the as-built timeline was obtained and used for the analysis and all sequences in the build process were considered. A couple specific considerations in the build process included the falsework included in Spans 1, 2, and 5, the jacking sequence

prior to closure pours, and the friction at the expansion bearings. The jacking sequence involved each span being jacked apart longitudinally prior to pouring the closure pour. This initiates an outward bow of Piers 2 and 4 to account for a small amount of the long term creep and shrinkage effects.

Falsework was represented using stiff supports along the length of the supported span. This representation does not consider the specific falsework structure or ground and soil conditions, because it was only the vertical displacement restraint caused by the falsework that had an important effect on the structure. The supports could be easily added and removed in the staged construction analysis.

The closure pours in each span involved another consideration taken into account in the modeling. At each closure, the two joining spans were vertically adjusted to obtain matching elevations for the closure pour. In the field, this is done for the closures in Span 2 and 5 by adding weight the opposite side of one of the cantilevers to raise the section or placing weight on the closure side of the cantilever to lower it. For the closure pours in Spans 3 and 4, alignment beams are used to match the elevations of the two adjoining spans. An alignment beam consists of a very stiff steel beam that is attached to one of the spans and extends across the gap to the adjoining span. The beam is then either jacked or tensioned with respect to the un-attached span to match the elevations. The alignment processes here were not modeled explicitly but instead modeled as simple point loads at the end of the spans. Approximate values of the point forces were recommended by the onsite field engineer [7]. It is noted that the elevations of connecting spans were not exactly matched up in the model when closures were poured although they are within one or two inches, which is considered adequate. It was more important not to exceed the actual alignment forces as applied in the construction of the bridge than to perfectly match the elevations of the sections. Before the closure pours were cast in the structure, a horizontal jacking force was applied. This is accounted for in the model with the application of point loads.

Another general consideration was the friction representation of the expansion bearings at Pier 1 and the abutments. Friction was considered in the model through a multi-linear plastic model, which assumes an essentially rigid-perfectly plastic relationship. In the case of each expansion bearing, the coefficient of friction was obtained from the bridge design plans [3] and expected normal forces were computed in order to define the transition to plastic behavior for each joint.

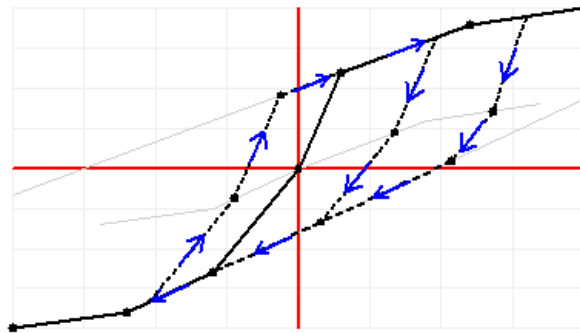


Figure 5.5: General multi-linear plastic kinematic relationship.

5.5 Footing Restraints

5.5.1 General

Appropriate restraints at the footings of Piers 2, 3, and 4 are important aspects for accurately modeling the forces in the pier walls, because as the superstructure expands and contracts, the footings will rotate and translate and thus relieve forces in the pier walls. It was necessary to obtain an approximation for the rotational and translational stiffnesses at the center of gravity of the footings to account for this effect. The stiffnesses can then be represented by the use of translational and rotational springs located at the footings. Footing movements at the abutments and Pier 1 are not as important in this case because of the presence of expansion bearings at the superstructure connection, which will relieve most of the lateral forces on the substructure components, therefore the footing restraints at these locations were assumed to be fixed as they will not translate or rotate significantly.

A brief discussion of the as-built footings was required before continuing with the analysis. The footings of Piers 2 and 3 consist of pile supported footings. The piles are steel shell pipes filled with a combination of structural concrete and sand/gravel. Each footing consists of 36 piles. The footing at Pier 4 is a spread footing resting directly on rock. Figure 5.6 shows the geometry of each footing.

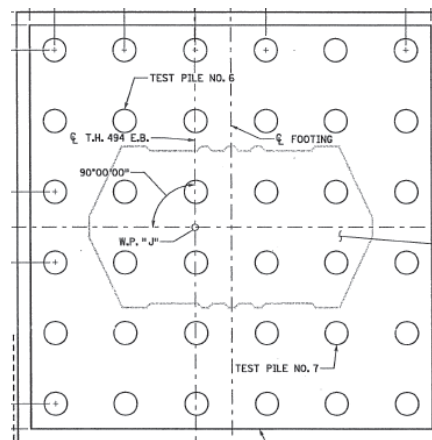


Figure 5.6: Pier 2 Pile supported footing.

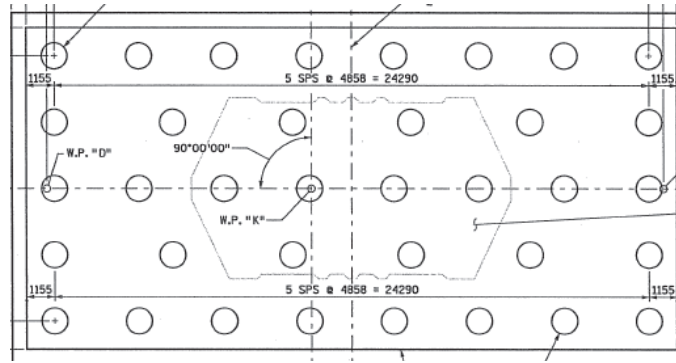


Figure 5.7: Pier 3 Pile supported footing.

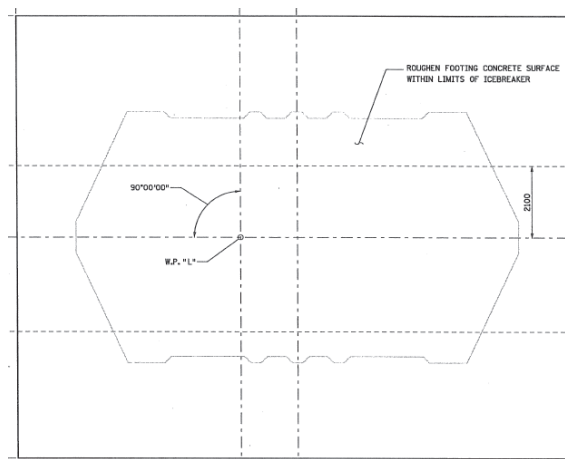


Figure 5.8: Pier 4 spread footing.

5.5.2 *Pile Analysis*

The most accurate method for determining appropriate spring stiffnesses at each footing requires a pile analysis for Piers 2 and 3 incorporating actual soil properties from the excavation site. Because a fully functioning pile analysis program capable of analyzing the full pile group could not be acquired, each footing was analyzed as smaller pile groups and the associated rotational and translational stiffnesses summed to produce the stiffness of the entire footing. The pile strips were oriented so that the reduction factors associated with each pile group were taken into account by the pile analysis program. Soil composition and elevation data was provided from the site excavation and used in the analysis program. Properties for each soil layer were calculated and input as required.

A full bridge analysis was run in SAP2000 prior to application of foundation springs to get an approximate value of forces that would be acting on the foundation at the stage in which the bridge would be analyzed. This was necessary because of the highly nonlinear nature of pile-soil interactions. It was necessary to investigate the forces just after jacking and at ultimate conditions, therefore forces at these stages were applied to the pile-soil interaction model and the associated stiffnesses found. Scour was not considered in this case because the model will be used for calibration to field data at service conditions at the beginning of the life of the bridge

and therefore significant scour will most likely not have occurred. Also, at ultimate conditions, assuming a “no scour” condition is conservative when pier forces are the concern because scour will alleviate stresses in the bridge piers.

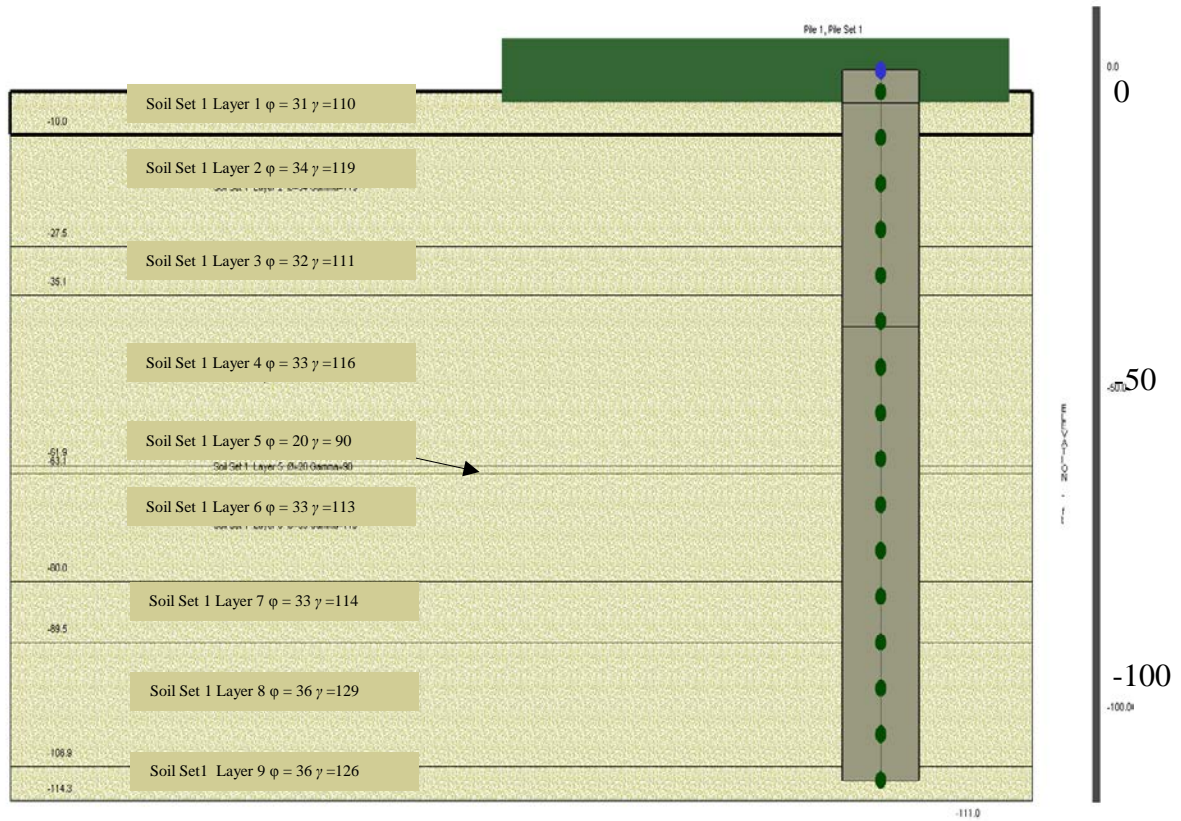


Figure 5.9: Pier 2 soil profile (ϕ = angle of internal friction, γ = unit weight in lb/ft³).

The axial force is approximately constant and the transverse shear and out-of plane moment at the foundations are very small, so these DOF's were assumed to be fixed at the base of the foundation. The soil profile used for both piers 2 and 3 are shown in Figure 5.9.

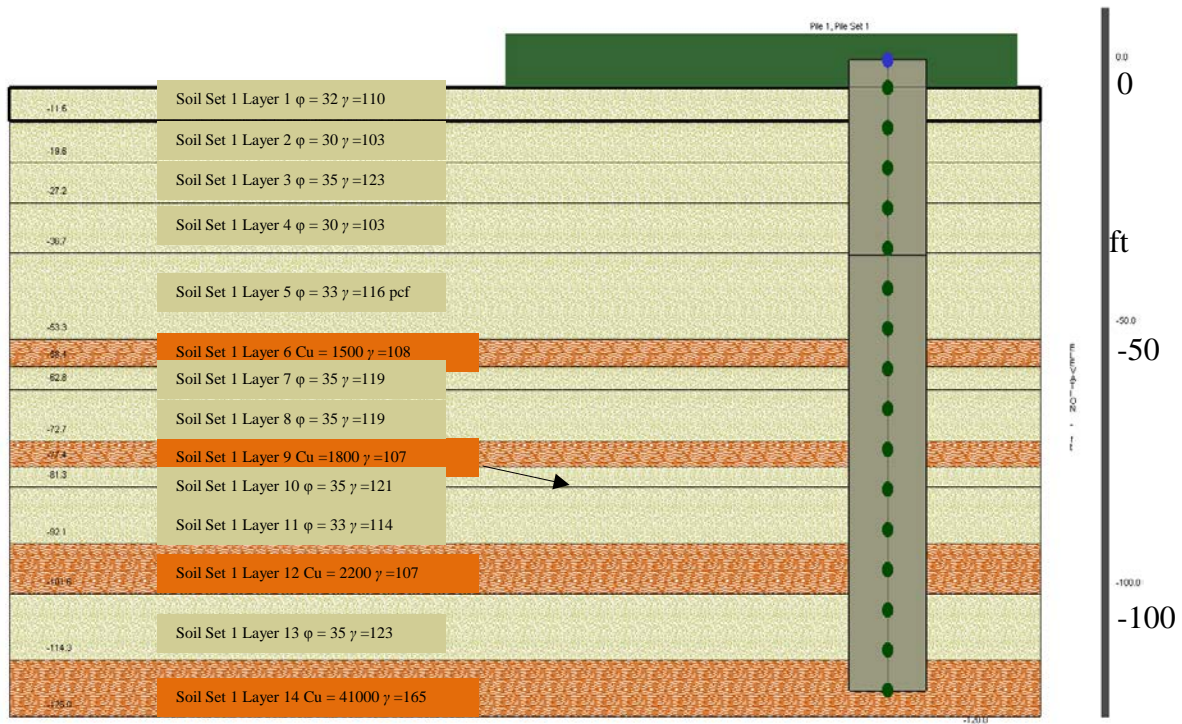


Figure 5.10: Pier 3 soil profile (ϕ = angle of internal friction, γ = unit weight in lb/ft³).

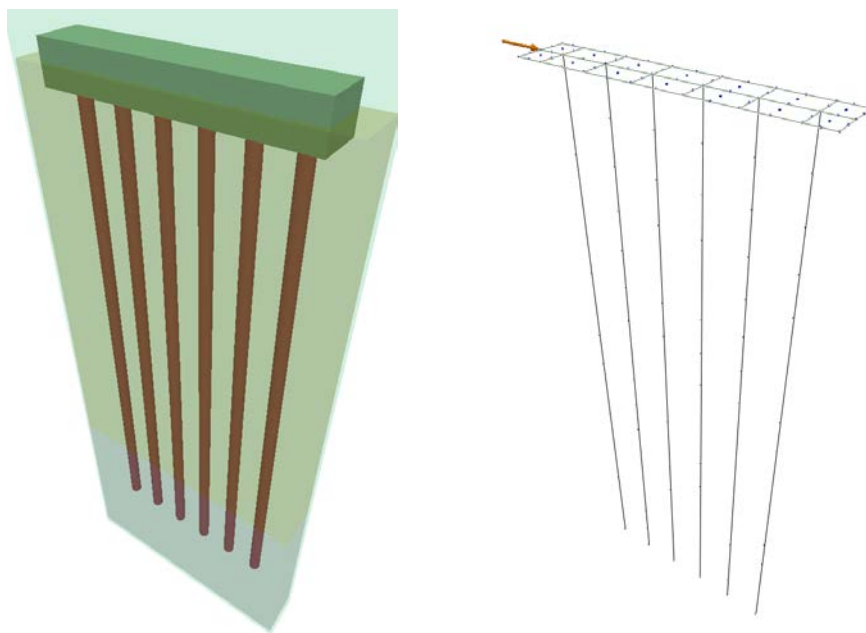


Figure 5.11: Pier 2 pile analysis strip and applied lateral load.

It was also useful to consider a simplified approximate procedure for determining the rotational and translational stiffnesses at the base of the piers in this type of pile footing. It would be beneficial to be able to define an effective length of the piles to which simple beam displacement

formulas can be applied. To investigate this possibility, simple beam bending and compression formulas were compared to the results of the pile analysis and an effective length was found for each bending case in each loading condition. This should give a good idea of the range of effective lengths for the loading range. The movement of the piles at the foundation can be likened to two different formulas assuming a fixed connection between the pile and pile cap, where L is an effective length.

$$K_{Translational} = \frac{V}{\Delta} = \frac{12EI}{L^3} \quad (9)$$

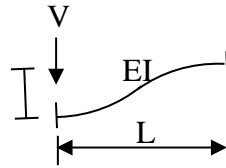


Figure 5.12: Translational stiffness diagram.

$$K_{Axial} = \frac{P}{\Delta} = \frac{AE}{L} \quad (10)$$

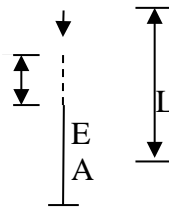


Figure 5.13: Axial stiffness formula diagram.

Taking the results from the pile analysis, an effective length could be found for each of the loading types: lateral load, rotational load, and axial load. The pile area and inertia were found based on steel area only.

For rotation, the effective length was found by assuming a rigid footing and thus compressing each pile proportionally on one side and pulling on those on the other side, considering both compression and tension in the pile footing (Figure 5.14).

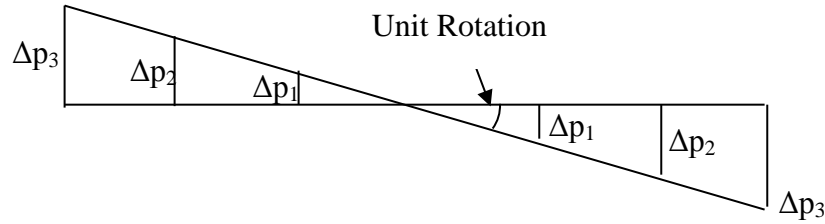


Figure 5.14: Simplified rotational stiffness in pile strip.

This same simplified analysis could be used when considering a pinned pile to pile-cap connection. Although the connection most closely simulates a fixed connection in the field, both fixed and pinned connections are generally analyzed when designing, giving a range of displacements and stiffnesses. The worst-case scenario is then taken for each situation. Because of this, a pinned connection was investigated and a range for stiffnesses was defined. The simple stiffness equation for shear in the pinned case takes the form:

$$K_{Translational} = \frac{3EI}{L^3}. \quad (11)$$

Table 5.5.2.1(a-b) shows the calculated stiffnesses for Foundations 2 and 3 at loading just after construction jack-apart and at ultimate. It also shows the associated beam bending stiffness and calculated effective length of the pier if using the simplified equations for both fixed and pinned connection situations. The evaluation of effective length for the theoretical calculations may be useful in future calculations. An estimate of the stiffness with different loads could be made without going back into the pier analysis and updating the loads.

Table 5.1 a): Foundation properties (fixed connection).

Loading Case	Pier	D.O.F	Approximate Loading magnitude	Stiffness from analysis	Applicable beam stiffness equation	Theoretical Effective Length (ft)	Pile Length (ft)
Construction Jack	2	Shear (longitudinal)	900 k	16513 k/in	$\frac{12EI}{L^3}$	127	107
		Moment (in-plane)	49000 'k	8.69*10 ⁸ 'k/rad	$\sum \frac{AE}{L}$	39	107
		Axial Force	21000 k	165354 k/in	$\frac{AE}{L}$	52	107
	3	Shear (longitudinal)	17 k	12852 k/in	$\frac{12EI}{L^3}$	110	120
		Moment (in-plane)	45000 'k	3.11*10 ⁸ 'k/rad	$\sum \frac{AE}{L}$	55	120
		Axial Force	24000 k	116338 k/in	$\frac{AE}{L}$	74	120
Ultimate	2	Shear (longitudinal)	6000 k	12793 k/in	$\frac{12EI}{L^3}$	139	107
		Moment (in-plane)	480000 'k	3.33*10 ⁸ 'k/rad	$\sum \frac{AE}{L}$	102	107
		Axial	26400 k	77193 k/in	$\frac{AE}{L}$	111	107
	3	Shear (longitudinal)	318 k	12848 k/in	$\frac{12EI}{L^3}$	110	120
		Moment (in-plane)	25000 'k	3.12*10 ⁸ 'k/rad	$\sum \frac{AE}{L}$	55	120
		Axial	30500 k	102250 k/in	$\frac{AE}{L}$	84	120

Table 5.1 b): Foundation properties (Pinned connection).

Loading Case	Pier	D.O.F	Approximate Loading magnitude	Stiffness from analysis	Applicable beam stiffness equation	Theoretical Effective Length (ft)	Pile Length (ft)
Construction Jack	2	Shear (longitudinal)	900 k	6338 k/in	$\frac{3EI}{L^3}$	111	107
		Moment (in-plane)	49000 'k	8.66*10 ⁸ 'k/rad	$\sum \frac{AE}{L}$	39	107
		Axial Force	21000 k	166667 k/in	$\frac{AE}{L}$	52	107
	3	Shear (longitudinal)	17 k	4018 k/in	$\frac{3EI}{L^3}$	102	120
		Moment (in-plane)	45000 'k	3.53*10 ⁸ 'k/rad	$\sum \frac{AE}{L}$	48	120
		Axial Force	24000 k	113762 k/in	$\frac{AE}{L}$	76	120
Ultimate	2	Shear (longitudinal)	6000 k	1932 k/in	$\frac{3EI}{L^3}$	164	107
		Moment (in-plane)	480000 'k	2.82*10 ⁸ 'k/rad	$\sum \frac{AE}{L}$	120	107
		Axial	26400 k	77193 k/in	$\frac{AE}{L}$	111	107
	3	Shear (longitudinal)	318 k	4024 k/in	$\frac{3EI}{L^3}$	102	120
		Moment (in-plane)	25000 'k	3.01*10 ⁸ 'k/rad	$\sum \frac{AE}{L}$	57	120
		Axial	30500 k	95862*10 ⁸ 'k/rad	$\frac{AE}{L}$	90	120

A few observations can be made from the results. It can be seen that the difference between the pinned and fixed pile-to-cap connection has a large effect on the translational stiffnesses of the foundation, whereas the rotational and axial stiffnesses are affected very little. Also, the effective lengths for the simplified bending formulas can be seen to extend beyond the actual length of the pile in high loading cases. In all cases the effective length gets larger as loading increases. In a recently acquired document from MnDOT, a simplified method for determining the rotational stiffness at the bottom of pile driven footings was presented, which yields the same results as the currently used method. In the MnDOT document [27], the effective length is specified to be a value between L/2 and L where L is the length of the pile. It can be noted that the current investigation yields values for effective lengths similar to this specification, although the range extends from about L/3 to L with the effective length increasing as loading increases. A representative graph of lateral deflections for the foundation is shown below for both a fixed and pinned pile-to-pile cap connection.

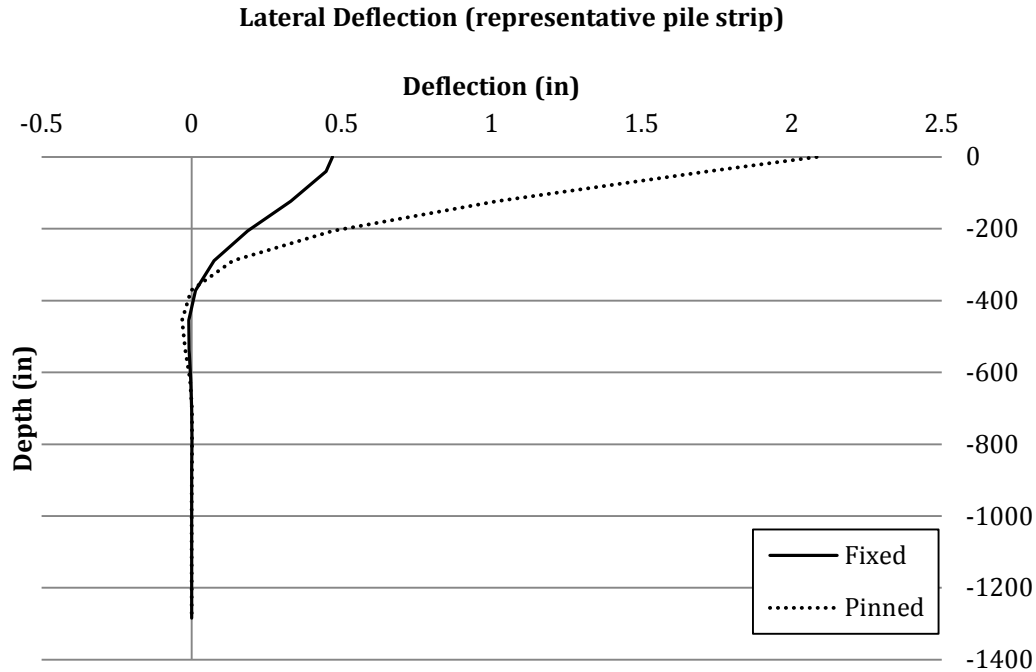


Figure 5.15: Lateral deflection range for approximate ultimate loadings.

5.6 Preliminary Correlation

Although continuous data collection had not yet begun throughout the structure at this point, one set of data was manually obtained. This data concerned the stresses and movements before and after the construction jacking events. Using this data, a quick verification of the predictive ability of the model was desired. Unfortunately, a large amount of time elapsed between strain gauge readings due to contractor request (~3 weeks). Because of this large gap in readings, the desired information was not able to be interpreted. There was simply too much activity in between the two data collection points and therefore pure strain behavior due to the jacking sequence was unachievable.

Although the strain gauges did not yield any intelligible results at this juncture, there were displacement readings that were taken during the Span 3 and Span 4 jacking sequences indicating the displacement of the expansion bearings at Pier 1 and the east and west abutments.

Table 5.2: Predicted and measured movements (mm) due to construction jack apart.

Jack Location	West Abutment		Pier 1		East Abutment	
	Predicted	Measured	Predicted	Measured	Predicted	Measured
Span 4	-3.7	-1	-2.4	-1	9.9	8
Span 3	-4.5	-1	-2.8	0	5.7	2

These displacements provide a means to check if the model is behaving accurately, but too much weight should not be put on this correlation because of the fact that the field measurements are not precise, as they are simply measured using marks on the joints and a ruler. The estimated least count in these measurements was on the order of 6 mm. Also, the predicted results are taken from the beam model and therefore are not taken precisely at the location of the expansion bearing, but instead at the center of the cross-section. In addition, the abutments are not modeled; therefore any movements of the abutments were not taken into account, which would reduce the movement of the expansion bearings. Although this is the case, a generally reasonable correlation is seen between the predicted and measured movements at the expansion bearings, where reasonable correlation is defined here as being within a couple of millimeters.

Chapter 6. Comparison of Linear Models

6.1 Introduction

In order to establish a correlation between the DLM1 model and the RLM1 model, bridge response to loading has been evaluated using each model and compared. The comparison of the two linearly behaving models should show the precision of the model representations and give confidence that the bridge is correctly modeled for further studies. The rationale for this chapter is that if the models behave similarly using simplified material properties, then significant confidence can be had that diverging results in future chapters of this report are not caused by basic modeling errors but rather by nonlinear solution methods such as the CRD method for the DLM1 model and the incorporated nonlinear material solution algorithm in the RLM2 model. This is necessary because the evaluation of the CRD method is a necessary outcome of this study.

6.2 Pier Lateral Movement

An easy way to evaluate if the DLM1 and RLM1 were behaving appropriately was to compare the values produced by the two models with linear materials to simple approximations of deflection and force. In order to accomplish this task, some expected values were estimated and compared with the results from the models. One easy way to estimate expected values for the pier walls was through the use of a purely thermal loading and the knowledge of the coefficient of thermal expansion (*CTE*). Using the *CTE*, the expected expansion between piers can be easily estimated and the corresponding pier moments can then be estimated based on the expansion.

Because the purpose of this study was to compare the DLM1 model with the more descriptive RLM1 model, values for all variable parameters were set identical in both models including concrete strengths, moduli, boundary conditions and the coefficient of thermal expansion, among others. The values used for material parameters were taken from the design plans for the Wakota Bridge. The design value for the coefficient of thermal expansion is $6 \times 10^{-6}/^{\circ}\text{F}$ and the pier concrete is specified as 4 ksi concrete, therefore, both models will be evaluated using these values. Also, the bases of all pier foundations are fixed against rotation and translation in the DLM1 and the RLM1 models.

Estimating reasonable values for the movement of the top of each pier in this case is fairly easy. The superstructure will expand about Pier 3 because only Piers 2, 3, and 4 are fixed and Spans 3 and 4 are of equal length. Using the coefficient of thermal expansion and a nominal 85°F temperature increase (the choice of an 85°F temperature loading is arbitrary and has no relation to the AASHTO LRFD design), the displacement of Piers 2 and 4 can be approximated as:

$$\Delta_{2,3} = \alpha L_p \Delta T$$

where $\Delta_{2,3}$ = lateral movement at top of Pier 2 or 3, L_p = span length, ΔT = change in temperature of the structure

$$\Delta_{2,3} = (6 \times 10^{-6}/^{\circ}\text{F}) \times (5590\text{in}) \times (85^{\circ}\text{F}) = 2.85\text{inches}$$

This is an upper bound limit assuming no restraint due to the stiffness of the pier walls. It can be noted that Piers 2 and 4 have different dimensions and heights and therefore will have slightly difference displacement values.

The following (Table 6.2.1) are the pier displacement results from the DLM1 model and the RLM1 model. These results are reasonable relative to the 2.85” estimate, and they are in close agreement with each other, so they are considered acceptable.

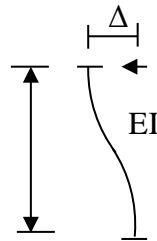
Table 6.1: Pier wall displacements at top under 85 °F temperature increase.

<u>Location</u>	<u>Displacement (in)</u>	
	<u>DLM1</u>	<u>RLM1</u>
P2D	-2.601	-2.699
P2U	-2.478	-2.584
P4D	2.539	2.533
P4U	2.660	2.659

In the table, “P2D” and “P2U” refer to the downstation and upstation blades of Pier 2 respectively, and “P4D” and “P4U” refer to the downstation and upstation blades of Pier 4 respectively.

6.3 Pier End-Moments

The moments at the ends of the piers must next be checked for reasonableness and correlation between models. In order to get an estimate of reasonable values for the moments at the ends of the pier walls, the displacements of the ends of the piers can be used to approximate the moment. If the pier wall was assumed to be fixed at both ends, a maximum moment could be found based on the upper displacement.



$$P = \frac{12EI\Delta}{l^3} \quad (12)$$

$$M_{max} = \frac{Pl}{2} \quad (13)$$

Figure 6.1: Estimate of appropriate moments at ends of piers.

Estimating I (moment of inertia) to be $2.63 \times 10^6 \text{ in.}^4$ and using the larger of the displacement values for Pier 4 from the preceding analyses, the moment at the base of Pier 4U turns out to be $5.72 \times 10^5 \text{ k-in}$ if no rotation is assumed. This gives a rough approximation of the expected

values when considering moments at the bottom of the pier walls. In this analysis, Pier 4U was arbitrarily chosen as the subject for verification purposes.

The results from analysis are as follows for a 85 °F uniform temperature expansion using linear material properties:

Table 6.2: a): Moments due to 85 °F temperature load.

Feature	Location	Moment (k-in)	
		DLM1	RLM1
P4U	Top face	5.32×10^5	4.42×10^5
P4U	Bottom Face	5.28×10^5	4.20×10^5
Footing Pier 4	Bottom Face	3.01×10^6	2.41×10^6

Table 6.2 b): Axial forces due to 85 °F temperature load.

Feature	Location	Force (k)	
		DLM1	RLM1
P4U	Top face	4333	3289
P4U	Bottom Face	4333	3247

Table 6.2 c): Shear forces due to 85 °F temperature load.

Feature	Location	Force (k)	
		DLM1	RLM1
P4U	Top face	2057	1662
P4U	Bottom Face	2057	1662

These values, while on the same order of magnitude are significantly different at the ends of the pier walls (by approximately 20%). The reason for this difference is the presense of local rotations in the RLM1 model. While the DLM1 model piers are fixed to a 90 degree angle with respect to the superstructure as well as the icebreaker, the RLM1 model allows for some relative rotation between the icebreaker-pier wall connection and the pier wall-superstructure connection. This relative rotation relieves a significant amount of moment in the pier walls that the DLM1 model does not take into account. The reason is that the pier walls in the DLM1 model are attached via rigid link elements based on the assumption that the diaphragm and the icebreaker are infinitely stiff compared to the slender pier walls. The local rotations arise from the stem walls being cast and supported on an elastic foundation (the icebreaker at the bottom and diaphragms at the top). This rotation can be accounted for in the DLM1 model through the use of rotational springs (DLM2 model), the influence of which will be investigated in a following section.

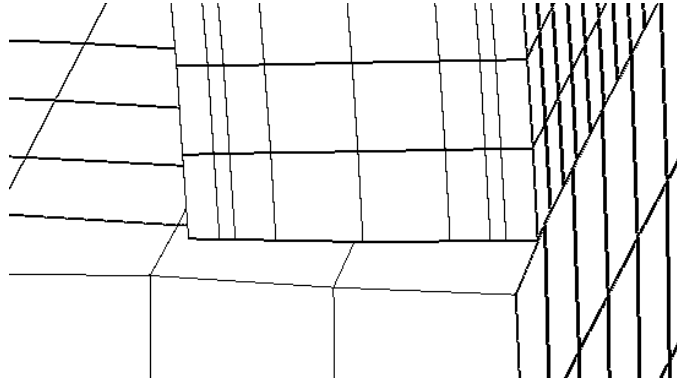


Figure 6.2: Local rotation of pier base due to elastic icebreaker.

It was desired to further confirm the hypothesis that the difference in moment at the ends of the piers was in fact due to the stated local rotations. To do so, each model was analyzed another time, but this time with fixed constraints at the bottom of the pier stem walls instead of the fixed constraints at the foundations. The results showed a significant convergence between the moment values of the two models. This agreement supports the argument regarding local rotations.

Table 6.3: Moments with pier wall base fixed (85° F expansion load).

Feature	Location	Moment (k-in)	
		DLM1	RLM1
P4U	Bottom Face	5.62×10^5	5.65×10^5

Another way of confirming this hypothesis is to compare the end rotations of the piers for the two models. The DLM1 predicted a rotation of 6×10^{-4} rad. and 1.032×10^{-11} rad. at the top and bottom faces of the pier walls, respectively, whereas the RLM1 predicted rotations of 8×10^{-4} and 1.2×10^{-3} . The bottom rotations were significantly different, which is the main contributor to the moment reduction in the RLM1 model. The values given by the RLM1 were further confirmed by imposing the displacement and rotation loads given by the RLM1 on the corresponding pier in the DLM1. The values agreed very favorably. This observation leads to the conclusion that the models were both giving appropriate values considering the modeling techniques at the piers.

6.4 Superstructure Bending

It was then desired to check the bending of the superstructures of the two models to verify that they were both behaving as expected. If both models show similar deflections, it is assumed that they are both valid. The self weight dead load was applied to each model for this purpose and deflections observed. As can be seen for self weight loads (Figure 6.3), the DLM1 and RLM1 models act very similarly under dead loads which shows the validity of the superstructure models as well as the models as a whole. One should note that the deflections in this case are not representative of the actual Wakota Bridge deflections due to the fact that neither model contains

post tensioning or construction loads at this point. The deflections are meant only for confirming modeling techniques. Because of this fact, the below graph does not indicate units for the deflections.

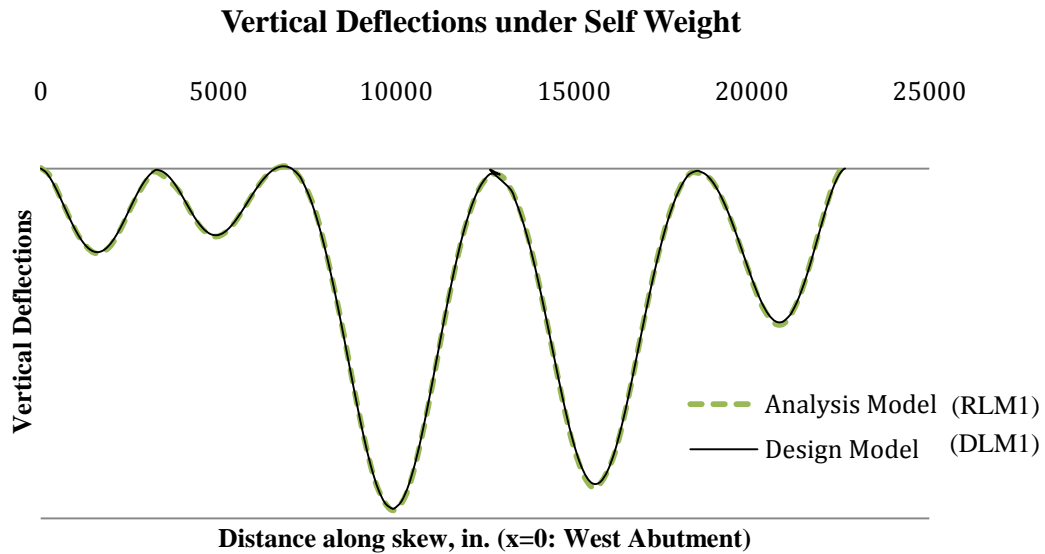


Figure 6.3: Qualitative vertical deflections of superstructure under self weight.

Because the DLM1 and RLM1 were shown to behave similarly, there was significant confidence that both were sufficiently accurate for continuing investigation of the design method for fixed twin wall flexible pier systems.

6.5 Rotational Spring Considerations

It was necessary to investigate the use of rotational springs as mentioned earlier in order to evaluate their effect on the modelling. In order to do this, rotational springs were applied to the bottom and top of the pier walls. To get a base estimate of what the rotational stiffness of the piers should be, the moment and rotation were simply taken from the RLM1 model and the relation $k_{\theta} = \frac{M}{\theta}$ used. For the base of Pier 4, this yields a value of 3.5×10^8 k-in/rad. While this was used as a starting value, actual values were obtained by guessing and checking the moments at the top and bottom of the 4 stem walls of Piers 2 and 4 until acceptable agreement (<1%) between the DLM2 and RLM1 models was achieved. The values used for the rotational spring stiffnesses were on the order of 10^8 k-in/rad for the top and bottom of the stem walls. It can be seen that all the values of forces and moments in the DLM2 model are very close to the RLM1 results for pier 4U. Forces at other piers exhibited similar correlation.

Table 6.4: a): Moments due to 85° F temperature load (with rotational springs).

Feature	Location	Moment (k-in)	
		DLM2	RLM1
P4U	Top face	4.43×10^5	4.42×10^5
P4U	Bottom Face	4.19×10^5	4.20×10^5
Footing Pier 4	Bottom Face	2.53×10^6	2.41×10^6

Table 6.4 b): Axial forces due to 85° F temperature load (with rotational springs).

Feature	Location	Force (k)	
		DLM2	RLM1
P4U	Top face	3736	3289
P4U	Bottom Face	3736	3247

Table 6.4 c): Shear forces due to 85° F temperature load with rotational springs).

Feature	Location	Force (k)	
		DLM2	RLM1
P4U	Top face	1675	1662
P4U	Bottom Face	1675	1662

For the purpose of further confirming the values of the DLM2 model with respect to the RLM1, another loading case was defined. This time a 120° F temperature loading was used. The results are not shown for brevity, but the values for moment were again within about a 1% correlation. A loading condition including self weight and a uniform thermal loading was also checked for correlation. The values, which are not shown for brevity, were again very close, this time within about 3% due mainly to the slight difference in dead load values in the two models because of slightly different geometries. In light of these comparisons, it was presumed that the DLM2 model (with rotational springs at the ends of the pier walls) was properly calibrated to the more descriptive RLM1. This DLM2 model could then be used to investigate the use of rotational springs at the ends of the piers in the CRD method, although the use of springs may not be practical in most designs.

Chapter 7. Evaluation of Common Refined Design Method

7.1 Introduction

It was then necessary to incorporate nonlinearity into the model representations. The CRD method for incorporating cracked sections can be applied to the DLM1 and DLM2 models and can be compared with the results of the RLM2 model, which incorporates nonlinear materials. In order to accomplish this, each model was analyzed with arbitrary loadings imposing lateral movements on the piers. Again, no time-dependent effects or post-tensioning were considered here, but in this case, nonlinear materials were used in the RLM2 model and the concrete stiffnesses in the DLM1 and DLM2 models were reduced via the iterative process described in the CRD method.

7.2 Pier Discretization Questions

The first question to be answered with respect to the CRD method concerned the number of stiffness updating segments that need to be used for each pier to produce an accurate result. Accuracy was determined by comparison to the cracking-capable RLM2 model. This is an important aspect of the analysis because a solution that is not refined correctly with respect to stiffness may lead to either an unconservative or an uneconomical design. On the other hand, a solution that is unnecessarily overrefined with respect to stiffness may result in valuable time lost for little or no gain. In order to investigate this question of the appropriate stiffness refinement (number of stiffness updating segments) and the accuracy of different refinement choices, a nominal temperature loading was applied to the bridge structure to initiate cracking in the piers. A number of stiffness refinement techniques were used in the DLM1 and DLM2 models and compared with the results of the nonlinear RLM2 model.

The procedure for the CRD method employed by most bridge designers is rather simple. The bridge model based on gross section properties is first analyzed with appropriate loading conditions. The moments along the pier height are then extracted and compared with a moment curvature plot for the pier wall section. This plot can be easily generated using a sectional analysis program. Response-2000 [26] was used for this purpose in this study. Stiffness was then updated and cracking accounted for by reducing Young's modulus at certain intervals along the height of each pier. The question to be addressed here concerned the number of stiffness updating segments along the height of the pier that are necessary, and whether this method generally yields accurate results.

First, the method for updating the pier stiffnesses as used in this study is summarized (CRD method).

- Analysis is conducted using gross section properties
- Moments are recorded at both ends of each stiffness segment
- End moments are averaged over the stiffness segment
- Updated curvature found based on a $M-\phi$ plot.
- Updated modulus found based on $E_{new} = \frac{M}{\phi * I_T}$ for each discretization

- Updated modulus is input into frame model to reduce stiffness
- Repeat with updated stiffnesses until convergence (i.e. change in modulus of elasticity < 1%)

In order to evaluate the accuracies of different discretization schemes, three different analyses were performed with 2, 4, and 6 stiffness updating segments along each pier of the DLM1 and DLM2 models. The geometry, loading, and mesh remained the same in all three analyses. The only variable in the analyses was the number of stiffness updating segments along the height of each pier wall. All material properties were identical in the two models for comparison purposes.

A nominal temperature loading of 100° F was applied first as the loading condition. This loading condition was chosen because it causes the pier walls to be well into their cracked state and the stiffnesses of the walls were significantly reduced.

The results for the RLM2 Pier 4 moments and forces are shown in Table 7.2.1. Again, Pier 4 was chosen as the focus of the study because it is the one that will experience the most cracking and the mesh refinement in the RLM2 model was refined adequately to provide convergent results.

Table 7.1: RLM2 moments and forces due to 100° F temperature load (Pier 4).

Location	Moment (*10 ⁵ k-in)	Axial Force (k)	Shear Force (k)
Pier 4U-top	4.034	-2589	1509
Pier 4U-bot	3.888	-2661	1509
Pier 4D-top	3.746	2821	1451
Pier 4D-bot	3.715	2684	1450

These values were then used as reference for comparison to the different values achieved through the refined design process (CRD method) described above and applied to the DLM1 and DLM2 models. The DLM1 and DLM2 models were both analyzed for a 100°F temperature loading with 2, 4, and 6 stiffness update segments spaced approximately evenly along the height of each pier. It should be noted that because the geometry of the piers changes along the height of the pier, average sectional properties were assumed for the stiffness updates that included varying geometry although the geometry itself remained unchanged. This averaging technique is accurate because the pier geometry changes in width only and therefore the stiffness (*EI*) scales linearly with the changing width. The results of the design method with a 100°F temperature loading applied to the initially unstressed structure are shown for the three chosen stiffness updating schemes for both the DLM2 model (only including 2 stiffness updates) and the DLM1 model in Table 7.2.2 (a-b) below.

Table 7.2: a): DLM1 (100°F, Pier 4).

# Stiffness Updates	Location	Moment (*10 ⁵ k-in)	Axial Force (k)	Shear Force (k)
2	Pier 4U-top	4.07	-3106	1608
2	Pier 4U-bot	4.10	-3106	1608
2	Pier 4D-top	3.97	3015	1543
2	Pier 4D-bot	3.94	3015	1543
4	Pier 4U-top	3.94	-3038	1564
4	Pier 4U-bot	4.01	-3038	1564
4	Pier 4D-top	3.77	3035	1499
4	Pier 4D-bot	3.85	3035	1499
6	Pier 4U-top	3.86	-2979	1549
6	Pier 4U-bot	4.01	-2979	1549
6	Pier 4D-top	3.70	2975	1485
6	Pier 4D-bot	3.85	2975	1485

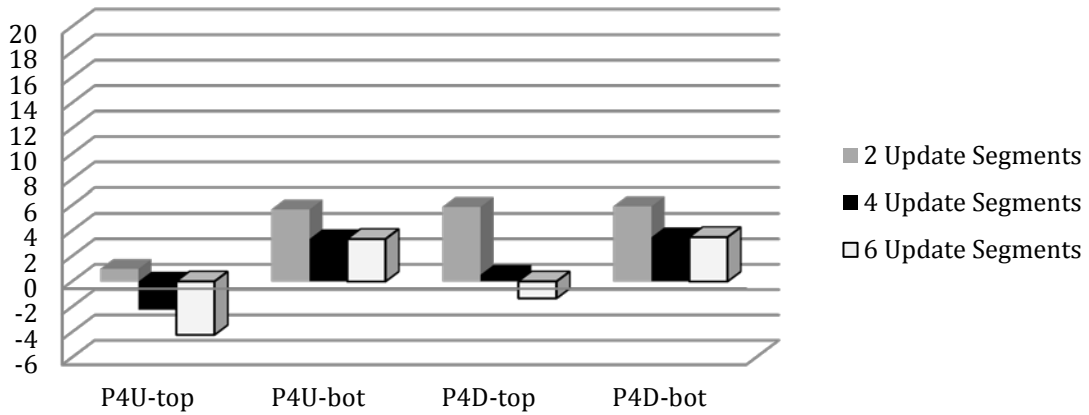
Table 7.2 b): DLM2 (100°F, Pier 4).

# Stiffness Updates	Location	Moment (*10 ⁵ k-in)	Axial Force (k)	Shear Force (k)
2	Pier 4U-top	3.60	-2696	-1380
2	Pier 4U-bot	3.50	-2696	-1380
2	Pier 4D-top	3.56	2689	1368
2	Pier 4D-bot	3.49	2689	1368

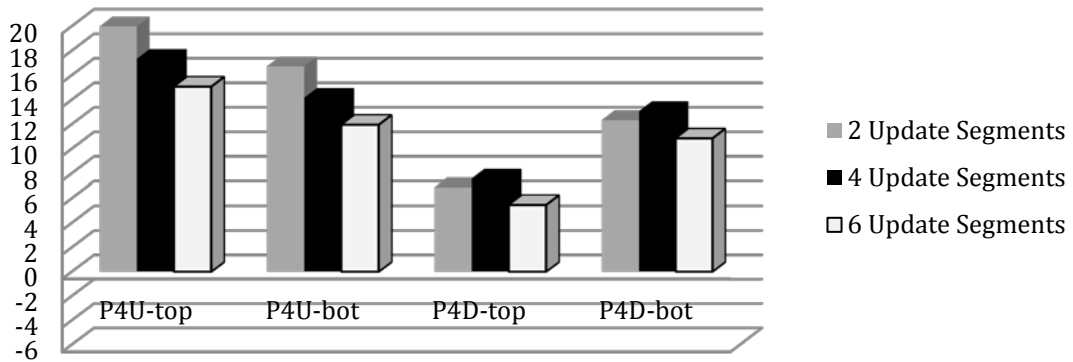
Although the particular numbers resulting from these analyses are artificial due to the fact that only a temperature load is applied, some significant observations can be drawn from the comparison of the results. First of all, it can be observed that the CRD method is far more accurate when rotational springs are not assigned at the ends of the pier walls (i.e. the DLM1 model is more accurate than the DLM2 model). The most likely reason for this is that the interaction of the connection is highly nonlinear, and employing a linear spring to model a connection that displays nonlinear behavior cannot yield good results for all loading cases. The influence of the connection interaction became less important as loading magnitude is increased. The DLM2 model is unconservative with respect to moment, although a more accurate value of axial force is achieved. Because of this unconservatism with respect to moment, which is the main contributor to stiffness reduction, and the fact that adding these rotational springs is not common or desirable in design practice, the DLM2 model was removed from discussion at this point.

It can also be observed that the values achieved using the DLM1 model and the CRD methodology are very close to the three-dimensional RLM2 analysis results, which incorporate the actual physical geometry of the bridge including rebar in the piers and nonlinear material behavior.

Deviation of Moments from RLM (%)



Deviation of Axial Forces from RLM (%)



Deviation of Shear Forces from RLM (%)

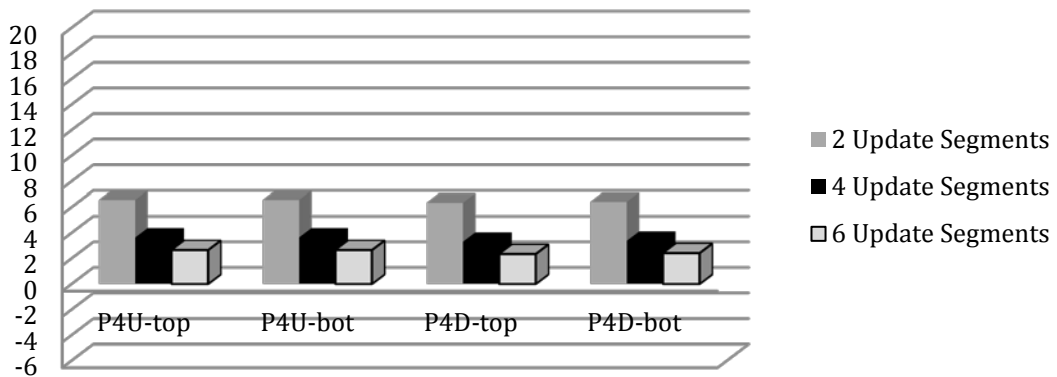


Figure 7.1: Pier force and moment comparison of DLM1 with CRD stiffness updating method and RLM2 with nonlinear materials.

It was slightly concerning that the axial force values were so much different in the DLM1 and RLM2 models whereas the moment and shear forces seem to converge more closely. However, this loading case does not include any direct axial loading on the piers although in actual bridge loadings, the piers will have significant axial loads induced by the vertical dead and live loads acting on the bridge. In order to investigate the case with both lateral and axial loads acting on the piers, the DLM1 and RLM2 were analyzed with a series of point loads acting on the top of the bridge deck concurrently with the temperature loading. The applied loading induced a very large axial compression load in one of the Pier 4 stem walls and a very small tensile axial force in the other (Table 7.2.3). What is seen in this situation is a very close correlation of axial forces in the stem wall with high compression forces (~4%) and poor correlation of axial forces in the stem wall with low tensile forces (~50%) when comparing the two modeling techniques. Therefore, the CRD method is shown to be more accurate for axial forces, as presumed, for load cases including gravity load effects. Also, it has been shown that the CRD method should be used very carefully with significant conservatism when dealing with small axial loads, as there could be a level of inaccuracy in the method.

Table 7.3: Results from axial and lateral loading.

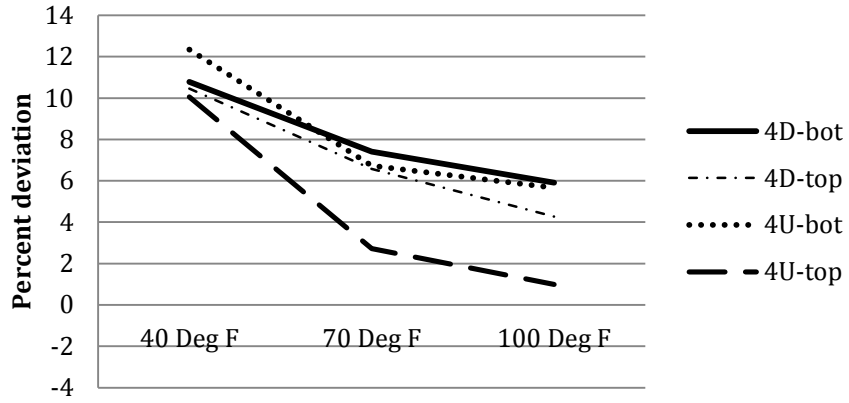
Model	Location	Moment (*10⁵ k-in)	Axial Force (k)	Shear Force (k)
DLM1	P4U-bot	3.56	409	1421
DLM1	P4D-bot	3.54	-9324	1418
RLM2	P4U-bot	3.12	818	1246
RLM2	P4D-bot	3.87	-9731	1500

The DLM1 model incorporating the CRD method tends to average the moments and shear forces of the more descriptive RLM2 model for loadings that produce large magnitude differences in stem wall axial loading between the twin pier walls. It is also recognized that the discrepancy of the DLM1 model axial forces compared to those of the RLM2 is equal in magnitude for both stem walls (~400 kips in this case). This difference could very well be produced by the modeling difference and not the CRD updating procedure. Overall, what is seen is that the DLM1 model using the CRD method distributes the forces more evenly over the two stem walls than does the RLM2 model. This behavior should be kept in mind when designing with this method and appropriate conservatism should be used to account for this effect.

7.3 Dependence on Loading Magnitude

Another aspect of the reduced stiffness design method is the question of how loading magnitude affects the accuracy. For the purpose of investigating this aspect, the uniform temperature loading condition as discussed earlier was analyzed for three different magnitudes: 40, 70, and 100° Fahrenheit. Again, no vertical loads were applied. The results are shown below for both 2 and 4 stiffness updates along each pier.

Moment Deviation vs. Temp. load - 2 Stiffness Segments



Moment Deviation vs. Temp. Load - 4 Stiffness Segments

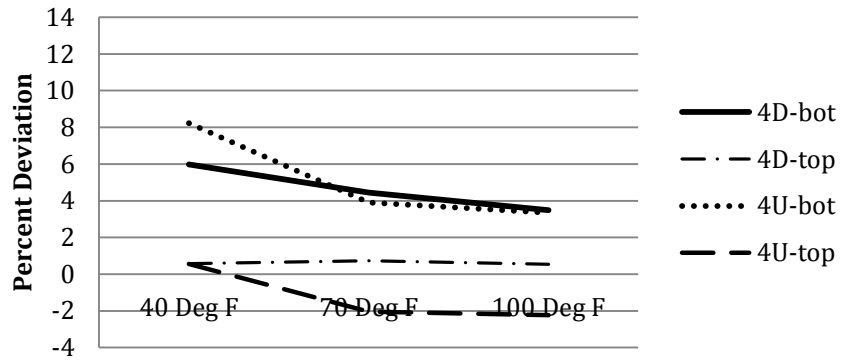
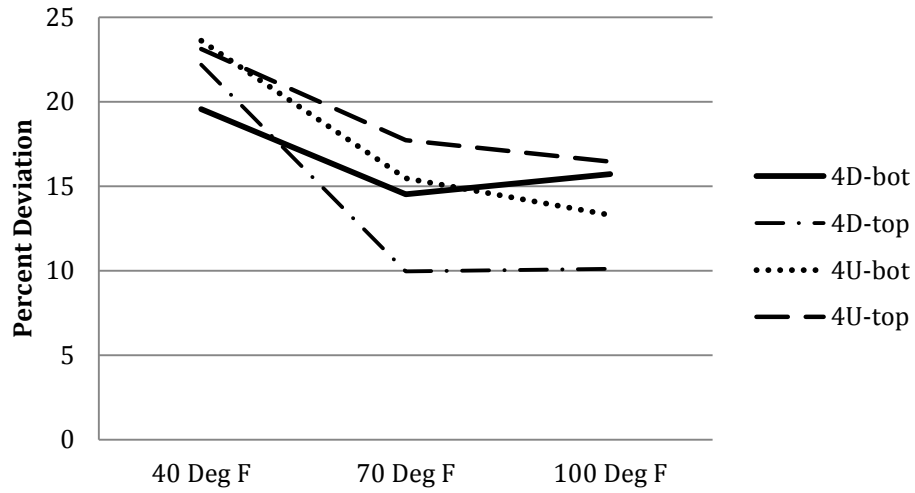


Figure 7.2: Moment deviation with respect to loading magnitude using: 2 Stiffness Segments (top), 4 Stiffness Segments (bot).

Axial Force Deviation vs. Temp. Load - 2 Stiffness Segments



Axial Force Deviation vs. Temp. Load - 4 Stiffness Segments

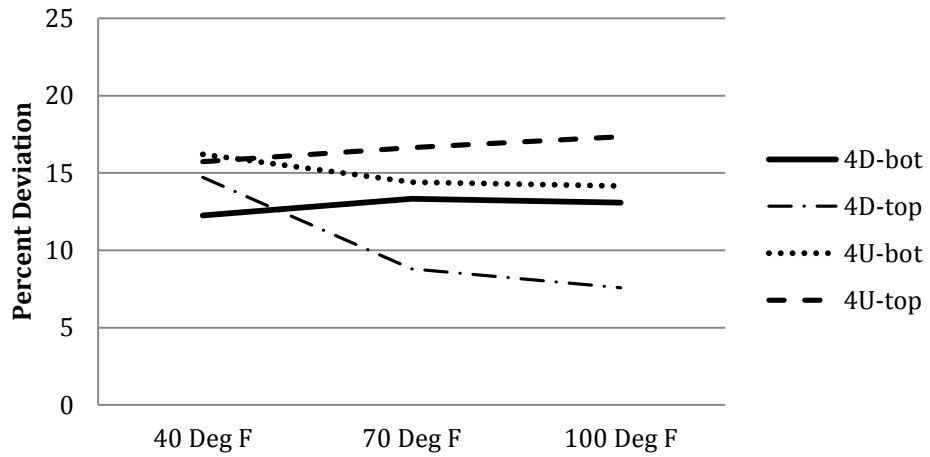


Figure 7.3: Axial force deviation with respect to loading magnitude using: 2 Stiffness Segments (top), 4 Stiffness Segments (bot).

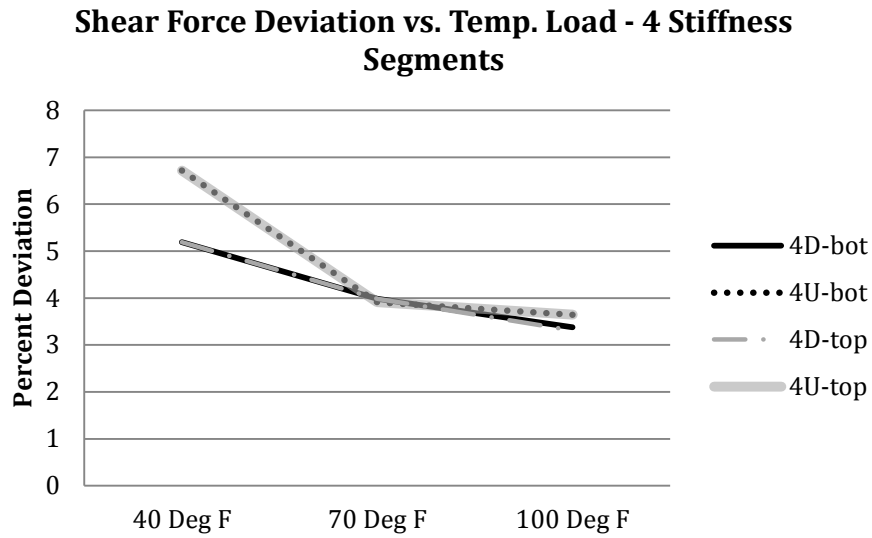
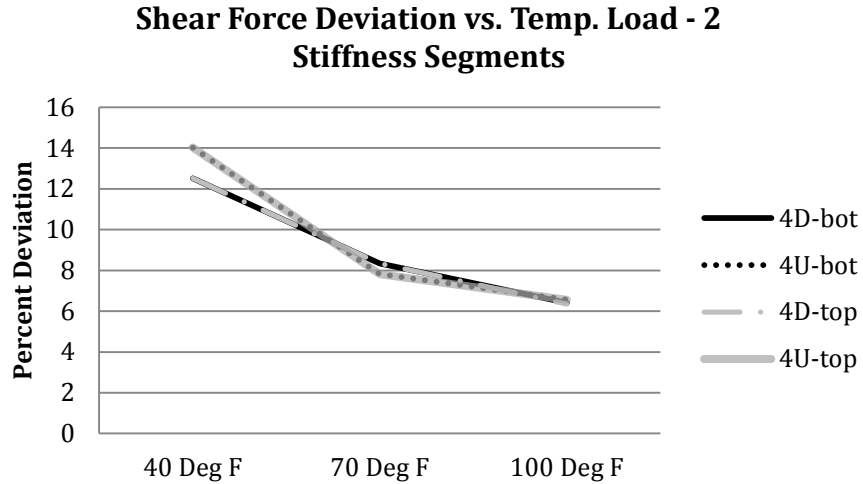


Figure 7.4: Shear force deviation with respect to loading magnitude using: 2 Stiffness Segments (top), 4 Stiffness Segments (bot).

It is clear from this data that moment and shear force get more accurate as the lateral loading increases, which is very beneficial because of the fact that design is performed at ultimate loading conditions. The reason for this convergence with increasing lateral load on the piers may be the effect of the complex connection characteristics between the stem walls and the pier base. Recall that previously, rotational springs were considered to account for this effect when no cracking was introduced because of large discrepancies in moment values at the faces of the stem walls. As cracking was introduced, the relative rotations of the stem walls with respect to the base of the pier becomes less important because the cracking releases large amounts of moment and thus the relative rotations become smaller and the models converge.

Axial forces are not as dependent on loading, as can be seen by the data. This is understandable because axial forces are not as affected by the lateral stiffness of the piers and rotations at the faces of the piers.

Chapter 8. AASHTO LRFD Design Option Evaluation

8.1 Introduction

The last objective of this report was to investigate the different design options presented in the AASHTO LRFD for accounting for the reduced section properties due to temperature loads in fixed pier walls (using a refined method (such as the CRD method) or the gross section method, as discussed in chapter 3) as well as the different temperature load application options. For the purpose of evaluating the different design options, the DLM3 model, which incorporates all post-tensioning and time-dependent loads was evaluated at ultimate loading conditions using each of the accepted design options stated by AASHTO LRFD.

8.2 Loading Considerations

In order to properly conduct this investigation, a brief discussion of the loading is needed. The case of maximum moment at the base of Pier walls 2 and 4 is needed when evaluating for lateral effects and cracked section properties. All strength load cases specified in the AASHTO LRFD were considered (Table 9.2.1) and the case producing the maximum moment at the pier stem wall bases was applied.

Table 8.1: AASHTO LRFD strength load cases.

Load Combination State	DC, DD, DW, EH, EV, ES, EL, PS, CR, SH	LL, IM, CE, BR, PL, LS	WA	WS	WL	FR	TU	TG	SE
Strength I	γ_p	1.75	1	-	-	1	1.2/0.5	γ_{TG}	γ_{SE}
Strength II	γ_p	1.35	1	-	-	1	1.2/0.5	γ_{TG}	γ_{SE}
Strength III	γ_p	-	1	1.40	-	1	1.2/0.5	γ_{TG}	γ_{SE}
Strength IV	γ_p	-	1	-	-	1	1.2/0.5	γ_{TG}	γ_{SE}
Strength V	γ_p	1.35	1	0.40	1	1	1.2/0.5	γ_{TG}	γ_{SE}

(Abbreviations are defined in the List of Abbreviations at the beginning of this document and in the following)

Loads considered:

1. *Dead Loads*

- Reinforced concrete (*DC*) 150 pcf
- Concrete wearing course (*DW*) 150 pcf
- Utilities (*DW*) 0 pcf

2. *Live Loads*

- HS25 vehicle load (*LL*) As specified by AASHTO LRFD
- Dynamic impact factor (*IM*) 33% vehicle axle weight
- Pedestrian (*PL*) 0.075 ksf

3. *Temperature (TU)*

Two methods

- 75 °F rise and fall
- 35 °F rise and 45 °F fall
- $\alpha = 6.0 \times 10^{-6} / ^\circ\text{F}$

4. *Creep and Shrinkage (CR, SH)*

CEB/FIP model for creep and shrinkage, 1990

5. *Construction Loads (EL)*

Included with load factor 1.0

6. *Load Factors*

- γ_p (Dead load factors)

Table 8.2: Dead weight load factors (γ_p).

<i>DC</i> (Dead load of structural Components)	1.25/1.5 for Strength IV
<i>DW</i> (Wearing surface and utilities)	1.5
<i>EL</i> (Locked in Forces)	1.0
<i>PS</i> (Secondary Forces)	1.0
<i>CR</i> (Creep)	1.0
<i>SH</i> (Shrinkage)	1.0

- Temperature gradient load factor, $\gamma_{TG} = 0$ for strength
- Settlement load factor, $\gamma_{SE} =$ not considered

Please note that a load factor of 1.0 is used for both creep and shrinkage although there is a range of values specified in the AASHTO LRFD. This was chosen because it was the load factor used for the design of the Wakota Bridge as presented in the design documents. Also note that the HS-25 vehicle load is larger than the current AASHTO LRFD specified HL-93 load. The use of the higher load produced an upper bound on the live load.

Through inspection and by running various analyses, Strength Load Case I was found to control the ultimate moment on the critical piers (Piers 2 and 4). As the controlling load case, all of the following analyses were conducted using Strength Load Case I.

8.3 Comparison of Options

As mentioned previously, there are two different options in the AASHTO LRFD and the MnDOT BDM for accounting for the reduced stiffness in the cracked piers,

- 1) Use a refined method (such as the CRD method) and load factor of 1.0 (AASHTO LRFD allows a load factor of 1.0 if the reduced section properties are accounted for with a refined analysis as stated in Article 3.4.1)
- 2) Use gross section properties and load factor of 0.5

There are also two different methods described in the AASHTO LRFD and the MnDOT BDM for the magnitude of uniform temperature change to be applied,

- 1) Procedure A: Use a temperature range centered at 45 °F (per MnDOT) with a decrease of 45 °F and increase of 35 °F [23].
- 2) Procedure B: Use the temperature contour maps, which define a 75 °F decrease and a 75 °F increase from a central 45 °F temperature for Minnesota [23].

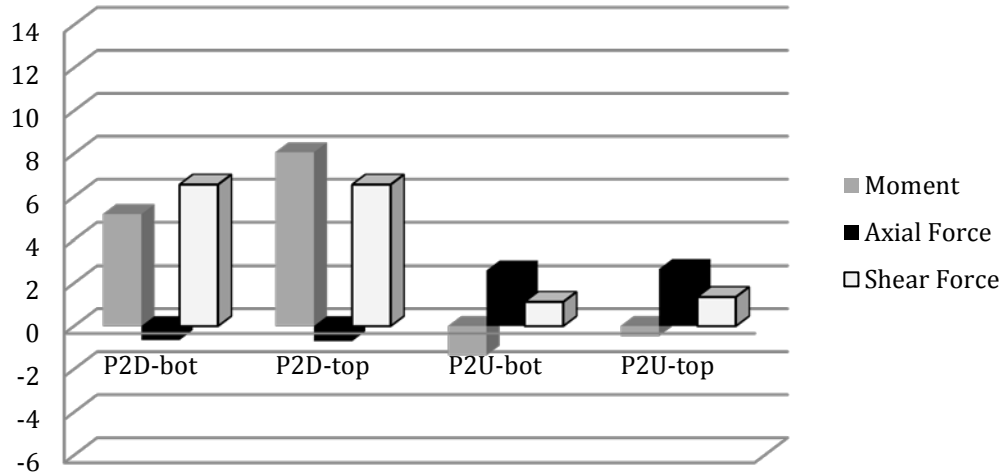
Because of this ambiguity and the fact that it is difficult for bridge designers to know which procedure is appropriate for their application, it was necessary to compare the different options for the case of the Wakota Bridge using the constructed staged construction model (DLM3) with applied ultimate loading conditions and appropriate foundation springs. This comparison sheds some light on the correlation of the options and provides insight into the appropriate design option when considering thermal loads.

8.3.1 Comparing Cracked Stiffness Methods

In order to compare the two cracked stiffness options, both Procedure A and Procedure B temperature application methods were analyzed using: 1) the refined method at ultimate conditions and 2) the gross section method using a load factor of 0.5. The maximum moment is likely to occur near the end of the bridge's service life when all creep and shrinkage have occurred and when the maximum negative temperature change is applied to the structure. The creep, shrinkage and temperature change will then contribute additively to the moments and forces at the ends of the pier walls. The results comparing the refined and gross section methods (Figure 8.1 and 8.2) show a correlation within 10% for the majority of the values, where the vertical axis is the percent difference in the results of the two design methods. In Figure 8.1-2, a positive value corresponds to the gross section stiffness method being conservative with respect

to the refined analysis method. It can be seen that the gross section method generally becomes less conservative with the higher temperature loading (Procedure B), although it is closer to the actual values. Note that these results show that the response of Pier 2 is opposite to that of Pier 4.

Pier 2 twin wall difference in end forces due to refined vs. gross section methods (%) - Procedure A



Pier 4 twin wall difference in end forces due to refined vs. gross section methods (%) - Procedure A

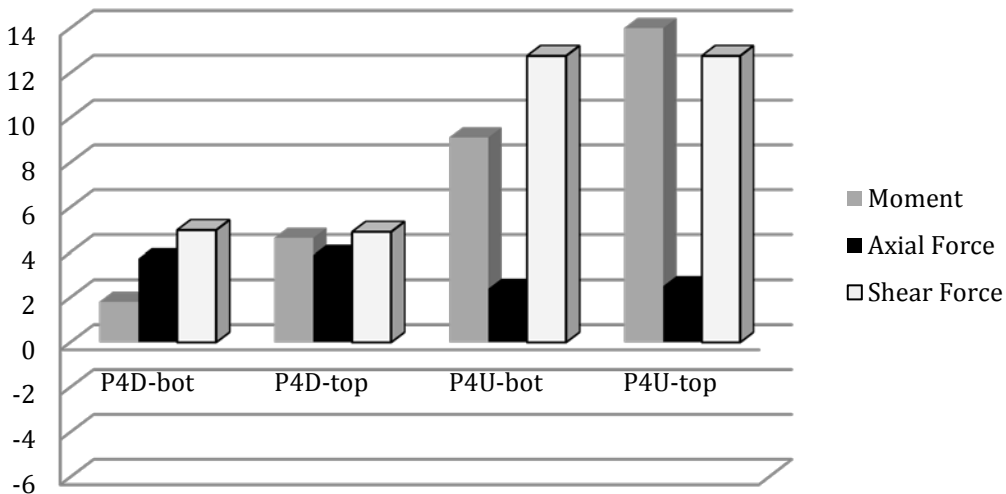
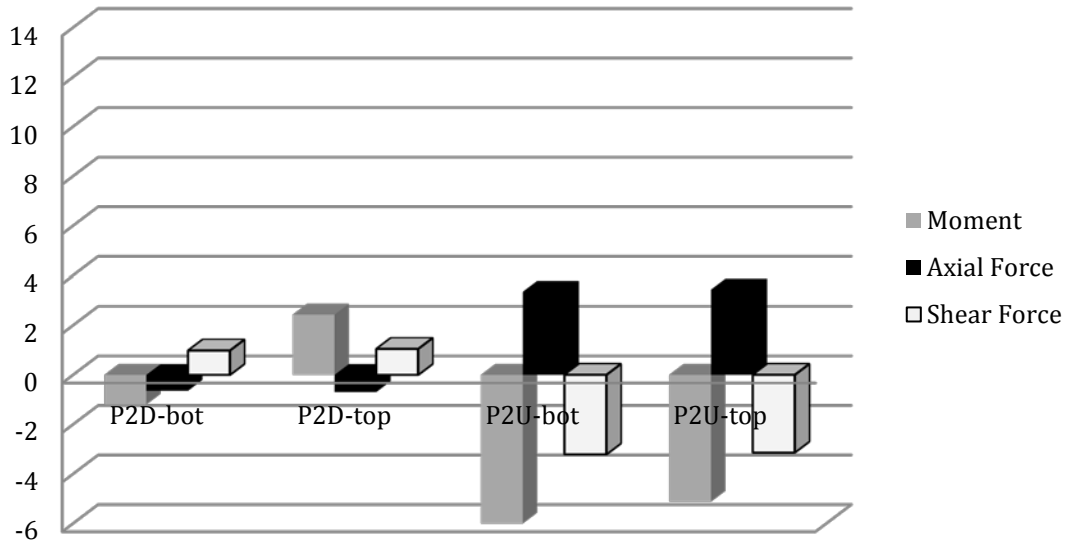


Figure 8.1: Comparison of predicted pier wall end forces and moments using the refined and gross section cracked section procedure (Temperature Procedure A).

Pier 2 twin wall difference in end forces due to refined vs. gross section methods (%) - Procedure B



Pier 4 twin wall difference in end forces due to refined vs. gross section methods (%) - Procedure B

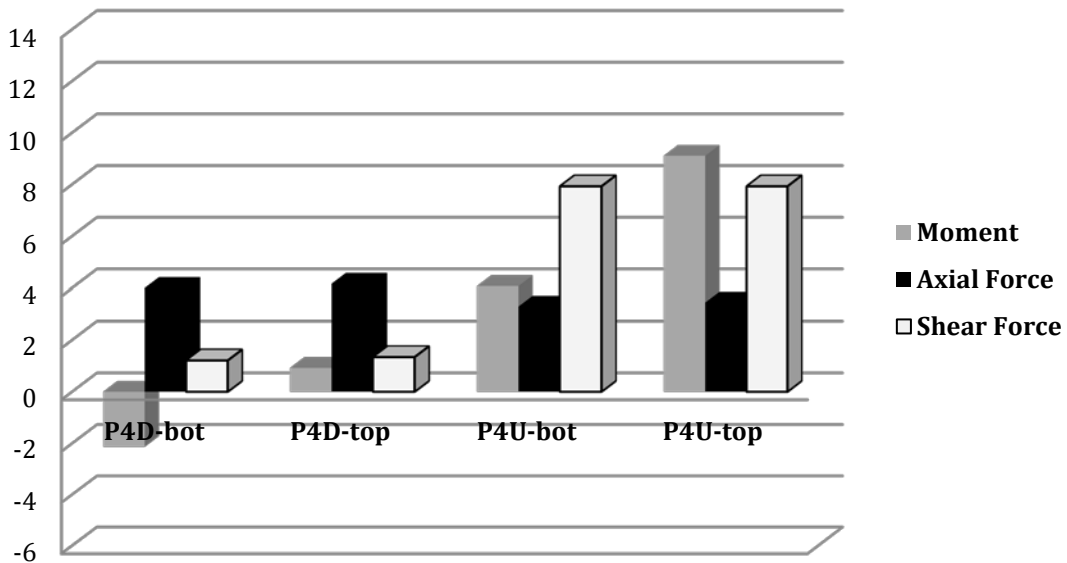


Figure 8.2: Comparison of predicted pier wall end forces and moments using the refined and gross section cracked section procedure (Temperature Procedure B).

8.3.2 Comparing Temperature Application Methods

It is intuitive that Procedure B will produce larger moments at the pier ends than Procedure A and that the piers will be more extensively cracked because of the larger temperature change imposed on the structure. Although this is the case, it was still useful to confirm this hypothesis

and compare the procedures and investigate the stiffnesses produced by each procedure. The differences (%) in moment produced by Procedure A and Procedure B are shown in Figure 8.3 below. As expected, there was a large difference in design forces between the design Procedure A and B although axial forces are similar.

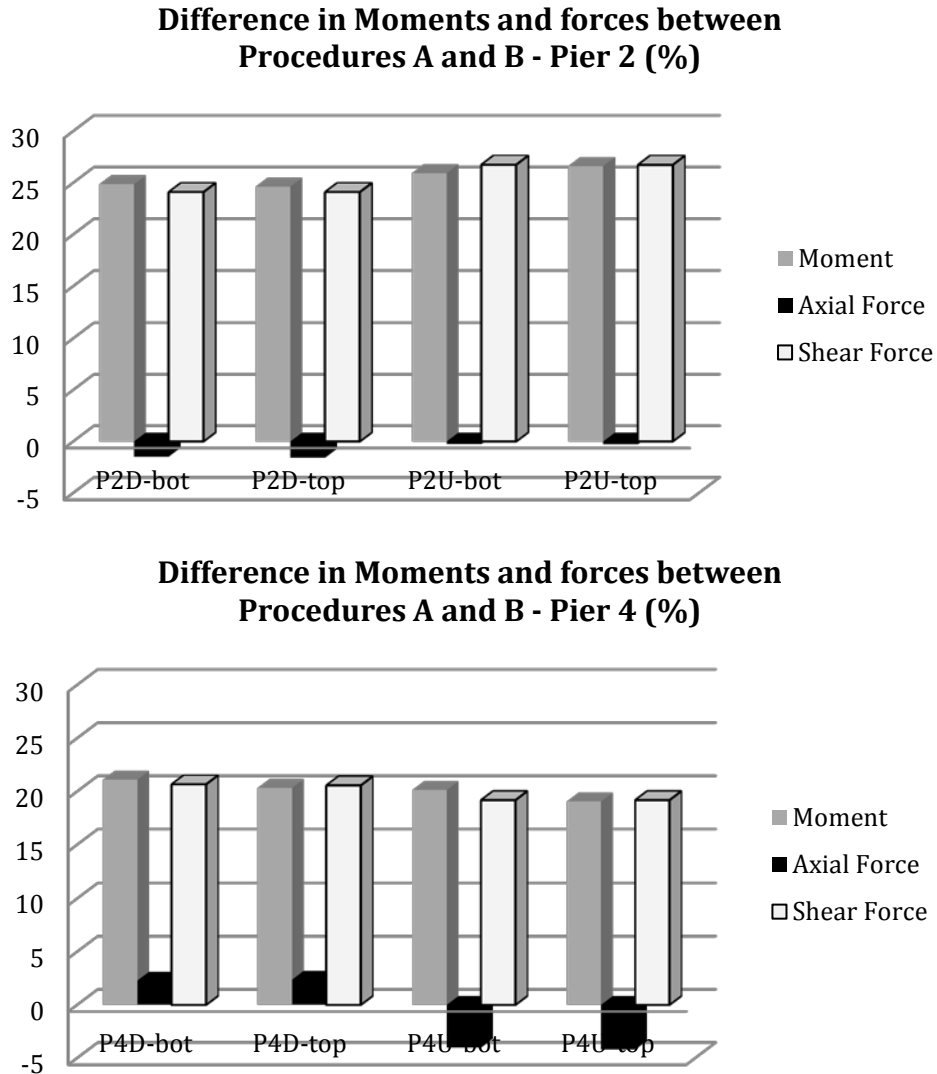


Figure 8.3: Percent difference in design forces when using Procedure B vs. Procedure A.

For future reference, it was considered valuable to document the relative stiffness values. For this purpose, the relative stiffnesses along the height of Piers 2 and 4 for the refined stiffness (CRD) method are reported in Table 8.3.2.1. Each pier wall was divided into 4 stiffness update segments, segment 1 being at the bottom and segment 4 being at the top.

Table 8.3: Pier wall relative stiffnesses.

Procedure (A or B)	Pier Wall	Section	$EI_{\text{Refined}}/EI_{\text{Gross}}$	Avg $EI_{\text{refined}}/EI_{\text{gross}}$
A	2D	1	0.66	0.78
		2	0.88	
		3	0.98	
		4	0.60	
	2U	1	0.68	0.8
		2	0.89	
		3	1.00	
		4	0.63	
	4D	1	0.63	0.75
		2	0.80	
		3	1.00	
		4	0.58	
	4U	1	0.62	0.74
		2	0.78	
		3	1.00	
		4	0.56	
B	2D	1	0.64	0.72
		2	0.79	
		3	0.88	
		4	0.57	
	2U	1	0.65	0.75
		2	0.81	
		3	0.94	
		4	0.58	
	4D	1	0.61	0.72
		2	0.73	
		3	1.00	
		4	0.55	
	4U	1	0.60	0.70
		2	0.71	
		3	0.95	
		4	0.54	

8.4 Discussion

Although all of the options discussed above are allowed by AASHTO LRFD, a balance between conservatism and accuracy must be kept in mind. It is seen through the above results that the methods for determining cracked section (refined and gross section) stiffnesses yield results that are relatively similar for the case of the Wakota Bridge ($< \sim 10\%$). Although this is the case, the refined method probably yields more accurate results due to the process of refinement, but the gross section method could be very valuable in preliminary design to get quick estimates of design force and moment demand.

It was also seen that the traditional Procedure (A) for the thermal design loads yields moments and shear forces that are significantly different than those produced by the more recently added Procedure B in the AASHTO LRFD, as was expected. Relative reduced stiffness values for the Wakota pier walls using four stiffness updates per wall can also be seen as reference for future design using the refined stiffness method. Having starting values for the relative stiffness can prove valuable when analyses take excessive computational time. A good estimate for the refined stiffness will speed up convergence and reduce the number of analyses that are needed for convergence.

Chapter 9. Summary, Conclusions, and Recommendations

9.1 Summary

In this work, a common refined design method for the analysis of lateral forces on flexible twin-walled bridge piers as seen on the Wakota Bridge in South St. Paul, Minnesota, was reviewed. Finite element models were produced in two different programs; ABAQUS, a research-level program that has the ability to perform nonlinear analyses for the cracking of concrete, and SAP2000, a design-level program often used in structural design. A common refined design method for the refinement of concrete reduced section properties in the piers was used with the design-level models, and parameters in the method were varied. The design-level model results were then compared to those produced by the research-level model with similar loading conditions. Results were affected by the varying parameters used in the refined method, but were found to correlate fairly well for the two modeling techniques.

A design-level staged construction model was also produced for the evaluation of pier moments and forces at ultimate design conditions. Using this model, different design options for lateral loads that are available in the AASHTO LRFD and the MnDOT BDM were evaluated and compared. The different options showed some similarities and some differences that should be noted by bridge design professionals.

An instrumentation plan was also developed for monitoring the lateral forces due to temperature changes and long-term deflections in the Wakota Bridge.

9.2 Conclusions

Several conclusions regarding thermal design and the refined design method can be drawn as a result of the finite element simulations that have been constructed and evaluated:

- 1) Based on a more accurate and descriptive modeling approach, the refined design method as defined in this study predicts shear forces and moments at the ends of fixed pier walls to a sufficiently accurate degree.
- 2) The refined method could have a degree of inaccuracy with respect to axial force predictions. This inaccuracy is reduced significantly with the presence of large initial axial loadings, as is the case with most bridge pier structures. But when dealing with small axial forces, this method could be inaccurate.
- 3) Rotational springs at the base of the pier walls could be important when calibrating the design model to actual bridge behavior with service loads and loads that produce very little cracking. The connection interaction becomes less important as loading increases.
- 4) The accuracy of the refined cracked section design method increases as the lateral loading magnitude on the piers increases. This is most likely because the cracking in the pier becomes more uniform and the pier wall to icebreaker connection becomes less significant.
- 5) Four and six stiffness update segments along the height of each pier wall was sufficient to achieve a rather accurate prediction of cracked section stiffness and pier forces and moments.

- 6) Foundation rotational and translational springs were found and approximate effective lengths were found for each case. For rotational springs, an effective length of approximately $L/3$ to L , L being the pile length, was found to estimate the rotational stiffness using simple beam formulas. The effective length increases as loading increases. For translational springs, an effective length of approximately L to $1.5L$ was found to approximate the translational stiffness using appropriate beam bending formulas. Note that these effective lengths were calculated specifically for the soil conditions at the Wakota Bridge.
- 7) The refined stiffness analysis method and gross section method produce similar results for the Wakota Bridge critical piers (to within about 10% correlation). This leads to the belief that both are reliable methods, although the refined method is more accurate and should be used in final designs. The gross section method with a load factor of 0.5 is a good method for preliminary design to achieve quick estimates of force demand on the piers in a fixed pier system, and also for approximating behavior of less complicated (i.e. “typical”) bridges. The refined analysis method with 1.0 load factor should be used with “non-typical” bridges.
- 8) Procedure A and Procedure B as defined in the AASHTO LRFD produce much different moment and force requirements at the base of the pier walls in Minnesota.

9.3 Recommendations

9.3.1 For Practice

- 1) The CRD Method, as discussed in chapter 3, is an appropriate method for the analysis of cracked section properties in concrete piers that experience cracking. This method, or a similar one, should be used when performing final designs concerning lateral forces on this type of bridge pier. Although this is the case, the gross section method, which employs a 0.5 temperature load factor, can be used for preliminary design, as it generally produces conservative results.
- 2) When using the CRD Method, a minimum of 4 stiffness updating segments should be used along the height of each pier wall.
- 3) The CRD method should be used with considerable conservatism when dealing with small axial loads as it may not be a precise predictor of axial load magnitude.
- 4) For conservatism, the magnitude of the uniform temperature load should be applied as per Procedure B in the AASHTO LRFD when considering longitudinal effects, as this procedure produces much larger moments at the ends of the pier walls. Ambient air temperature at the bridge will be compared to the internal concrete temperatures in the field portion of the research, allowing for a better judgment on whether the Procedure A or B temperature range is the best range to use for design in Minnesota. Even though the finite element models are three-dimensional representations that simulate both longitudinal and transverse effects, the focus of the study was on effects in the longitudinal direction, ∴ no judgment can be made on the effects of temperature loading in the transverse direction.

9.3.2 For Research

- 1) Field data was collected and will be compared to the results from this first half of the report in Phase 2. This will be completed using the described instrumentation plan and a monitoring of the Wakota Bridge. Using the DMCD, the field data should be calibrated to the model and the global behavior of the bridge should be studied.
- 2) Other bridges containing fixed flexible reinforced concrete piers should be studied to determine the applicability of this research to different geometries and locations around the country.

References

- [1] Peng, Yousong. *Analytical Solution to Temperature Variations in Highway Concrete Bridges Due to Solar Radiation*. International Conference on Transportation Engineering 2007, Chengdu, China, ICTE 2007. (2007).
- [2] Minnesota Department of Transportation. 2010. Web. 2010. <<http://www.dot.state.mn.us/metro/projects/wakota/>>.
- [3] HNTB, *Wakota Bridge Plans and Documents*. Oakdale, MN: MnDOT, 2007.
- [4] *Geokon Vibrating Wire Strain Gauge Manual - Model 4200/4202/4204/4210*. Lebanon, NH: Geokon, Inc, 2008.
- [5] Unimeasure, *Linear Potentiometer, Position Transducer, Displacement Sensors, String Pot*. Accessed 25 May 2010. <<http://unimeasure.com/>>.
- [6] *AVW200 User's manual*. Logan, UT: Campbell Scientific, 2009.
- [7] Cavallin, Jeffrey. Personal interview. 9 April. 2010.
- [8] Burgess, Chris. Personal interview. 26 Jan. 2010.
- [9] American Concrete Institute, *Building code requirements for structural concrete and commentary*. ACI Standard ACI 318-08. Farmington Hills, MI; 2008.
- [10] *SAP2000*. Vers. 14. Berkeley, CA: Computers and Structures, Inc, 2009.
- [11] Isenberg, J., ed. *Finite Element Analysis of Reinforced Concrete Structures II*. New York, NY: American Society of Civil Engineers, 1993.
- [12] Wang, Taijun. "Nonlinear finite element analysis of concrete structures using new constitutive models." *Computers & Structures* 79.32 (2001): 2781-2791.
- [13] Jiang, J. "Nonlinear analysis of reinforced concrete slabs by a discrete finite element approach." *Computers & Structures* 65.4 (1997): 585-592.
- [14] Nayal, Rim, and Hayder, A. Rasheed. "Tension Stiffening Model for Concrete Beams Reinforced with Steel and FRP Bars." *Journal of Materials in Civil Engineering* Nov/Dec (2006): 831-41.
- [15] Stramandinoli, Renata S.B., and Henriette L. La Rovere. "An efficient tension stiffening model for nonlinear analysis of reinforced concrete members." *Engineering Structures* 30 (2008): 2069-080.
- [16] *ABAQUS Analysis User's manual*. Providence, RI: Dassault Systems, 2008. ABAQUS Documentation. Web.

- [17] Sietta, Anna, Roberto Scotta, and Renato Vitaliani. "Stress analysis of concrete structures subjected to variable thermal loads." *Journal of Structural Engineering* 121.3 (1995): 446-57.
- [18] Branco, F.A., and Mendes, P.A. (1993). "Thermal actions for concrete bridge design." *J. Struct. Engrg.*, ASCE, 119(8), 2313-1331.
- [19] Shushkewich, Kenneth W. "Design of segmental bridges for thermal gradient." *PCI Journal* 43.4 (1998):120-137.
- [20] Priestley, Nigel. "Design of Concrete Bridges for Temperature Gradients." *ACI* May (1978): 209-16.
- [21] Roeder, Charles W. "Proposed Design Method for Thermal Bridge Movements." *Journal of Bridge Engineering* January/February (2003): 12-19.
- [22] American Association of State Highway and Transportation Officials, ed. *AASHTO LRFD Bridge Design Specifications*. 4th ed. Washington, DC: AASHTO, 2007.
- [23] MnDOT Bridge Office, comp. *LRFD Bridge Design Manual*. Oakdale, MN: MnDOT, 2009.
- [24] *AASHTO Guide Specifications: Thermal Effects in Concrete Bridge Superstructures*. Washington, DC: AASHTO, 1989.
- [25] *CATIA*. Vers. 5 Student. Dassault Systems, 2009. Computer software.
- [26] *Response-2000*. Vers. 1.0.5. 2000.
- [27] *Influence of Footing Fixity Constants of Support Reactions*. 2009. TS. MnDOT, Saint Paul, MN.
- [28] "Wakota Bridge." *Wikipedia*. Accessed 25 May 2010. <<http://www.wikipedia.org>>.

Appendix A: Wakota Bridge Monitoring Program Instrumentation Plan

A.1 Background

This appendix describes the instrumentation plan for the Minnesota Department of Transportation (MN/DOT) Bridge 82855. The instrumentation plan contained here is part of a monitoring program aimed at monitoring the effects of temperature variations on the forces in the bridge piers as well as the superstructure of Bridge 82855. This appendix describes the instrumentation that has been placed in the piers and superstructure as well as the data acquisition system that was installed to collect the data transmitted from the instruments. Note that this Appendix was originally submitted as a separate deliverable for the Wakota Monitoring Project. As such, some of the information presented here is repeated from that presented in Chapter 2 of this report. No information was excluded so as not to remove context from additional instrumentation information presented in this Appendix.

A.2 Rationale

The plan described in this document provides instrument descriptions and specifications, locations and installation notes as well as data acquisition equipment descriptions, specifications, approximate installation locations and installation notes. The basic premise for the instrumentation plan is that daily and seasonal temperature changes generate fluctuations in the length of the bridge superstructure. Due to bridge support conditions, the length fluctuations generate changes in member forces. Of primary interest to the monitoring program are the magnitudes of the changes in pier axial forces, bending moments and shear forces. Likewise, the pier support conditions will generate changes in forces and moments in the box girder superstructure sections, causing axial strains in the superstructure members.

The instrumentation described here is designed to capture the behavior of the changing forces, moments, and strains. The gauges are placed in positions that are assumed to be most affected by the change in length of the superstructure due to thermal loading caused by the changing of temperature throughout the seasons and thus having the largest change in axial strains. The positions determined to capture this behavior are in Pier 2 and 4 in the substructure and Spans 3 and 4 in the superstructure. These positions were determined because Pier 1 contains an expansion bearing and Pier 3 is close to the calculated neutral point in the superstructure longitudinal displacement, therefore these piers are assumed to be exposed to small strain changes. Also, since Spans 1, 2, and 5 have at least one end of the span containing an expansion bearing (each abutment contains an expansion bearing), these three spans are assumed to also undergo a small strain change due to temperature loading. All pier instrumentation is limited to the pier walls. Strain changes due to temperature fluctuations are assumed to be much smaller in the icebreakers compared to the other components of the pier. In addition, the piles were not selected for instrumentation due to complications associated with measurement of pile strains (i.e., saturated conditions, potential gauge damage during pile driving, and uncertainty associated with soil-pile interaction).

A.3 Pier Instrumentation

A.3.1 Overview

The two piers to be instrumented (Piers 2 and 4) are shown in the elevation of Bridge 82855 in Fig A.3.1.1. The instrumentation consists of 44 vibrating wire strain gauges installed in the walls of Piers 2 and 4, and the PVC conduit needed to carry the wires to the top of the pier walls. At each instrumented pier, both walls (upstation and downstation) are instrumented at two elevations that are near the top and bottom of the pier walls. The instrumented sections are located 1000 mm away from the top and bottom of the pier walls to avoid disturbance of the strain fields and the potential for cracking posed by member termination. The top instrumented sections for each pier are at the same elevation for both walls. The bottom instrumented sections for both walls of both piers are the same elevation (214 m).

Pier 2 Instrumented

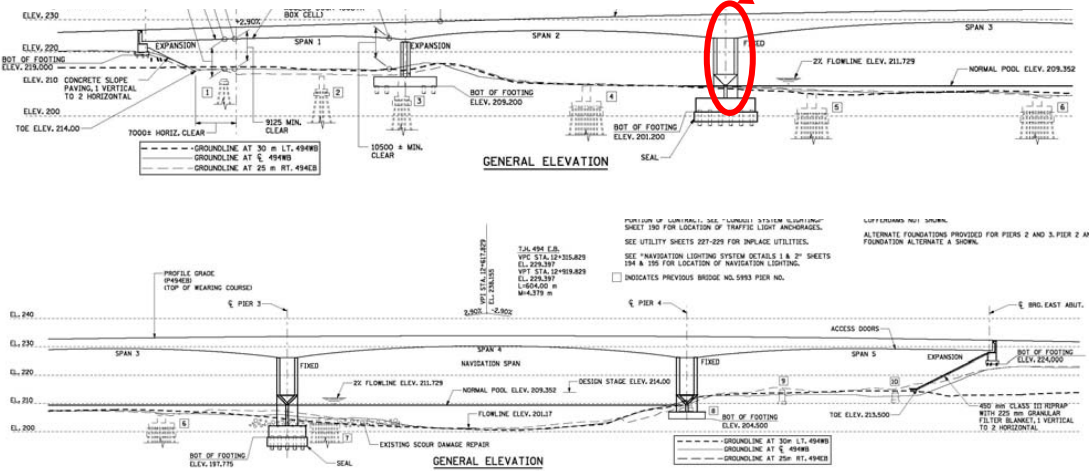


Fig A.3.1.1: Elevation of Mn/DOT Bridge 82855 with instrumented Piers 2 and 4.
All units in mm unless shown otherwise. 1 mm = 0.0039 in., 1 m = 3.28 ft.

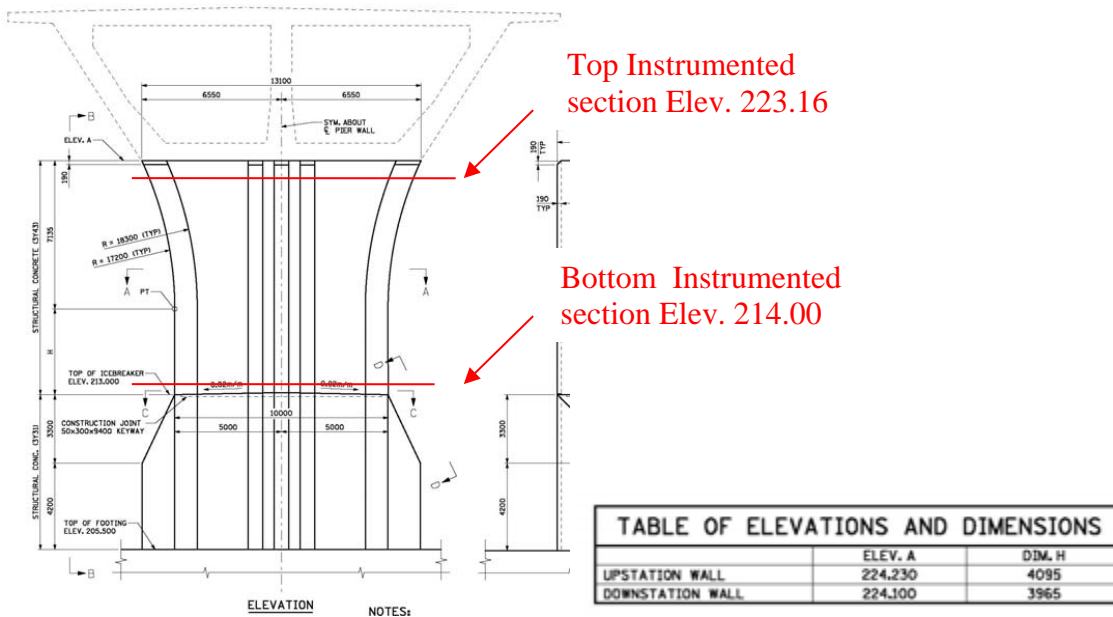


Fig A.3.1.2: Pier 2 instrumented sections. All units in mm unless shown otherwise. 1 mm = 0.0039 in., 1 m = 3.28 ft

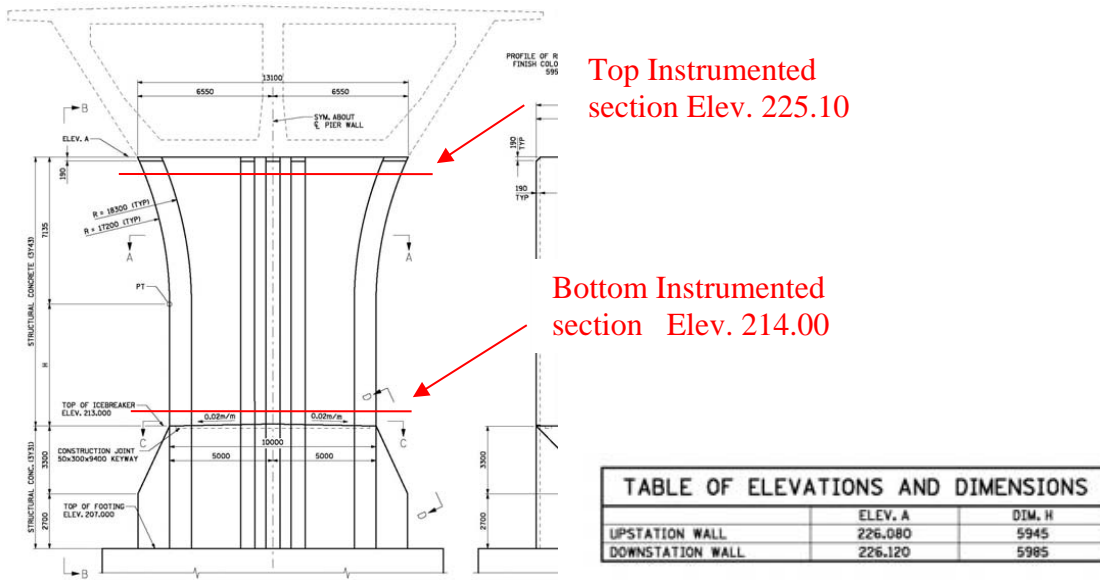


Fig A.3.1.3: Pier 4 instrumented sections. All units in mm unless shown otherwise. 1 mm = 0.0039 in., 1 m = 3.28 ft

A.3.2 Instrument Locations and Designations

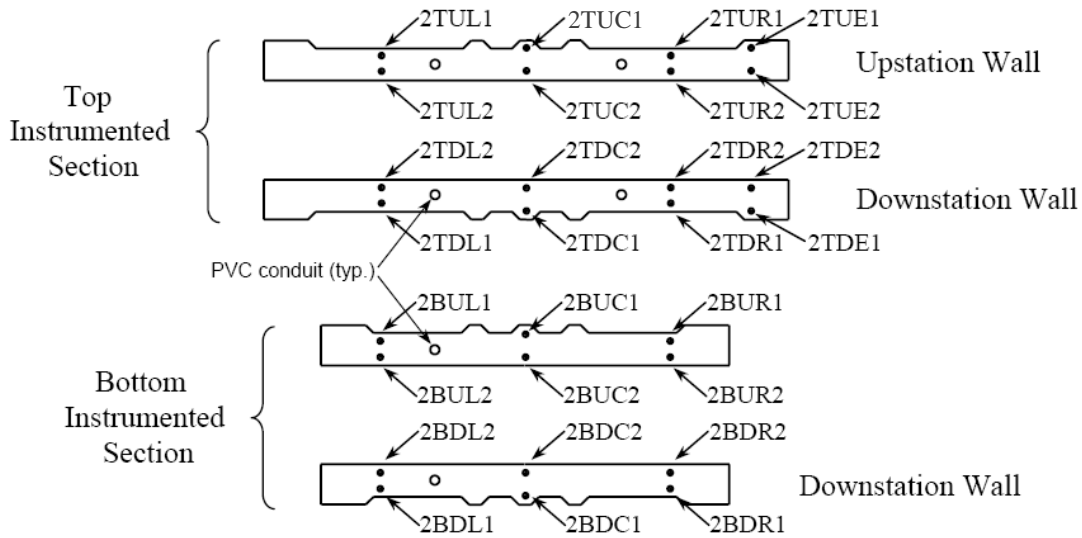


Fig A.3.2.1: Gauge designations for Pier 2.

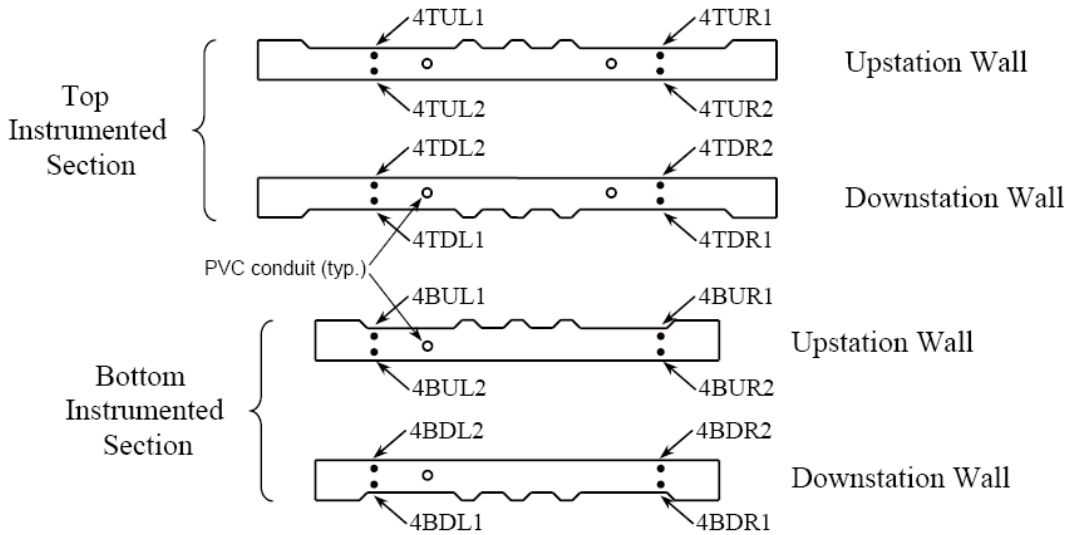


Fig A.3.2.2: Gauge designations for Pier 4.

Instrument locations along wall width are given in Fig A.3.2.2 relative to wall centerline. Only one half of the walls are shown by virtue of symmetry. The gauges in the “center” position (2TUC1, 2TUC2, 2TDC1, 2TDC2, 2BUC1, 2BUC2, 2BDC1, 2BDC2) are slightly off center. The location of the long PVC conduit in Fig A.3.2.3 for running the bottom section gauge leads to the top of the pier was modified an unspecified distance during construction due to the fact that the leads of the gauges farthest away from the PVC conduit were too short to travel the specified distance. To remedy this, the long PVC was moved closer to the center point of the pier, thus shortening the distance of travel of the leads farthest away.

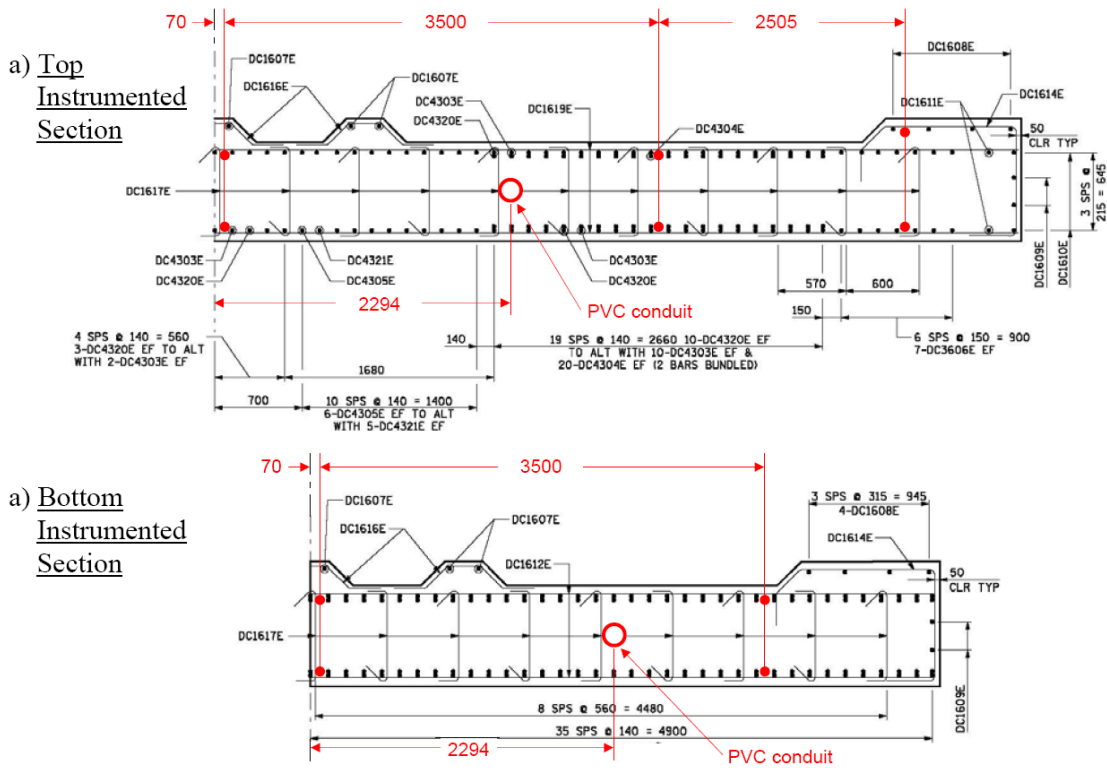


Fig A.3.2.3: Gauge Locations along Wall Width. All units in mm unless shown otherwise. 1 mm = 0.0039 in., 1 m = 3.28 ft

Each gauge has a five-digit designation with the first digit being the pier number (2 or 4). The second digit defines the top (T) or bottom (B) instrumented section. The third digit designates the upstation (U) or downstation (D) wall. The fourth digit indicates the location of the gauge along the width of the wall (L – left, C – center, R – right, E – right edge). The last digit indicates the nearest face (1 – rusticated, 2 – flat).

Table A.3.2.1: Gauge Designations. All units in mm unless shown otherwise. 1 mm = 0.0039 in., 1 m = 3.28 ft

Gage	Pier	Section	Wall	Location	Face	Distance [†]		
2TUL1	2	top (T)	upstation (U)	left (L)	rusticated (1)	-3570		
2TUC1				center (C)		+70		
2TUR1				right (R)		+3570		
2TUE1				edge (E)		+6075		
2TUL2				left (L)		flat (2)	-3570	
2TUC2			center (C)	+70				
2TUR2			right (R)	+3570				
2TUE2			edge (E)	+6075				
2TDL1			downstation (D)	left (L)	rusticated (1)		-3570	
2TDC1				center (C)		+70		
2TDR1		right (R)		+3570				
2TDE1		edge (E)		+6075				
2TDL2		left (L)		flat (2)		-3570		
2TDC2		center (C)			+70			
2TDR2		right (R)			+3570			
2TDE2		edge (E)			+6075			
2BUL1		bottom (B)			upstation (U)	left (L)	rusticated (1)	-3570
2BUC1				center (C)		+70		
2BUR1			right (R)	+3570				
2BUL2			left (L)	flat (2)		-3570		
2BUC2	center (C)		+70					
2BUR2	right (R)		+3570					
2BDL1	downstation (D)		left (L)		rusticated (1)	-3570		
2BDC1			center (C)	+70				
2BDR1			right (R)	+3570				
2BDL2			left (L)	flat (2)		-3570		
2BDC2			center (C)			+70		
2BDR2			right (R)		+3570			
4TUL1			4		top (T)	upstation (U)	left (L)	rusticated (1)
4TUR1				right (R)			+3570	
4TUL2		left (L)		flat (2)			-3570	
4TUR2	right (R)	+3570						
4TDL1	downstation (D)	left (L)				rusticated (1)	-3570	
4TDR1		right (R)					+3570	
4TDL2		left (L)		flat (2)			-3570	
4TDR2		right (R)					+3570	
4BUL1	bottom (B)	upstation (U)		left (L)	rusticated (1)	-3570		
4BUR1				right (R)		+3570		
4BUL2				left (L)		flat (2)	-3570	
4BUR2				right (R)			+3570	
4BDL1				downstation (D)			left (L)	rusticated (1)
4BDR1		right (R)			+3570			
4BDL2		left (L)	flat (2)		-3570			
4BDR2		right (R)			+3570			

[†]Distance in mm from centerline along wall width (+/- indicates right/left of centerline).

A.3.3 Gauge Description

All gauged locations are instrumented with Model 4200 vibrating wire strain gauges manufactured by the Geokon Inc. (www.geokon.com). These gauges are designed for direct embedment in concrete and manufacturer specifications are given in Table A.3.3.1. The gauges have wire leads attached by the manufacturer and two different wire lengths are used. The gauges that are installed in the top sections of the piers have a 35-ft wire lead, and those that are installed in the bottom sections have a 70-ft lead.

Table A.3.3.1: Gauge Specifications

Parameter	Value
Standard Range	3000 $\mu\epsilon$
Resolution	1.0 $\mu\epsilon$
Accuracy	$\pm 0.5\%$ (of full scale)
Nonlinearity	$< 0.5\%$ (of full scale)
Temperature Range	-20°C to $+80^{\circ}\text{C}$
Active Gage Length	153 mm
Thermal Expansion Coefficient	12 ppm/ $^{\circ}\text{C}$
Coil Resistance	180 Ω
Cable Type	4 conductor shielded 22 awg

A.3.4 Installation

Installation of the strain gauges is made to adjacent reinforcing bars using steel wire ties. The gauges have a barbell configuration (Fig A.3.4.1) which facilitates the installation by tying steel wires ties around the heads of the gauges. The gauges are placed in a stable configuration by using at least two wire ties at each end (e.g., horizontal wires tied to adjacent vertical reinforcing bars and vertical wires tied to adjacent horizontal reinforcing bars). The gauges are placed in a vertical configuration in the same plane as the vertical reinforcing bars, and at the horizontal locations as specified in Table A.3.2.1. The center of the gauges coincides with the elevations for the corresponding section elevation (Fig A3.2.1.2-3) and the wire leads are pointing downward in all installed gauges.



Fig A.3.4.1: Geokon Vibrating Wire Strain Gauge Model 4200

All gauges placed in the top sections of the wall piers (i.e., with second digit “T” in the designations given in Table A.3.2.1 and Fig A.3.2.1-2) have a 35-ft wire lead installed by the manufacturer. The gauges in the bottom sections (i.e., with second digit “B” in the designations given in Table A.3.2.1 and Fig A.3.2.1-2) have a 70-ft wire lead. The wire leads are extended to the corresponding PVC conduit for that section (“top” sections are serviced by the short conduit

and “bottom” sections are serviced by the long conduit). The wire leads are tied to the vertical bars using wire ties and leaving enough slack lead wire to provide stress relief. Care was taken when tying the wire leads to the reinforcing bars to prevent the plastic insulation in the wire leads from being damaged. The wire leads were inserted into the PVC conduit and extended to the top of the wall pier and an elbow was attached so as to facilitate the leads exiting the stem wall diaphragm in a horizontal configuration, where all lead wires were wound into a coil and taped securely to the outside of the PVC conduit. The top of the PVC was covered with duct tape to prevent concrete from dropping into the conduit during casting. After casting, the PVC conduits were cut flush with the inner diaphragm wall of the box girder and the leads were trimmed. The leads were left accessible for future splicing and the installation of data acquisition equipment.

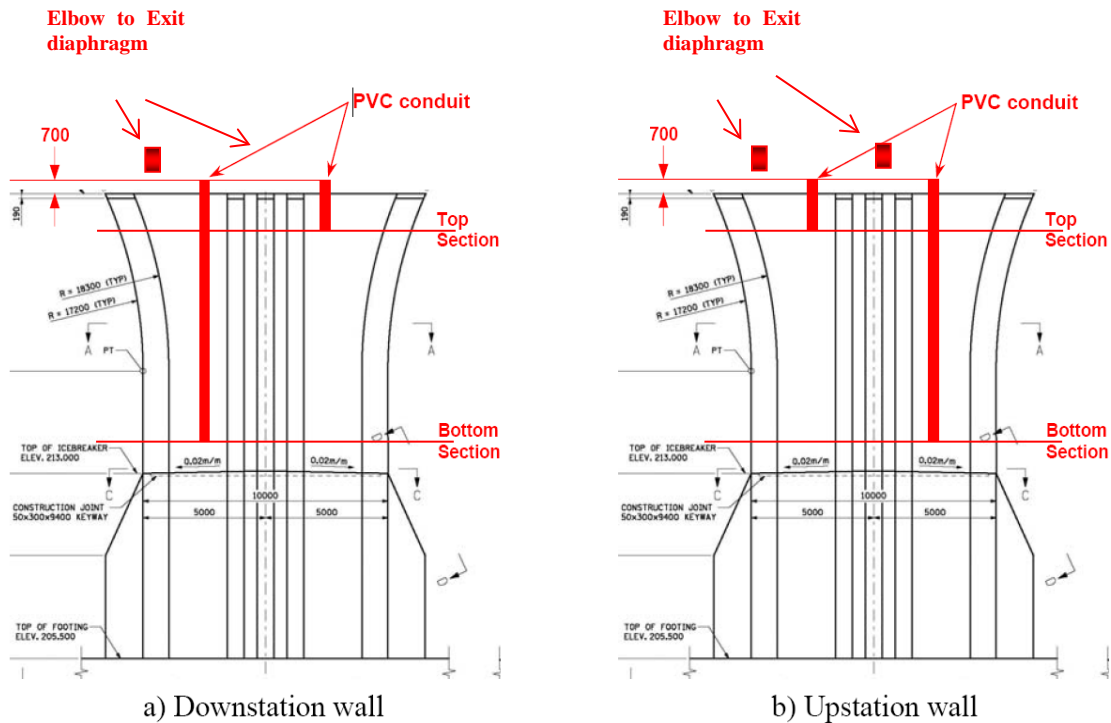


Fig A.3.4.2: View of Pier 2 with the PVC conduit as seen from the rusticated face. All units in mm unless shown otherwise. 1 mm = 0.0039 in., 1 m =3.28 ft

Prior to the installation of the strain gauges, the PVC conduit was installed as shown in Fig A.3.4.2. The PVC conduit was cut into straight lengths as indicated in Table A.3.4.3 and they were placed such that the top of the conduit protruded 700 mm above the top of the pier walls. An elbow was attached to the straight PVC to facilitate a horizontal exit configuration from the corresponding pier wall diaphragm. The PVC conduit was tied to reinforcing bars at sufficient locations along its height to prevent movement of the conduit during the casting process. The bottom of the conduit was covered with duct tape to prevent concrete from entering during casting.

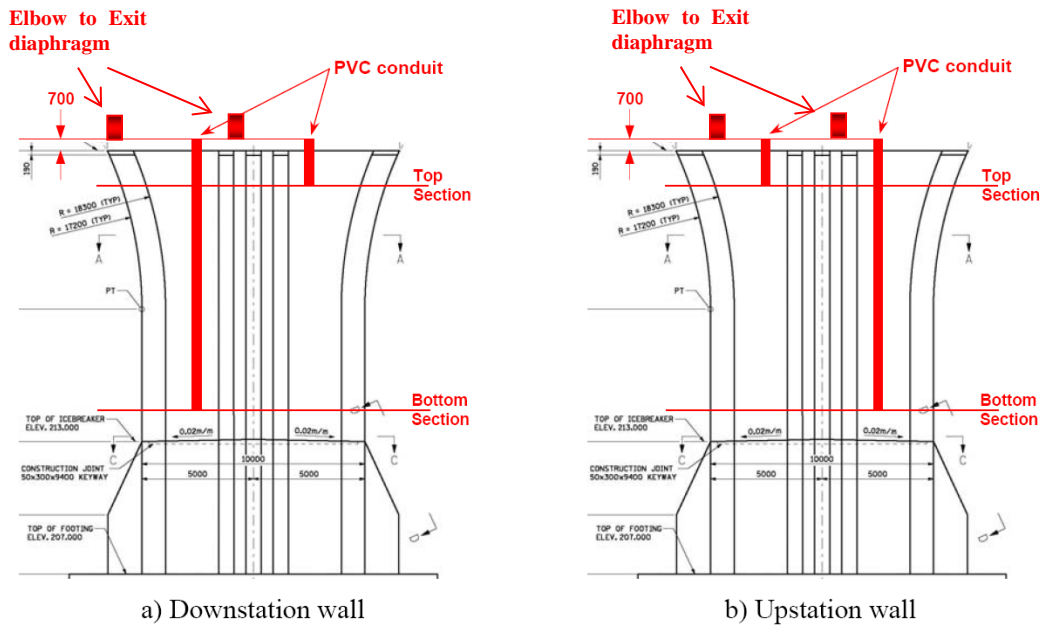


Fig A.3.4.3: View of Pier 4 with the PVC conduit as seen from the rusticated face.
All units in mm unless shown otherwise. 1 mm = 0.0039 in., 1 m = 3.28 ft

Table A.3.4.1: PVC Conduit Lengths.

Pier	Pier Wall	Section	Length (m)
2	Upstation	Top	1.77
		Bottom	10.93
	Downstation	Top	1.64
		Bottom	10.80
4	Upstation	Top	1.68
		Bottom	12.78
	Downstation	Top	1.72
		Bottom	12.82

A.3.5 Installation Pictures



Fig A.3.5.1: PVC Exiting top of pier wall.

Fig A.3.5.2: Strain gauges tied to vertical reinforcing bar.



Fig A.3.5.3: Gauge leads being run to PVC transfer pipe.

Prior to casting and after gauge installation, all strain gauges were manually checked to verify that they were operable. Upon checking the 48 gauges installed in Piers 2 and 4, it was found that three gauges were not working properly. These gauges were: 2TUE2, 2BUL1, and 2BUC1.

A.3.6 Gauge Labeling

The vibrating wire strain gauges are labeled using two complementary techniques. The first of these comprises the attachment of adhesive labels with the designations listed in Table A.7.2. The labels are printed using permanent (non-water soluble) ink, and labels are attached to the wire leads (not the gauge itself). Two labels are attached to each wire lead, one at the free end and the other at the end where the lead is attached to the strain gauge. These labels are necessary to identify the correct location of each gauge during data collection and analysis. The second labeling scheme is meant for rapid visual inspection of gauge installations. This scheme comprises the use of three successive loops of colored electrical tape that are coordinated to identify the location of the gauges. The colored tape combinations are placed at both ends of the wire leads of all strain gauges. The electrical tape colors are linked to specific locations, as noted in Table A.3.6.1. The combinations arising from this scheme are given in Table A.3.6.2.

Table A.3.6.1: Gauge Color Labeling Scheme.

Number	Parameter	Condition	Color
1	Instrumented Section	top (T)	white (Wh)
		bottom (B)	red (Re)
2	Gage Location	left (L)	yellow (Yw)
		center (C)	grey (Gy)
		right (R)	purple (Pu)
		edge (E)	orange (Og)
3	Wall Face	rusticated (1)	green (Gn)
		flat (2)	brown (Br)

Table A.3.6.2: Gauge Color Schemes.

Gage	Color 1	Color 2	Color 3
2TUL1	Wh	Yw	Gn
2TUC1		Gy	
2TUR1		Pu	
2TUE1		Og	
2TUL2		Yw	Br
2TUC2		Gy	
2TUR2		Pu	
2TUE2		Og	
2TDL1		Yw	Gn
2TDC1		Gy	
2TDR1		Pu	
2TDE1		Og	
2TDL2	Yw	Br	
2TDC2	Gy		
2TDR2	Pu		
2TDE2	Og		
2BUL1	Re	Yw	Gn
2BUC1		Gy	
2BUR1		Pu	
2BUL2		Yw	
2BUC2		Gy	
2BUR2		Pu	
2BDL1		Yw	Gn
2BDC1		Gy	
2BDR1		Pu	
2BDL2		Yw	
2BDC2		Gy	
2BDR2		Pu	
4TUL1	Wh	Yw	Gn
4TUR1		Pu	
4TUL2		Yw	Br
4TUR2		Pu	
4TDL1		Yw	Gn
4TDR1		Pu	
4TDL2		Yw	Br
4TDR2		Pu	
4BUL1	Re	Yw	Gn
4BUR1		Pu	
4BUL2		Yw	Br
4BUR2		Pu	
4BDL1		Yw	Gn
4BDR1		Pu	
4BDL2		Yw	Br
4BDR2		Pu	

A.4 Superstructure Instrumentation

A.4.1 Introduction

The instrumentation for the superstructure is limited to the members of the structure that are expected to undergo the largest axial strains due to change in temperature. Those members are Spans 3 and 4. Spans 1, 2, and 5 are all fitted with expansion joints at one or both ends and therefore will not experience the magnitude of forces that Span 2 and 3 will. Because axial strains are desired, the sections in Span 2 and 3 to be instrumented were chosen close to the live load inflection points of the structure. This way, the bending strains from live loads will be minimized and axial forces can be more clearly computed. The inflection points are near if not over the pier tables, so sections close to the piers were chosen. In order to best coincide with the

timelines of the construction schedule and the monitoring project progress, gauges were installed in section P4-6D in Span 4, and section P2-4U in Span 3. The instruments were spaced evenly around the box-girder cross section in order to obtain a full representation of the axial strains in the cross section.

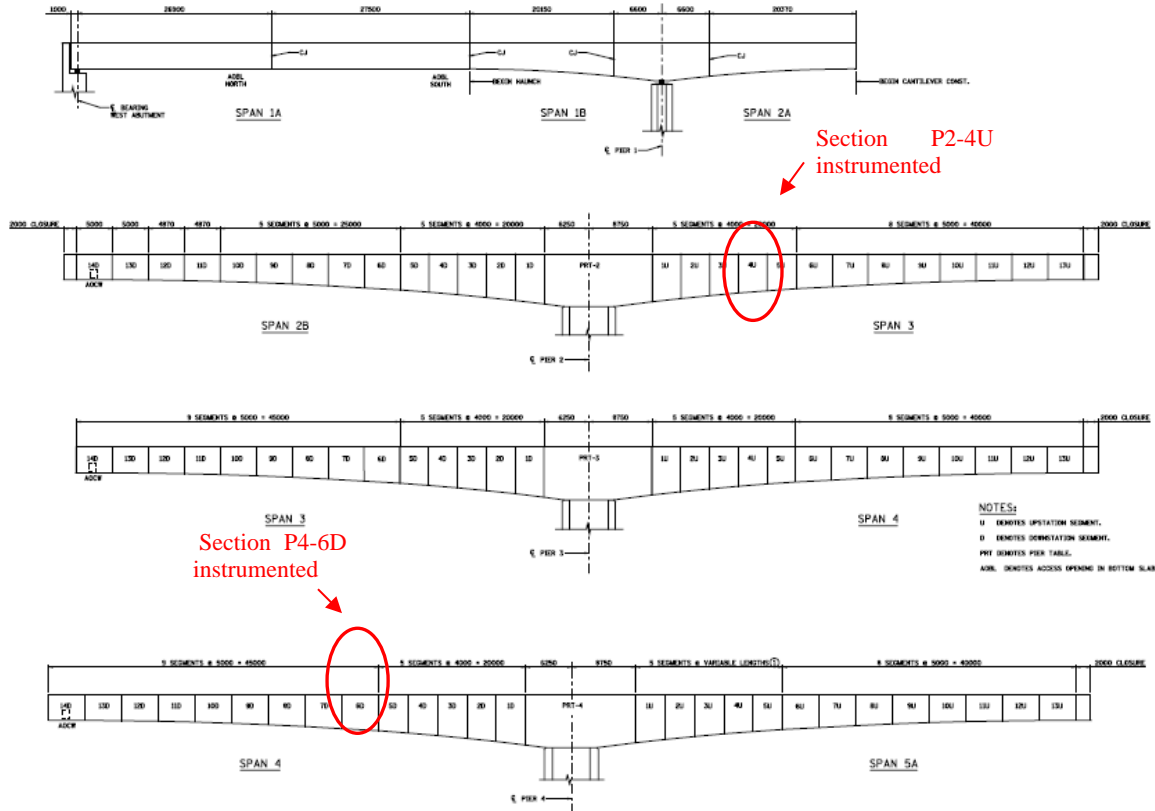


Fig A.4.1.1: Elevation of MN/DOT Bridge 82855 with instrumented spans 3 and 4. All units in mm unless shown otherwise. 1 mm = 0.0039 in., 1 m =3.28 ft

A.4.2 Overview

The two spans instrumented (Spans 3 and 4) are shown in Fig A.4.1.1. The instrumentation consists of 40 vibrating wire strain gauges with incorporated thermistors as well as a PVC outlet in each section to provide an exit point for the leads of the strain gauges. Twenty (20) strain gauges are embedded in each cross section and spaced uniformly around each cross section at a point midway through the length of the section in order to avoid end effects of the section. The spacing of gauges is shown in Fig A.4.3.1. While Fig A.4.3.1 shows only one-half the cross section, gauge placements are symmetric except on the center vertical component. The instrumentation of Span 3 and Span 4 are identical. Therefore Fig A.4.3.1 represents both span instrumentations.

A.4.3 Instrument Locations and Designations

Instrument locations and designations are shown in Fig A.4.3.1 and A.4.3.2. The gauges were installed with respect to the section dimensions in which they were installed. Sections P2-4U and P4-6D have different dimensions and therefore the gauges were spaced differently. Dimension specifications for each section are shown in the below table of dimensions.

Table A.4.3.1: Table of Dimensions pertaining to Fig A.4.3.1.

	Dim. A (mm)	Dim. D (mm)	Station
P2-4U	~2612	~5310	12+427.650
P4-6D	~2705	~4873	12+660.150

In each section, the top slab gauges were placed in the same plane as the top layer of longitudinal rebar in the slab and the bottom slab gauges were placed likewise, tied to the top layer of rebar in the bottom slab. The outer web gauges were placed in the same plane as the outermost layer of longitudinal rebar, and the inner web gauges were placed on alternating sides of the web as shown in Fig A.4.3.1. This being the case, all gauges have a concrete cover to the respective surfaces as indicated in the Wakota Bridge design drawings of at least 50 mm clear cover.

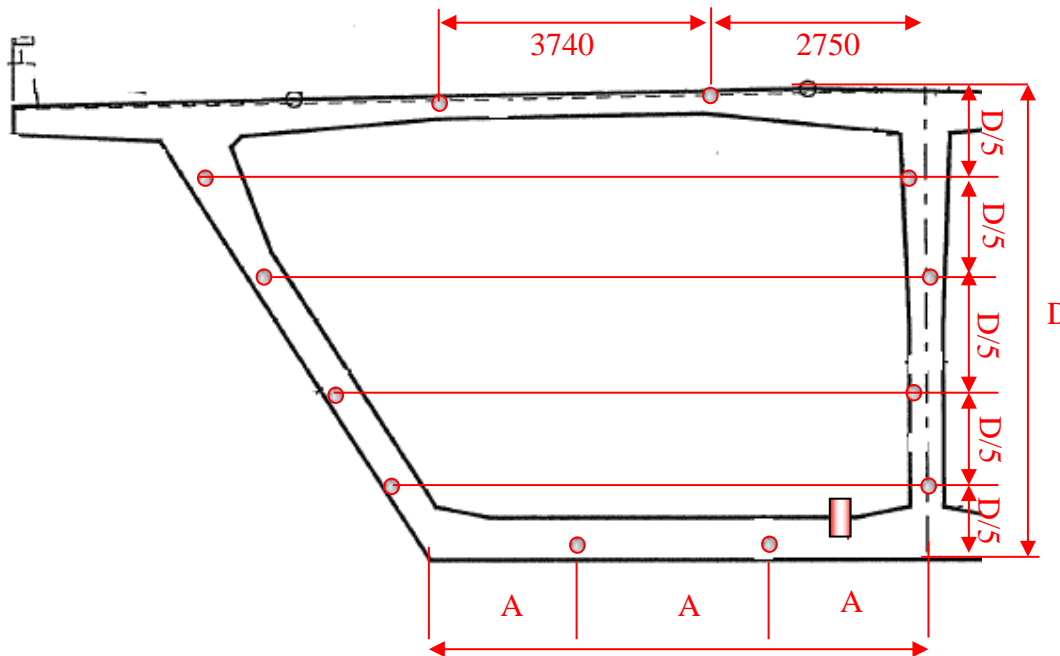


Fig A.4.3.1: Gauge Locations in cross sections with respect to section dimensions. All units in mm unless shown otherwise. 1 mm = 0.0039 in., 1 m =3.28 ft

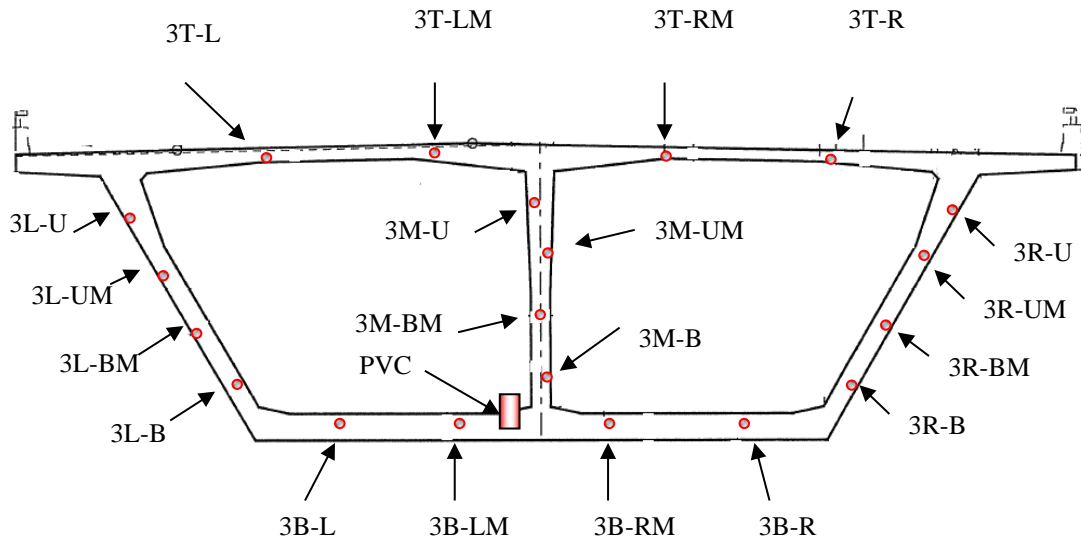


Fig A.4.3.2: Gauge designations for instrumented section (Span 3 – looking upstation).

Each gauge has a 3-part designation with the first part being the span number in which it is located (3 or 4). The second part designates the side the gauge is located in the section (T - top, B - bottom, L - left (looking upstation), R - right (looking upstation), M - middle). The third part (after the dash) designates the location within the side (L - left, LM - left middle, RM - right middle, R - right).

Table A.4.3.2: Gauge Designations.

Gauge	Span	Side	Location
3T-L	3	T (top)	Left (L)
3T-LM			Left middle (LM)
3T-RM			Right middle (RM)
3T-R			Right (R)
3B-L		B (bottom)	Left (L)
3B-LM			Left middle (LM)
3B-RM			Right middle (RM)
3B-R			Right (R)
3L-U		L (left)	Upper (U)
3L-UM			Upper middle (UM)
3L-BM			Bottom middle (BM)
3L-B			Bottom (B)
3M-U		M (middle)	Upper (U)
3M-UM			Upper middle (UM)
3M-BM			Bottom middle (BM)
3M-B			Bottom (B)
3R-U		R (right)	Upper (U)
3R-UM			Upper middle (UM)
3R-BM	Bottom middle (BM)		
3R-B	Bottom (B)		
4T-L	4	T (top)	Left (L)
4T-LM			Left middle (LM)
4T-RM			Right middle (RM)
4T-R			Right (R)
4B-L		B (bottom)	Left (L)
4B-LM			Left middle (LM)
4B-RM			Right middle (RM)
4B-R			Right (R)
4L-U		L (left)	Upper (U)
4L-UM			Upper middle (UM)
4L-BM			Bottom middle (BM)
4L-B			Bottom (B)
4M-U		M (middle)	Upper (U)
4M-UM			Upper middle (UM)
4M-BM			Bottom middle (BM)
4M-B			Bottom (B)
4R-U		R (right)	Upper (U)
4R-UM			Upper middle (UM)
4R-BM			Bottom middle (BM)
4R-B			Bottom (B)

A.4.4 Gauge Description

All gauged locations are instrumented with Model 4200 vibrating wire strain gauges manufactured by Geokon Inc. (www.geokon.com). These gauges are designed for direct embedment in concrete and manufacturer specifications are given in Table A.4.3.2 shown in the pier instrumentation section. The gauges have 100 ft leads attached by the manufacturer.

A.4.5 Installation

Installation of the strain gauges has been accomplished by attaching the gauges to adjacent reinforcing bars using zip ties. The gauges have a barbell configuration which facilitates the installation by tying the zip ties around the heads of the gauges. The gauges are placed in a stable configuration by using a tie at each end of the gauge. The gauges are placed in a horizontal configuration in the same plane as the horizontal reinforcing bars, and at the locations as close to those specified in Fig A.4.3.2 without interfering with the reinforcing bars. The centers of the gauges coincide with the centerline of the section in elevation view and the wire leads are pointing towards Pier 3 in all installed gauges. The leads of the gauges are attached to existing reinforcing bar and run around the section in the shortest manner to the PVC outlet located as shown in Fig A.4.5.2.



Fig A.4.5.1: Gauge leads in P4-6D are run to the PVC outlet pipe.



Fig A.4.5.2: Vibrating wire strain gauge installed in P4-6D.



Fig A.4.5.3: Strain gauge installed in P2-4U.

The PVC lead outlet is oriented vertically and one end placed flush with the interior surface of the box-beam. The dimensions of the outlet are such as to accommodate the bundle of 20 leads coming from the 20 strain gauges housed in the section. Once the leads are all placed in the outlets, the ends of the outlets were taped so as to prevent concrete from entering during the casting process. After casting was complete, the tape was removed from the exposed end and the leads were exposed.

Gauge Labeling

The vibrating wire strain gauges are labeled using two complementary techniques. The first of these comprises the attachment of adhesive labels with the designations listed in Table A.4.3.2. The labels are printed using a desktop printer on white paper and are attached to the wire leads (not the gauge itself). Two labels are attached to each wire lead, one at the free end and the other at the end where the lead is attached to the strain gauge. On the free end, the labels are shrink-wrapped onto the lead whereas on the other end, the labels are simply taped on. The shrink wrap will ensure the exposed ends are not damaged by outside factors. These labels are necessary to identify the correct location of each gauge during data collection and analysis.

Table A.4.6.1: Gauge color labeling scheme.

Number	Parameter	Condition	Color
1	Instrumented side	T (top)	white (Wh)
		B (botton)	blue (Bl)
		L (left)	yellow (Ye)
		M (middle)	red (Rd)
		R (right)	grey (Gy)
2	Location	Left (L) / Upper (U)	purple (Pu)
		Left middle (LM) / Upper middle (UM)	orange (Or)
		Right middle (RM) / Bottom middle	green (Gr)
		Right (R) / Bottom (B)	brown (Br)

The second labeling scheme is meant for rapid visual inspection of gauge installations. This scheme comprises the use of two successive loops of colored electrical tape that are coordinated to identify the location of the gauges. The colored tape combinations are placed at both ends of the wire leads of all strain gauges. The electrical tape colors are linked to specific locations, as noted in Table A.4.6.1. The combinations arising from this scheme are given in Table A.4.6.2.

Table A.4.6.2: Gauge Color Scheme

Gauge	Color 1	Color 2	Gauge	Color 1	Color 2
3T-L	Wh	Pu	4T-L	Wh	Pu
3T-LM		Or	4T-LM		Or
3T-RM		Gr	4T-RM		Gr
3T-R		Br	4T-R		Br
3B-L	Bl	Pu	4B-L	Bl	Pu
3B-LM		Or	4B-LM		Or
3B-RM		Gr	4B-RM		Gr
3B-R		Br	4B-R		Br
3L-U	Ye	Pu	4L-U	Ye	Pu
3L-UM		Or	4L-UM		Or
3L-BM		Gr	4L-BM		Gr
3L-B		Br	4L-B		Br
3M-U	Rd	Pu	4M-U	Rd	Pu
3M-		Or	4M-		Or
3M-		Gr	4M-		Gr
3M-B		Br	4M-B		Br
3R-U	Gy	Pu	4R-U	Gy	Pu
3R-		Or	4R-		Or
3R-BM		Gr	4R-BM		Gr
3R-B		Br	4R-B		Br

A.5 Data Acquisition System

A total of 84 vibrating wire strain gauges from Piers 2 and 4 and Spans 3 and 4 were wired to data acquisition equipment that collected, organized, and stored data at a prescribed rate. The data acquisition equipment includes six multiplexers, four vibrating wire modules, two dataloggers, three multidrops, and one wireless modem. Expansion/contraction information was also collected and stored at each expansion joint at the abutments using the equipment. Each datalogger required a power source consisting of a rechargeable lead-acid battery, current regulator, and wall charger (to be plugged into the 125 V electrical outlets located in the box girder).

A.5.1 System Description

As shown in this instrumentation document, Piers 2 and 4, as well as Spans P4-6D and P2-4U were instrumented with Geokon vibrating wire strain gauges. The data transmitted by these gauges was collected and organized by equipment from Campbell Scientific. Strain gauge data from Pier 2 and Span P2-4U and the west abutment string pot readings were collected by one datalogger system while data from pier 4 and span P4-6D and the east string pot readings were collected by another. Each system consists of the same basic components from Campbell Scientific: 3 model AM16/32B multiplexers, two AVW200 vibrating wire interfaces, and a CR1000 datalogger. Each of the vibrating wire strain gauge leads was connected to one of 16 inputs on a AM16/32B multiplexer (36 leads in the Pier 4 - Span 4 system, 48 leads in the Pier 2 - Span 2 system). The use of multiplexers allows a vibrating wire interface to be able to read up to 32 gauges in succession at a time. Each multiplexer was then connected to a vibrating wire interface. The vibrating wire interface (AVW200) converts the frequency signal of the VW gauge to a recognizable signal to the datalogger. Each vibrating wire interface can accept up to two multiplexers at a time, therefore two interfaces are required in each system to accept the three multiplexers. The two vibrating wire interfaces in each section were then connected to the CR1000 datalogger which collected, organized, and stored the data at a programmed rate. This data was then transferred to a computer and erased from the datalogger memory for analysis. Fig. A.5.3.1-2 show the system configuration with respect to the bridge piers and spans.

In addition to the data acquired from the aforementioned VW strain gauges, overall expansion and contraction information of the bridge due to temperature loading was desired. To achieve this, a measurement device was placed at each expansion joint located at the abutments of the bridge. The device chosen to accomplish this was a linear potentiometer. Linear potentiometers are capable of measuring large displacements very accurately and are very resistant to environmental conditions. These qualities make them desirable in this situation as they will be placed in exposed environments and a displacement range of ~12 inches is desired according to the bridge plans. The linear potentiometer ordered is the HX-P420 from Unimeasure, Inc. This model was selected because of its rugged design, ability to handle a wide temperature range, and the option of using long lead wires due to a current output instead of a voltage output.

A.5.2 Equipment Description

Campbell Scientific (www.Campbellsci.com) manufactures the data acquisition equipment used in the data acquisition system described above. These instruments are compatible with the Geokon model 4200 vibrating wire strain gauges already installed in the structure as well as the Unimeasure linear potentiometers installed in the abutments. The specifications for all Campbell equipment can be found on the Campbell Scientific website. The specifications for the string pots are shown below.

Table A.9.2.1: HX-P420 Linear Potentiometer Specifications

<p>General Measurement range: 15”</p> <p>Performance Linearity....±0.20% FS Repeatability.....±0.015% FS Resolution.....Essentially Infinite</p> <p>Electrical Output.....User adjustable 4-20 mA Excitation Voltage....9 to 35 V DC Min. Supply voltage..(.02 x Load Res.) + 9 VDC Insulation Resistance.....100 Megaohms min. at 100 VDC</p>	<p>Adjustment Range 4mA.....0 to 30% of Range 20 mA.....80% to 100% of Range Protection.....Reversed Polarity</p> <p>Environmental Thermal Coefficient of Sensing Element.... ±100PPM/°C Max Operating Temp.....-40°C to +95°C Operating Humidity.....100% Shock.....50 G @ 0.1 ms Max. Vibration.....10 Hz to 2000 Hz, 15 G peak Ingress protection Exclusive of Wire Rope area NEMA 4</p>
---	--

A.5.3 Installation of DAQ Equipment

As mentioned, there were two main data acquisition systems for the strain gauges installed in the substructure and superstructure. The data acquisition equipment that was used to collect data from Pier 2 and Span P2-4U was placed partly at a location midway between the pier and span P2-4U and partly in the pier table. The equipment placed in the pier table consisted of one multiplexer, whereas the equipment placed at the midway location consists of two multiplexers, two vibrating wire interfaces, and one datalogger as well as supplies to power the system.

The leads from the gauges located in the pier walls exit at four different locations in the pier table. The 14 leads from the upstation wall exit at two different points through the upstation pier table diaphragm: seven exit on the north side of the web and seven exit on the south side. Likewise, the 14 leads from the downstation wall exit through the downstation diaphragm, seven on each side of the center box girder web. The leads in the pier table were spliced and run to one location on the north side of the center web in the box girder, this was done by running the south side leads through the holes created in the center web by the form traveler. A total of 16 leads were then connected to the multiplexer in the pier table. The remaining 12 leads as well as the multiplexer communication wires were bundled and run along the center of the box girder to the equipment location midway between the instrumented span and the pier.

The 20 leads exiting in span P2-4U were also bundled and run to the midway equipment location. These leads along with the 12 pier leads were connected to the two multiplexers at the location, the multiplexers were connected to the vibrating wire interfaces, and the interfaces connected to the datalogger. All equipment was placed in enclosures on the interior girder floor. Power was provided by a 7 Ahr rechargeable battery with a float charger and regulator connected to the 125 V receptacle located inside the box girder.

The strain gauge leads and DAQ equipment in the instrumented sections near Pier 4 were configured similarly although Pier 4 had only 16 leads to be connected. Because of this, all Pier four leads were connected to the multiplexer located in the pier table and no leads will need to be bundled and run to the midway equipment location in Span 3 although the multiplexer connection wires will still need to be run to the midway location. The equipment locations corresponding to the instrumented sections are shown in FIG A.5.3.1-2.

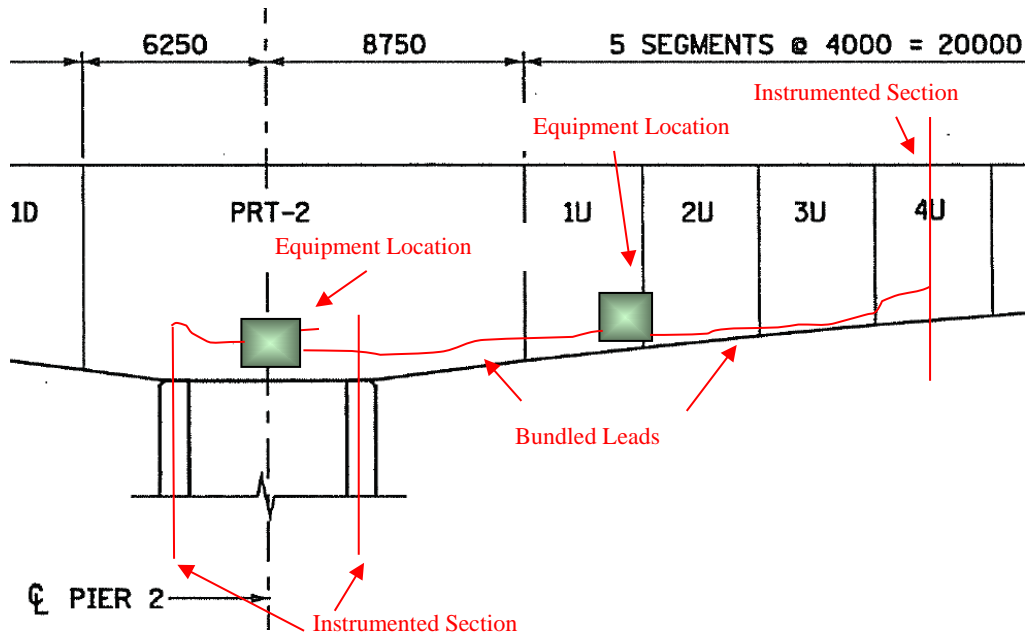


Fig A.5.3.1: DAQ equipment locations (pier 2). All units in mm unless shown otherwise. 1 mm = 0.0039 in., 1 m =3.28 ft

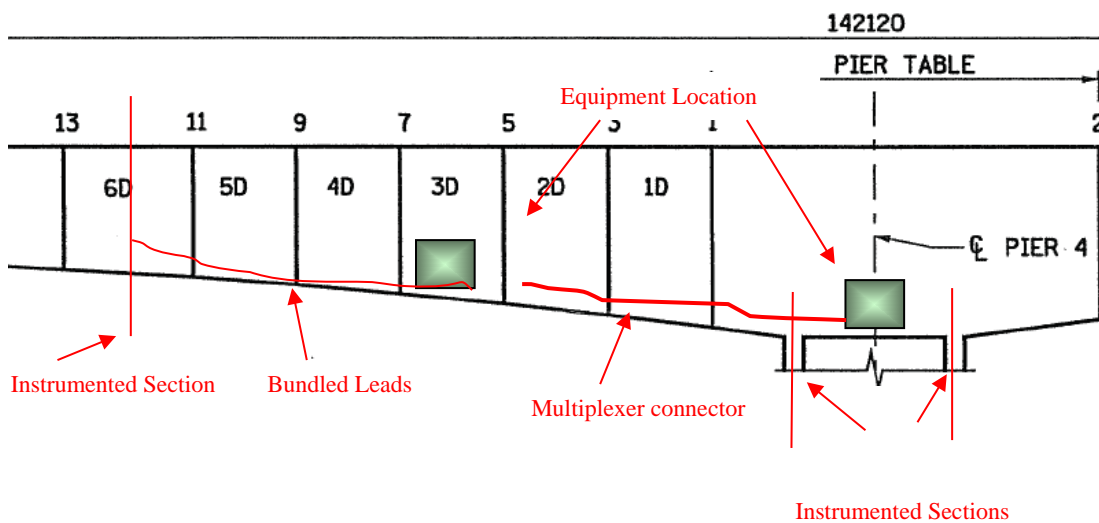


Fig A.5.3.2: DAQ equipment locations (pier 4). All units in mm unless shown otherwise. 1 mm = 0.0039 in., 1 m =3.28 ft

A.5.4 Installation of Linear potentiometers

One P-420 linear potentiometer was installed at each end of the superstructure. The linear potentiometer (a.k.a. string pot) was mounted on the exterior surface of the end diaphragm of the superstructure at the centerline of the box girder. It was mounted under the ledge of the diaphragm as shown in Fig A.5.4.1. The measuring cable from each pot was then extended to the abutment face and fastened in order to measure the amount of expansion and contraction between the superstructure and abutment throughout the yearly temperature changes. The string pot range of measurement was chosen based on the design range of the expansion joints in each abutment. The design of the bridge required an expansion joint range of plus or minus 6 inches for a total of 12 inches. Because of this required range, the string pot range was chosen to be 15 inches to accommodate the 12 inch required design expansion and leave some room for variability in installation due to the position in the range that the string pot is installed.

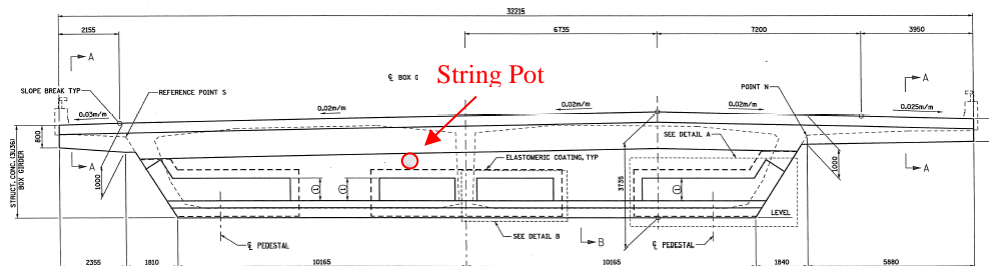


Fig A.5.4.1: Placement of Linear potentiometers in superstructure at abutment. All units in mm unless shown otherwise. 1 mm = 0.0039 in., 1 m =3.28 ft

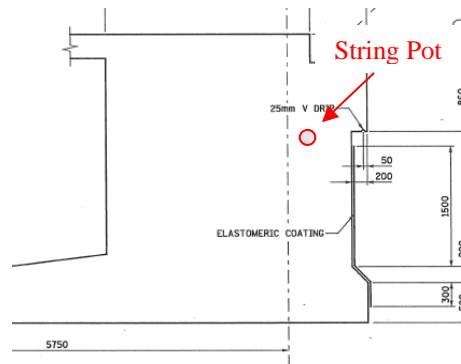


Fig A.5.4.2: String pot placement (elevation view). All units in mm unless shown otherwise. 1 mm = 0.0039 in., 1 m =3.28 ft

The string pots were mounted directly to the concrete box section by drilling anchor points and securing the devices with mounting bolts. The measuring cable from the string pot was extended and mounted in a similar fashion to the face of the abutment.

The data produced by these instruments was collected by the CR1000 dataloggers located on the interior of the superstructure box as discussed earlier. The leads from the potentiometer were run through the diaphragm at each end via the 78 mm electrical conduit on the west end of the

superstructure and via the formed voids for future post-tensioning on the east end. A current shunt was used to read the 4-20 mA output of the linear potentiometer by the datalogger.

Multidrop interfaces were used to connect all devices via the CR1000 dataloggers to a cell phone modem at the west end of the superstructure which transmitted the data over a broadband cell phone signal.

A.5.5 Summary

There were five equipment locations total as shown in Fig A.5.5.1, four of which were sensor connection locations and one in which the cell phone modem was located. The four aforementioned locations required power from the interior power/lighting plan described in the bridge plans.

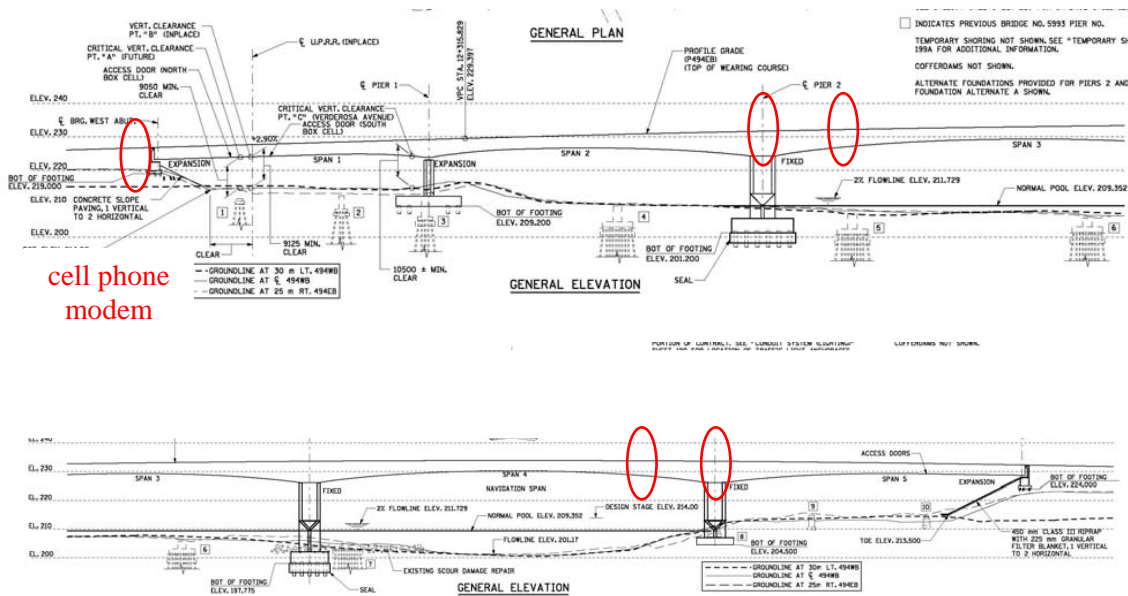


Fig A.5.5.1: Equipment and cell phone modem locations along bridge. All units in mm unless shown otherwise. 1 mm = 0.0039 in., 1 m =3.28 ft